UNIVERSITY OF OKLAHOMA
GRADUATE COLLEGE

GEOMETRICAL INVESTIGATIONS OF THE CASIMIR EFFECT: THICKNESS AND CORRUGATION DEPENDENCIES.

A DISSERTATION
SUBMITTED TO THE GRADUATE FACULTY
in partial fulfillment of the requirements for the
Degree of
DOCTOR OF PHILOSOPHY

By

PRACHI PARASHAR
Norman, Oklahoma
2011

GEOMETRICAL INVESTIGATIONS OF THE CASIMIR EFFECT:
THICKNESS AND CORRUGATION DEPENDENCIES.

A DISSERTATION APPROVED FOR THE
HOMER L. DODGE DEPARTMENT OF PHYSICS AND ASTRONOMY

BY

Dr. Kimball A. Milton, Chair

Dr. Phillip Gutierrez

Dr. Ronald Kantowski

Dr. Nikola Petrov

Dr. Michael Santos

Dedicated to my parents–Prabha and Nagendra Nath Jha.

Acknowledgements

First and foremost I want to thank my thesis advisor Prof. Kimball A. Milton, from whom I have learned a diverse spectrum of physics knowledge and without whom I would not be writing this acknowledgement! He allowed complete independence in choosing the thesis project and was always there to guide me through the crucial stages. Most importantly he was always extremely patient and supportive, specifically during the period of my father's illness for which I can never ever thank him enough.

Much of the work presented here was done in collaboration with Kim, Martin Schaden, Inés Cavero-Peláez, and K. V. Shajesh. I wish to extend my warmest thanks to all of them specially Shajesh with whom I discussed and worked most extensively during his stay in Norman and afterwards through innumerable EVO video conference meetings through the internet. I also wish to include my appreciation towards my other research collaborators–Stephen Fulling, Iver Brevik, Simen Ellingsen, and August Romeo- with whom I have worked on various projects.

The research group meetings, which we had everyday, were extremely productive. I take this opportunity to thank my research group members during my graduate student period–Inés, Shajesh, Jef Wagner, Archana Anandakrishnan, Elom Abalo, and Nima Pourtolami.

I also thank my Ph.D. committee members–Dr. Phillip Gutierrez, Dr. Ronald

Kantowski, Dr. Nikola Petrov, and Dr. Michael Santos- for their time and support.

My stay in Norman would not have been so pleasant without the warmth extended by Margarita and Kim Milton, who always accepted students as part of their family. I never felt alone due to the presence of my friends and their families here in Norman, elsewhere in US, and abroad, who brought balance and alternate outlook to life.

I wish to express my deepest appreciation towards my brother Anshul who has been my biggest critic and strongest support, my sister-in-law Babita who brought immense love and happiness to our family, and our little bundle of joy–my nephew Samanyu- who can always bring smile to my face and relieve all the stress without uttering a single word.

Thank you everyone!

Contents

List of Tables

List of Figures

Abstract

In the quantum theory the vacuum is not empty space. It is considered as a state of infinite energy arising due to zero point fluctuations of the vacuum. Calculation of any physically relevant process requires subtracting this infinite energy using a procedure called normalization. As such the vacuum energy is treated as an infinite constant. However, it has been established beyond doubt that mere subtraction of this infinite constant does not remove the effect of vacuum fluctuations and it cannot be treated just as a mathematical artifact. The presence of boundaries, which restricts the vacuum field, causes vacuum polarization. Any non-trivial space-time topology can cause similar effects. This is manifested as the Casimir effect, whereby the boundaries experience a force due to a change in the energy of the vacuum. To calculate the vacuum energy we treat the boundaries or other restrictive conditions as classical backgrounds, which impose boundary conditions on the solution of the vacuum field equations. Alternatively, we can incorporate the classical background in the Lagrangian of the system as classical potentials, which automatically include the boundary conditions in the field equations. Any change in the boundary conditions changes the vacuum energy and consequently the Casimir force is experienced by the boundaries.

In this dissertation we study the geometric aspect of the Casimir effect. We con-

sider both the scalar field and the physically relevant electromagnetic field. After a brief survey of the field in Chapter 1, we derive the energy expression using the Schwinger's quantum action principle in Chapter 2. We present the multiple scattering formalism for calculating the vacuum energy, which allows us to calculate the interaction energy between disjoint bodies and subtract out the divergent terms from the beginning. We then solve the Green's dyadic equation for the electromagnetic field interacting with the planar background surfaces, where we can decompose the problem into two transverse scalar modes. In Chapter 3 we collect all the solutions for the scalar Green's functions for the planar and the cylindrical geometries, which are relevant for this dissertation.

In Chapter 4 we derive the interaction energy between two dielectric slabs of finite thickness. Taking the thickness of the slabs to infinity leads to the Lifshitz results for the two infinite dielectric semi-spaces, while taking the dielectric permittivity to infinity gives the well-known Casimir energy between two perfect conductors. We then present a simple model to consider the thin-plate limit (taking the thickness of the slabs to zero) based on Drude-Sommerfeld free electron gas model, which modifies the plasma frequency of the material to include the finite size dependence. We get a non-vanishing result for the Lifshitz energy in the slab thickness going to zero limit. This is remarkable progress as it allows us to understand the infinitesimal thickness limit and opens a possibility of extending this model to apply it to graphene and other two dimensional surfaces. The Casimir and Casimir-Polder results in the perfect conductor limit give us the expected results.

In Chapter 5 we study the lateral Casimir torque between two concentric corrugated cylinders described by δ-potentials, which interact through a scalar field. We derive analytic expressions for the Casimir torque for the case when the corrugation

amplitudes are small in comparison to the corrugation wavelengths. We derive explicit results for the Dirichlet case, and exact results for the weak coupling limit, in the leading order. The results for the corrugated cylinders approach the corresponding expressions for the case of corrugated parallel plates in the limit of large radii of the cylinders (relative to the difference in their radii) while keeping the corrugation wavelength fixed.

In Chapter 6 we calculate the lateral Casimir energy between corrugated parallel dielectric slabs of finite thickness using the multiple scattering formalism in the perturbative approximation and obtain a general expression, which is applicable to real materials. Taking the thickness of the plates to infinity leads us to the lateral Lifshitz formula for the force between corrugated dielectric surfaces of infinite thickness. Taking the dielectric constant to infinity leads us to the conductor limit which has been evaluated earlier in the literature. Taking the dilute dielectric limit gives the van der Waals interaction energy for the corrugated slabs to the second order in corrugation amplitude. The thin plate approximation proposed in Chapter 4 is used to derive the Casimir energy between two corrugated thin plates. We note that the lateral force between corrugated perfectly conducting thin plates is identical to the ones involving perfectly conducting thick plates. We also evaluate an exact expression (in terms of a single integral) for the lateral force between corrugated (dilute) dielectric slabs.

Chapter 1

A brief survey of the Casimir effect

H. B. G. Casimir in 1948 [1] studied the change in the zero point energy (ZPE) of the electromagnetic field in the presence of two neutral perfectly conducting parallel plates, which were separated by a distance larger than the wavelength corresponding to the atomic frequencies, and predicted that they would experience an attractive force. This phenomenon of modification of the vacuum state in the presence of macroscopic objects is called the *Casimir effect* in the literature. It has widespread implications from fundamental to applied physics as well as in chemical and biological processes. In the following few decades after Casimir's prediction it received relatively little attention, mostly theoretical, due to lack of convincing experimental evidence. However, in the last fifteen years the interest in the field has sparked again with the new advances in experimental techniques, like atomic force microscopy, which has allowed experimentalists to measure forces at small scales with great accuracy. The major thrust in the study of the Casimir effect has come from the field of nanotechnology, where the miniaturization of electro-mechanical devices to MEMS (micro-electro-mechanical systems) and NEMS (nano-electro-mechanical

systems) has brought us into a regime in which quantum effects can no longer be neglected and the Casimir force dominates. On the other hand, Casimir effects for quantized fields in curved spaces can provide considerable insight into the problems related to gravitation, cosmology, extra dimensions, and unification theories. For an up-to-date account see [2].

The purpose of this Chapter is to present a brief historical survey and familiarize the reader with the basic understanding of the field. The rest of the Chapter is organized as follows. In Section 1.1, we present the interaction of macroscopic bodies with the radiation field from two different viewpoints – one in which the macroscopic bodies are fluctuating and the field is treated as classical and the other in which the field is fluctuating and the macroscopic bodies are considered classical. In Section 1.2 we present a basic example calculation of the Casimir energy using the zeta function regularization scheme. Section 1.3 introduces major theoretical and experimental advances in the field with emphasis on the effect of geometry, material and temperature on the Casimir energy.

1.1 Fluctuating Molecules versus Fluctuating Fields

1.1.1 Fluctuating molecules viewpoint and Casimir-Polder result

Two neutral molecules experience the weak van der Waals force whose precise nature was understood only after the birth of quantum mechanics. The spontaneous random distribution of electrons inside an atom causes self polarization of the atom. This temporary dipole can induce mutual polarization in nearby atoms and cause an

attractive force between them. In 1930 London [3, 4], using second order perturbation theory, showed that the interaction of two fluctuating dipoles falls with distance as $1/R^6$, where R is the separation distance between the two dipoles. However, while studying the stability of colloids, Verwey and Overbeek observed that colloids of coarse particles were more stable than that predicted by the theory [5]. They also observed that the attractive interaction should decay faster than the London potential $1/R^6$. Overbeek then pointed out that due to the finite value of the speed of light retardation effects should be taken into account when the separation between atoms becomes larger than the wavelength corresponding to atomic frequencies. Casimir and Polder [6] included retardation effects in analyzing the London-van der Waals interaction between an atom and a perfectly conducting plate, and between two atoms. Using second and fourth order perturbation theory in the two cases they obtained rather simple results given by

$$U_{\rm ap}=-\frac{3\hbar c}{8\pi R^4}\alpha, \tag{1.1a}$$

$$U_{\rm aa}=-\frac{23\hbar c}{4\pi R^7}\alpha_1\alpha_2, \tag{1.1b}$$

where $U_{\rm ap}$ is the interaction energy of the atom-plate configuration and $U_{\rm aa}$ is the interaction energy of the atom-atom configuration. α_i refers to the polarizability of the corresponding atom and R is the separation distance between two objects. For the case of two atoms they obtained the $1/R^7$ dependence consistent with the observation by Verwey and Overbeek.

1.1.2 Fluctuating fields viewpoint and Casimir result

In the concluding remarks of their paper [6] Casimir and Polder mentioned that the simplicity of the results suggest that it might be *"possible to derive these results from more elementary considerations."* In 1948 Casimir [7, 1] analyzed the problem considering the macroscopic bodies to be static but the electromagnetic field interacting with them to be now fluctuating [1]. In [7] he was able to reproduce the results given by Eq. (1.1) while in [1] he considered the case of interaction two perfectly parallel conductors. This change in viewpoint from the fluctuating objects to the fluctuating fields requires us to consider local action of the fields in contrast to the action at a distance between atoms in the former. This also requires the use of quantum field theory instead of quantum mechanics for analyzing the problem.

We associate each point in space with fluctuations of the electromagnetic field. The energy of each mode is given by that of the harmonic oscillator energy $E_n = \hbar\omega(n + 1/2)$, where n is the number of particles in the particular state under consideration. For the ground state of the vacuum, when there are no particles, $n = 0$. The energy of the vacuum state is

$$E_0 = \sum_{\mathbf{k}} \frac{1}{2}\hbar\omega_{\mathbf{k}}, \tag{1.2}$$

associated with the vacuum field, which can take any value. Therefore, this energy is infinite. The presence of the macroscopic bodies leads to the boundary conditions on the electromagnetic field, which modifies the characteristic frequencies of the field. The possible modes of the electromagnetic field are now restricted by the presence of the boundaries. Consequently, the ZPE refers to different allowed frequencies. The

[1] During a visit to Copenhagen, Casimir mentioned this work to Neils Bohr and explained his quest for a *"simpler and elegant derivation"*. Bohr thought over it and commented "must have something to do with zero-point energy"

ZPE of the vacuum state in the presence of the external bodies is given by

$$E_{0\mathrm{pp}} = \sum_{\mathbf{k}} \frac{1}{2}\hbar\bar{\omega}_{\mathbf{k}_{\mathrm{pp}}}, \tag{1.3}$$

where $\mathbf{k}_{\mathrm{pp}}$ is the wavevector in presence of the macroscopic body. The sum is still over an infinite range and consequently this energy is also infinite. Subtracting Eq. (1.3) from Eq. (1.2) may yield a finite result for the vacuum energy. This procedure is subtle and requires regularization.

1.2 Need for regularization and renormalization

As mentioned in Section 1.1, results obtained for the vacuum energy are infinite. The divergence arising from infinite degrees of freedom as described in previous section are ultraviolet divergences. These types of divergences can be controlled by a regularization procedure. We begin by introducing a regularization parameter to make the divergent expression finite, which in some limit reproduces the original expression. This limit is taken at the end of the calculation. Different regularization procedures should give the same finite value of the energy, which makes the analysis unambiguous. On the other hand there are divergences arising due to the topology of the system since the configuration space is bounded. Mostly in the cases where only single bodies are present one has to consider the renormalization procedure, i.e., subtracting proper counter terms leading to redefinition of physical parameters. Various geometric parameters like volume, surface area, curvatures are used for this purpose. In cases where the coupling of the fluctuating field with gravity is considered, mass can be used for renormalization [8]. However, so far there is no standard renormalization

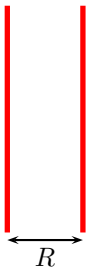

Figure 1.1: Two parallel perfectly conducting metal plates separated by distance R.

procedure which works for every case similar to the renormalization in quantum electrodynamics, for example. The Casimir force between separate bodies, in contrast, is in general finite. More information on renormalization in presence of background potentials can be found in Chapter 4 of the book by Bordag *et al* [9] and the review article by Nesterenko *et al* [10].

Using zeta-function regularization for obtaining Casimir's result – Example calculation

In the following we sketch an example calculation for the two parallel plate configuration using the zeta-function regularization procedure [11]. Consider two perfectly conducting infinite long parallel plates separated by a distance R as shown in Fig. 1.1. The presence of conducting parallel plates imposes boundary conditions on the electromagnetic field

$$\mathbf{E} \times \hat{\mathbf{n}} = 0, \qquad \mathbf{B} \,.\, \hat{\mathbf{n}} = 0, \tag{1.4}$$

where $\mathbf{E}$ and $\mathbf{B}$ are electric and magnetic fields respectively and $\hat{\mathbf{n}}$ is the unit vector normal to the surface of the boundary. The field can be decomposed into transverse electric and transverse magnetic modes, where each can be described by a massless

scalar field $\varphi(\mathbf{x}, t)$ obeying free Klein-Gordon equation

$$\Box\varphi(\mathbf{x}, t) = 0. \tag{1.5}$$

Using the fact that parallel plate geometry has translational invariance in two directions we can write the vacuum energy starting from Eq. (1.3) as

$$\mathcal{E}_{0\text{pp}} = \frac{\hbar}{2}\int \frac{d^2k}{(2\pi)^2} 2 \sum_{m=1}^{\infty} \omega_{\mathbf{k}_\perp, m}, \tag{1.6}$$

where $\mathcal{E}_{0\text{pp}}$ is the energy per unit area, $\mathbf{k}_\perp = \sqrt{k_x^2 + k_y^2}$, and the oscillator frequency $\omega_{\mathbf{k}_\perp, m}$ is given by

$$\omega_{\mathbf{k}_\perp, m} = c\sqrt{k_\perp^2 + \left(\frac{m\pi}{R}\right)^2}. \tag{1.7}$$

Eq. (1.6) now reads

$$\mathcal{E}_{0\text{pp}} = \frac{\hbar c}{2}\int \frac{d^2k}{(2\pi)^2} 2 \sum_{m=1}^{\infty} \left(k_\perp^2 + \left(\frac{m\pi}{R}\right)^2\right)^{\frac{1}{2}}, \tag{1.8}$$

where the factor of 2 takes care of the contributions from the two modes. This expression, as it sits, is divergent. In the zeta-function regularization procedure we replace the power $\frac{1}{2}$ by $-s$. The resulting integral is now convergent as long as $\operatorname{Re} s > \frac{3}{2}$. Evaluation of Eq. (2.1) with this change gives

$$\mathcal{E}_{0\text{pp}}^{reg} = \frac{\hbar c}{4\pi}\left(\frac{\pi}{R}\right)^{-2s+2} \zeta(2s-2)\frac{\Gamma(s-1)}{\Gamma(s)}. \tag{1.9}$$

Analytically continuing the value of s to $-\frac{1}{2}$ reproduces the result for the Casimir

energy per unit area

$$\mathcal{E}_{0\text{pp}} = -\frac{\pi^2}{720}\frac{\hbar c}{R^3}. \tag{1.10}$$

The Casimir force is defined as

$$F_{0\text{pp}} = -\frac{\partial E_{0\text{pp}}}{\partial R}. \tag{1.11}$$

Thus the Casimir force per unit area or the Casimir pressure P using Eq. (1.10) is given by

$$\text{P} = -\frac{\pi^2}{240}\frac{\hbar c}{R^4}, \tag{1.12}$$

which is attractive. For a separation distance of 1 micro-meter the Casimir pressure is 1.30 milli-Pascal and it increases rapidly as R decreases.

1.3 Important advances in the Casimir effect

The geometry and configuration confining the fluctuating field considered by Casimir are ideal, i.e., perfectly conducting infinitely long parallel plates with smooth surfaces at zero temperature. However, for experiments one has to consider finite-sized real materials with arbitrary surface roughness at non-zero temperature. To counter the problem of keeping two surfaces parallel most experiments are done with one curved object and another flat object. Calculation of the Casimir energy for geometries and configurations other than the parallel plates configuration, taking into account the aforementioned parameters, is challenging. Therefore, progress in fundamental understanding of the field has been rather slow. In the following we present the important theoretical and experimental landmarks in the field of the Casimir effect

along with their importance in the advancement of the field, which address some of these issues like geometry, material, and temperature dependences.

1.3.1 Theoretical advances

Effects of geometry and material

In 1955 Lifshitz [12] developed a macroscopic theory for the case of two semi-infinite slabs of real materials with arbitrary dielectric constants ϵ, thereby greatly generalizing Casimir's original work. Later papers by his group simplified the formalism and generalized the system to replace the intermediate vacuum by a third material. They also applied the theory to the thin films on the surface of the solid [13, 14]. The calculation, though lengthy, did not pose any new mathematical challenge. Nowadays, the Lifshitz calculation can be reproduced very simply, for example see chapter 3 of the book by Milton [15].

The first calculation for a curved geometry was performed by Boyer for a perfectly conducting spherical shell [16]. Casimir in 1953 [17] had suggested that stability of a classical electron could be explained by an attractive force due to ZPE. However, Boyer concluded that the Casimir energy of a perfectly conducting shell is repulsive, i.e, directed outward on the shell. This result was confirmed with greater precision by different calculations later [18, 19, 20]. However, the repulsive nature of the Casimir energy in this case generated more questions. One such being — How does the Casimir energy depend on the geometry of the bounding surface? Inclusion of material properties in the curved surface configuration leads to new structures of divergences. The first attempt to evaluate the Casimir energy for a dielectric sphere was undertaken by Milton in 1980 [21]. For the particular case of speed of light being different on

two sides for the spherical shell, the ZPE is infinite. However, for the dilute (weak) approximation, a finite part can be extracted [22]. Some of these results are listed in Table 1.1. It is interesting to note that in all the cases listed in Table 1.1, the Casimir energy for the single sphere is repulsive.

For the cylindrical geometry calculations turned out be more difficult as transverse electric and transverse magnetic modes cannot be separated except for perfect conductors. For the infinitely long conducting circular cylinder the first correct result was obtained by DeRaad and Milton [24] who found the Casimir energy for the electromagnetic case to be attractive, although its magnitude is small compared to the corresponding spherical case. The case of a dielectric cylinder was first considered by Brevik *et al* [25]. Various authors considered approximations similar to the spherical geometry, i.e., the dilute approximation and the speed of light being the same on either side of the cylindrical shell, and found that the Casimir energy, calculated up to the second order of the small parameter, vanishes. A summary of these results is listed in Table 1.1.

Various other geometries of the bounding surfaces like cylinders of triangular [32] and rectangular shapes, rectangular boxes [33, 34, 35], wedges [36, 37, 38], and objects of arbitrary shapes are being considered by researchers for a better understanding of the sign and magnitude of the Casimir energy and the divergences which arise. Calculations are performed using different dimensions, boundary conditions, confined fields, and models. Some of the important calculational approaches are the mode summation method, zeta function method [39], heat and cylinder kernel method [40], stress tensor method using Green's function, multiple scattering formalism [41, 19, 42], and worldline technique [43]. Description of all this is beyond the scope of the present

[1]This table is reproduced from [23] with author's permission.

Type	$E_{\text{Sphere}}R$	$\mathcal{E}_{\text{Cylinder}}R^2$	References
EM	+0.04618	-0.01356	[16][24]
D	+0.002817	+0.0006148	[26][27]
$(\varepsilon-1)^2$	$+0.004767 = \frac{23}{1536\pi}$	0	[22][28]
ξ^2	$+0.04974 = \frac{5}{32\pi}$	0	[29][30]
λ^2	$+0.009947 = \frac{1}{32\pi}$	0	[31][23]

Table 1.1: Summary of the Casimir energy (E) for a sphere and the Casimir energy per unit length ($\mathcal{E}$) for a cylinder both of radius R. Type describes different boundary conditions– perfectly conducting for electromagnetic fields (EM), Dirichlet for scalar fields (D), dilute (weak) dielectric for electromagnetic fields for coefficient of $(\epsilon-1)^2$, dilute dielectric for electromagnetic fields, with media having same speed of light on either side of the boundary, for coefficient of $\xi^2 = \frac{(\epsilon-1)^2}{(\epsilon+1)^2}$, and weak coupling for a scalar field with semi-transparent δ-function boundary. The last column lists the references.

thesis. Detailed references on advances in these areas can be found in recent book on the subject [9]. For the current status of the field see [2, 44].

Temperature effects

The cases described above are idealized in that only the geometric effects at zero temperature on quantum fluctuations of the vacuum state are considered. Any other form of excitation of the vacuum state is neglected. In a more general case one has to consider states with real thermal photons. Thus vacuum fluctuations can arise because of thermal effects in addition to the quantum effects. The energy of such a system is the Casimir energy at non-zero temperature and requires statistical treatment of the system in the realm of the quantum field theory [15, 9].

The first non-zero temperature effect calculation was carried out by Lifshitz [12] who did it for real materials. These results had some transcription errors, which were noted by Hargreaves [45] who analyzed the difference between Lifshitz's and other author's calculations. For history of other works see recent books [15, 9]. The case

of a perfect conductor can be obtained by taking the dielectric permittivity ϵ of the material to infinity. The procedure for taking this limit, though, is the cause of much debate in the field currently [2, 46] as it gives different low and high temperature dependences. Conventionally the $\epsilon \to \infty$ limit is taken before the $\omega \to$ limit so the contribution from TE (transverse electric) zero mode is retained. In the modified scheme this order of taking limits is reversed thereby removing the zero mode from the beginning. According to Milton [47], the low temperature result for the Casimir pressure of an ideal metal using the modified scheme is given by

$$P^T = -\frac{\pi^2}{240R^4}\left[1 + \frac{16}{3}(RT)^4\right] + \frac{\zeta(3)}{8\pi R^3}T, \tag{1.13}$$

where $RT \ll 1$. The term linear in T is absent in the conventional result obtained by Lifshitz and other authors [47]. Fig. 1.2 shows the low temperature effect on the fractional change in the Casimir pressure P with respect to the Casimir pressure at zero temperature P_0 plotted against the separation distance R. For distance between plates of the order $1\,\mu\,\mathrm{m}$ at room temperature ($300\,\mathrm{K}$) $RT \sim 0.1$. The linear dependence in T dominates other terms at low temperature limit and therefore, should be observable in experiments.

The high temperature result changes by a factor of $\frac{1}{2}$ from the conventional result in the modified scheme, and is given by

$$\mathrm{P}^T = -\frac{\zeta(3)}{8\pi R^3}T. \tag{1.14}$$

The linear dependence on temperature at high temperature limit shows the classical behavior of the system.

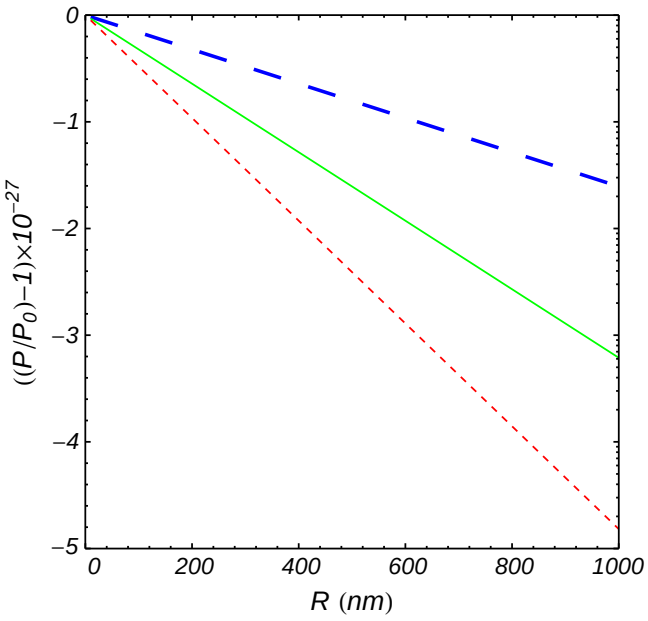

Figure 1.2: Variation of fractional change in the Casimir pressure with respect to the Casimir Pressure at zero temperature with the separation distance R between conducting plates. The large dashed curve(blue) is for $T = 100$K, line curve(green) is for $T = 200$K and small dashed curve(red) is for $T = 300$K.

1.3.2 Experimental advances

Many early experiments were performed to confirm the Casimir effect with inconclusive results [48, 49, 50, 51, 52, 53, 54, 55, 56]. These include experiments conducted on insulators as well as conductors. Specifically in [51] Sparnaay considered two parallel metal plates, which is the original configuration considered by Casimir. The experiment showed existence of the long range force, however, the error in the measurement was 100%. The first convincing proof came in a study of thin helium films done by Sabisky and Anderson in 1972 [57] confirming Lifshitz theory within an accuracy of 1%.

The first modern accurate experiment between conductors was performed by Lamoreaux in 1997 [58] in which he used a torsional balance to measure the force between

a gold plated plane and a gold coated sphere. The measurements agreed with Lifshitz theory within an accuracy of 5%. However, recently Lamoreaux had expressed more conservative estimates about the error [59]. In following years Mohideen *et al* [60, 61, 62] did experiments on the same configuration using atomic force microscopy. They claimed accuracy of within 5% with theory. Other groups have claimed similar precision [63]. In 2002, Bressi *et al* [64] performed the experiment for measuring the Casimir force between parallel metallic surface and claimed a precision of 15%. The Purdue group led by Decca has carried out several experiments using a micro-mechanical oscillator for measurement of the Casimir force at small separation distance [65, 66, 67, 68, 69]. These measurements are claimed to be so precise that they could put constraints on extra dimensions at short distances. They have also tested the low temperature thermal effects, which are still controversial as shown recently by another experiment and related discussions [68, 70, 71, 72].

Results for the parallel geometry were known exactly including the material properties and temperature correction while experiments struggled with keeping the surfaces parallel at such a small distance in early years. To avoid this, most of the experiments are done with one plane and other curved surface. These configurations until recently were studied using the proximity force approximation (PFA) developed by Derjaguin in 1934 [73]. PFA treats curved surfaces as made up of various parallel plates for which results are well known. This approximation works very well at small separation; however, its range of validity is debatable, specifically for the rough and corrugated surfaces. In the earlier experiments, reaching very small distances was also a major difficulty. In the last few years exact numerical techniques have been developed [74, 75], which can be applied to various geometries, for evaluating the Casimir energy and force. These results have been compared with the recent

experiments [76, 2].

1.4 Summary

The field of Casimir physics is currently a very active field. Considerable advances are achieved in both theoretical and experimental regimes [77]. These have, on the one hand, helped in improving our understanding of the behavior of the vacuum in presence of separate bodies and their material properties and to some extent of thermal effects. On the other hand they have generated more fundamental questions like the different forms of divergences arising due to the presence of the boundaries, coupling of the vacuum field to gravity, the attractive or repulsive nature of the Casimir energy, which model best describes the thermal behavior of the vacuum, or whether considering the Casimir effect as an effect of the zero point fluctuations is correct. Since the Casimir effect involves macroscopic bodies at large separation distances relative to the atomic distances most of the predictions based on material properties, geometry and thermal effects can be tested by current experiments. The purpose of this short sketchy review was to expose the reader to this field of open questions. The most up-to-date current status of the research done in this field can be found in [2, 44], which can direct the reader to the rich and diverse nature of research being done in this field.

Chapter 2

Mathematical foundations

The presence of boundaries, which restricts the fields, causes vacuum polarization. Any non-trivial space-time topology can cause similar effects. These restrictions manifest themselves as the Casimir effect, whereby the boundaries experience a force due to a change in the energy of the vacuum. To calculate the vacuum energy we treat the boundaries or the other restrictive conditions as classical backgrounds, which impose boundary conditions on the solution of the vacuum field equations. Alternatively, we can incorporate the classical background in the Lagrangian of the system as a classical potential, which automatically includes the boundary conditions in the field equation. There are several ways for evaluating the vacuum energy, for example, mode summation method, cylinder kernel expansion, Green's function approach, and worldline technique. Chapter 1 introduced a simple example calculation using the zeta-function regularization process. In this thesis, however, we will confine ourselves to the Green's function approach. In this Chapter, we present the derivation of the vacuum energy in terms of the Green's dyadic using standard field theory techniques. For the case of interaction between two separate rigid bodies the divergent terms can

be subtracted out from the onset thereby defining a finite interaction energy using the multiple scattering formalism, which we present next in the chapter. Following that we present the procedure for solving for the Green's dyadic.

2.1 Vacuum energy

2.1.1 Electromagnetic case

We start by assuming that space is filled with the electromagnetic field, which is interacting with background macroscopic dielectric bodies. The action is

$$W[\mathbf{E},\mathbf{H},\mathbf{A},\phi;\mathbf{P},\varepsilon,\mu] = \int d^3x \int dt\, \mathcal{L}(\mathbf{E},\mathbf{H},\mathbf{A},\phi;\mathbf{P},\varepsilon,\mu). \tag{2.1}$$

where ϕ is the scalar potential, $\mathbf{A}$ is the vector potential, $\mathbf{E}$ is the electric field, $\mathbf{H}$ is the magnetic field, $\mathbf{P}$ is the external polarization source, ε is the dielectric function, and μ is the dielectric permittivity. We shall neglect the dynamics (time dependence) of the dielectric bodies at the macroscopic level–for example we do not consider moving dielectrics. This still leaves us with two other venues for time dependence. First is the motion at the microscopic level of electrons and nuclei forming the dielectric body. This motion collectively contributes to the conductivity of a dielectric body, which will be one of the parameters in our study. The second form of time dependence is in the duration of the time for which a particular process is being investigated, which is introduced as the limits of integration of the time in Eq. (2.1). For most purposes it is sufficient to assume this time interval to be large enough to be replaced by $\pm\infty$. However, in the early 19th century while proposing a model for conductivity in metals, Sommerfeld studied the signal velocity in a dispersive medium, and in a

study of signal velocity in the wave propagation and its consequence on causality, Brillouin at Sommerfeld's suggestion in 1913, noticed the necessity to keep track of this formal fallacy of infinite time interval [78]. In general this needs to be taken into account primarily in relation to questions related to causality, and Nernst's heat theorem, which states that change in entropy of a system should approach zero at zero temperature.

The dielectric function codes the response of the system, as induced polarization, in the presence of an electric field. This effect should be causal and requires the time dependence in the construct $[\varepsilon \mathbf{E}]$ to be of the form

$$[\varepsilon \mathbf{E}](t) = \int_{-\infty}^{t} dt' \, \varepsilon(t - t') \mathbf{E}(t'), \tag{2.2}$$

where we suppressed the spatial dependence. The above statement of causality translates non-trivially into the frequency domain [79]. Nevertheless, we shall find it convenient to work in the frequency domain because our discussions will be restricted to static situations. This is achieved using the Fourier transform

$$f(t) = \int_{-\infty}^{\infty} \frac{d\omega}{2\pi} \, e^{-i\omega t} \tilde{f}(\omega) \tag{2.3}$$

written here for an arbitrary function of time, $f(t)$. We shall often drop the tilde in the Fourier transformed function.

The Fourier transformed action is

$$W[\mathbf{E}, \mathbf{H}, \mathbf{A}, \phi] = \int d^3x \int \frac{d\omega}{2\pi} \, \mathcal{L}(\mathbf{E}, \mathbf{H}, \mathbf{A}, \phi), \tag{2.4}$$

where the Fourier transformed Lagrangian density is

$$\begin{aligned}\mathcal{L}(\mathbf{E},\mathbf{H},\mathbf{A},\phi)=&\frac{1}{2}\mathbf{H}(\mathbf{x},-\omega)\cdot\mu(\mathbf{x},\omega)\mathbf{H}(\mathbf{x},\omega)-\frac{1}{2}\mathbf{E}(\mathbf{x},-\omega)\cdot\varepsilon(\mathbf{x},\omega)\mathbf{E}(\mathbf{x},\omega)\\&+\mathbf{E}(\mathbf{x},-\omega)\cdot\varepsilon(\mathbf{x},\omega)\Big[-\boldsymbol{\nabla}\phi(\mathbf{x},\omega)+i\omega\mathbf{A}(\mathbf{x},\omega))\Big]\\&-\mathbf{H}(\mathbf{x},-\omega)\cdot(\boldsymbol{\nabla}\times\mathbf{A}(\mathbf{x},\omega))+\mathbf{P}(\mathbf{x},-\omega)\cdot\Big[-\boldsymbol{\nabla}\phi(\mathbf{x},\omega)+i\omega\mathbf{A}(\mathbf{x},\omega)\Big],\end{aligned}\tag{2.5}$$

Using the least action principle we obtain

$$\begin{aligned}\delta\mathbf{H}:&\quad\mathbf{B}(\mathbf{x},\omega)=\boldsymbol{\nabla}\times\mathbf{A}(\mathbf{x},\omega),\\\delta\mathbf{E}:&\quad\mathbf{E}(\mathbf{x},\omega)=-\boldsymbol{\nabla}\phi(\mathbf{x},\omega)+i\omega\mathbf{A}(\mathbf{x},\omega),\\\delta\mathbf{A}:&\quad\boldsymbol{\nabla}\times\mathbf{H}(\mathbf{x},\omega)=-i\omega\Big[[\varepsilon\mathbf{E}](\mathbf{x},\omega)+\mathbf{P}(\mathbf{x},\omega)\Big],\\\delta\phi:&\quad\boldsymbol{\nabla}\cdot\Big[[\varepsilon\mathbf{E}](\mathbf{x},\omega)+\mathbf{P}(\mathbf{x},\omega)\Big]=0.\end{aligned}\tag{2.6a}$$

Here $\mathbf{B}=\mu\mathbf{H}$. The homogeneous Maxwell's equations can be obtained by taking the curl of the electric field and the divergence of the magnetic field, which we list here for completeness.

$$\boldsymbol{\nabla}\times\mathbf{E}(\mathbf{x},\omega)=i\omega\mathbf{B}(\mathbf{x},\omega),\tag{2.7a}$$

$$\boldsymbol{\nabla}\cdot\mathbf{B}(\mathbf{x},\omega)=0,.\tag{2.7b}$$

In general, the medium could be anisotropic and magnetic in which case the dielectric permittivity and permeability will be tensors. In this thesis we focus on non-magnetic, linear, isotropic, dispersive medium where $\mu(\mathbf{x},\omega)=1$. The Maxwell's equations in

Eqs. (2.6a) and (2.7a), in the frequency domain are

$$\boldsymbol{\nabla} \times \mathbf{E}(\mathbf{x},\omega) = i\omega \mathbf{H}(\mathbf{x},\omega), \tag{2.8a}$$

$$\boldsymbol{\nabla} \times \mathbf{H}(\mathbf{x},\omega) = -i\omega \Big[\varepsilon(\mathbf{x},\omega)\mathbf{E}(\mathbf{x},\omega) + \mathbf{P}(\mathbf{x},\omega) \Big]. \tag{2.8b}$$

Divergence of Eqs. (2.8a) and (2.8b) corresponds to Eqs. (2.7b) and (2.6a) in the frequency domain. Using Eq. (2.8a) in Eq. (2.8b) we have

$$-\Big[\boldsymbol{\nabla} \times \boldsymbol{\nabla} \times \ -\omega^2 \varepsilon(\mathbf{x},\omega)\mathbf{1} \Big] \cdot \mathbf{E}(\mathbf{x},\omega) = -\omega^2 \mathbf{P}(\mathbf{x},\omega). \tag{2.9}$$

Eq. (2.9) guides us to define the electric Green's dyadic satisfying the differential equation

$$-\left[-\frac{1}{\omega^2} \boldsymbol{\nabla} \times \boldsymbol{\nabla} \times \ +\varepsilon(\mathbf{x},\omega)\mathbf{1} \right] \cdot \boldsymbol{\Gamma}(\mathbf{x},\mathbf{x}';\omega) = \mathbf{1}\delta^{(3)}(\mathbf{x}-\mathbf{x}'), \tag{2.10}$$

and also defines the relation between the electric field and polarization source, mediated through the electric Green's dyadic $\boldsymbol{\Gamma}(\mathbf{x},\mathbf{x}';\omega)$,

$$\mathbf{E}(\mathbf{x},\omega) = \int d^3x' \, \boldsymbol{\Gamma}(\mathbf{x},\mathbf{x}';\omega) \cdot \mathbf{P}(\mathbf{x}',\omega). \tag{2.11}$$

To derive the vacuum energy we start with the action $W[\mathbf{E},\mathbf{H},\mathbf{A},\phi;\mathbf{P}]$,where it is a functional of $\mathbf{E},\mathbf{H},\mathbf{A},\phi$, and $\mathbf{P}$. The vacuum persistence amplitude is defined by

$$Z[\mathbf{P}] = \langle 0_+ | 0_- \rangle^{\mathbf{P}}. \tag{2.12}$$

We use Schwinger's quantum action principle [80, 81, 82, 83, 84, 85, 86]

$$\delta Z = i\langle 0_+|\delta W[\mathbf{E},\mathbf{H},\mathbf{A},\phi;\mathbf{P}]|0_-\rangle, \tag{2.13}$$

whose variation with the fields $\mathbf{E},\mathbf{H},\mathbf{A}$, and ϕ reproduces the equations of motion given in Eq. (2.7) is interpreted as referring to the operator fields now. Variation with respect to the external source $\mathbf{P}$ gives us

$$\delta\mathbf{P}: \qquad \delta Z = i\int d^3x \int \frac{d\omega}{2\pi}\,\delta\mathbf{P}(\mathbf{x},-\omega)\,\langle 0_+|\mathbf{E}(\mathbf{x},\omega)|0_-\rangle^{\mathbf{P}}, \tag{2.14}$$

which implies

$$\frac{1}{i}\frac{\delta Z[\mathbf{P}]}{\delta\mathbf{P}(\mathbf{x},-\omega)} = \langle 0_+|\mathbf{E}(\mathbf{x},\omega)|0_-\rangle^{\mathbf{P}}. \tag{2.15}$$

Using this in Eq. (2.9) we can write

$$-\left[-\frac{1}{\omega^2}\boldsymbol{\nabla}\times\boldsymbol{\nabla}\times\ +\varepsilon(\mathbf{x},\omega)\mathbf{1}\right]\cdot\frac{1}{Z[\mathbf{P}]}\frac{1}{i}\frac{\delta Z[\mathbf{P}]}{\delta\mathbf{P}(\mathbf{x},-\omega)} = \mathbf{P}(\mathbf{x},\omega). \tag{2.16}$$

Notice that operator is $\boldsymbol{\Gamma}^{-1}$ given in Eq. (2.10). So we can write the vacuum expectation value of $\mathbf{E}$ given by Eq. (2.16) using above equation as

$$\frac{1}{Z[\mathbf{P}]}\frac{1}{i}\frac{\delta Z[\mathbf{P}]}{\delta\mathbf{P}(\mathbf{x},-\omega)} = \int d^3x\,\boldsymbol{\Gamma}(\mathbf{x},\mathbf{x}';\omega)\cdot\mathbf{P}(\mathbf{x}',\omega)\,. \tag{2.17}$$

We can solve this functional differential equation for $Z[\mathbf{P}]$. One possible solution is

$$Z[\mathbf{P}] = Z[0]e^{\frac{i}{2}\int\frac{d\omega}{2\pi}\int d^3x\int d^3x'\mathbf{P}(\mathbf{x},-\omega)\cdot\boldsymbol{\Gamma}(\mathbf{x},\mathbf{x}';\omega)\cdot\mathbf{P}(\mathbf{x}',\omega)+Q[\varepsilon]}, \tag{2.18}$$

where $Q[\varepsilon]$ is a constant in $\mathbf{P}$. The argument of the exponential in the above equation

is defined as the effective action $W\Big[\mathbf{P}\Big]$. In absence of the background potential, i.e. for $\varepsilon = 1$, the effective action is given by

$$W_0[\mathbf{P}] = \frac{1}{2}\int \frac{d\omega}{2\pi}\int d^3x \int d^3x'\, \mathbf{P}(\mathbf{x},-\omega)\cdot\mathbf{\Gamma}_0(\mathbf{x},\mathbf{x}';\omega)\cdot\mathbf{P}(\mathbf{x}',\omega) \;+\; Q[1], \qquad (2.19)$$

where, $\mathbf{\Gamma}_0(\mathbf{x},\mathbf{x}';\omega)$ is the free Green's dyadic when no boundary is present and it satisfies

$$-\left[-\frac{1}{\omega^2}\boldsymbol{\nabla}\times\boldsymbol{\nabla}\times\;+\mathbf{1}\right]\cdot\mathbf{\Gamma}_0(\mathbf{x},\mathbf{x}';\omega) = \mathbf{1}\delta^{(3)}(\mathbf{x}-\mathbf{x}'). \qquad (2.20)$$

Next if we switch off the external source as well then vacuum does not decay and can be written in terms of a constant phase θ

$$Z_0[0] = \langle 0_+|0_-\rangle^{\mathbf{P}=0} = e^{i\theta} = e^{W_0[0]}. \qquad (2.21)$$

This implies that $Q[1] = \theta$, which is a pure constant. Varying the vacuum persistence amplitude with respect to the background potential parameter $\varepsilon(\mathbf{x},\omega)$ we get

$$\begin{aligned}\delta\varepsilon(\mathbf{x},\omega):\quad \delta Z[\mathbf{P}] &= \frac{i}{2}\int\frac{d\omega}{2\pi}\int d^3x\,\delta\varepsilon(\mathbf{x},-\omega)\langle 0_+|\mathbf{E}(\mathbf{x},-\omega)\cdot\mathbf{E}(\mathbf{x},\omega)|0_-\rangle^{\mathbf{P}} \\ &= \frac{i}{2}\int\frac{d\omega}{2\pi}\int d^3x\,\delta\varepsilon(\mathbf{x},-\omega)\frac{1}{i}\frac{\delta}{\delta\mathbf{P}(\mathbf{x},\omega)}\frac{1}{i}\frac{\delta}{\delta\mathbf{P}(\mathbf{x},-\omega)}Z[\mathbf{P}]. \qquad (2.22)\end{aligned}$$

We can formally write the solution for this as

$$Z[\mathbf{P}] = e^{\frac{i}{2}\int\frac{d\omega}{2\pi}\int d^3x[\varepsilon(\mathbf{x},-\omega)-1]\frac{1}{i}\frac{\delta}{\delta\mathbf{P}(\mathbf{x},\omega)}\frac{1}{i}\frac{\delta}{\delta\mathbf{P}(\mathbf{x},-\omega)}}\,Z_0[\mathbf{P}], \qquad (2.23)$$

which using Eq. (2.19) can be written as

$$Z[\mathbf{P}] = e^{\frac{i}{2}\int \frac{d\omega}{2\pi}\int d^3x[\varepsilon(\mathbf{x},-\omega)-1]\frac{1}{i}\frac{\delta}{\delta\mathbf{P}(\mathbf{x},\omega)}\frac{1}{i}\frac{\delta}{\delta\mathbf{P}(\mathbf{x},-\omega)}} e^{\frac{i}{2}\int \frac{d\omega}{2\pi}\int d^3x\int d^3x'\mathbf{P}(\mathbf{x},-\omega)\cdot\mathbf{\Gamma}_0(\mathbf{x},\mathbf{x}',\omega)\cdot\mathbf{P}(\mathbf{x}',\omega)+Q[1]}. \tag{2.24}$$

Notice that we can safely drop the term $Q[1]$ as it will not contribute to the solution. Using the exponential identity

$$e^{\frac{1}{2}\nabla^{\mathrm{T}}\cdot\mathbf{A}\cdot\nabla} e^{\frac{1}{2}\mathbf{x}^{\mathrm{T}}\cdot\mathbf{B}\cdot\mathbf{x}+\mathbf{c}^{\mathrm{T}}\cdot\mathbf{x}+r} = e^{\frac{1}{2}\mathbf{x}^{\mathrm{T}}\cdot\mathbf{B}\cdot\mathbf{K}\cdot\mathbf{x}+\mathbf{c}^{\mathrm{T}}\cdot\mathbf{K}\cdot\mathbf{x}+\frac{\mathbf{1}}{\mathbf{2}}\mathbf{c}^{\mathrm{T}}\cdot\mathbf{K}\cdot\mathbf{A}\cdot\mathbf{c}+r+\frac{1}{2}\mathrm{Tr}\ln\mathbf{K}}, \tag{2.25}$$

for matrices where $\mathbf{K}$ is the solution to the matrix equation

$$\Big[\mathbf{1}-\mathbf{A}\cdot\mathbf{B}\Big]\cdot\mathbf{K}=\mathbf{1}, \tag{2.26}$$

we conclude that

$$Z[\mathbf{P}] = e^{\frac{i}{2}\int \frac{d\omega}{2\pi}\int d^3x\int d^3x'\mathbf{P}(\mathbf{x},-\omega)\cdot\mathbf{\Gamma}(\mathbf{x},\mathbf{x}';\omega)\cdot\mathbf{P}(\mathbf{x}',\omega)+2\pi\delta(0)\frac{i}{2}\int\frac{d\omega}{2\pi}\mathrm{Tr}\ln\mathbf{\Gamma}\mathbf{\Gamma_0}^{-1}}, \tag{2.27}$$

where we have used Green's dyadic equation to obtain this final form. The trace is over space variables only. Trace over the frequency domain leads to $2\pi\delta(0)$ which will be interpreted as the infinite time τ of the process. For $Z[0]$ we get

$$Z[0] = \langle 0_+|0_-\rangle^{\mathbf{P}=0} = e^{iW[0]} = e^{\tau\frac{1}{2}\int\frac{d\omega}{2\pi}\mathrm{Tr}\ln\mathbf{\Gamma}\mathbf{\Gamma_0}^{-1}}. \tag{2.28}$$

Since $\langle 0_+|0_-\rangle^{\mathbf{P}=0} = \langle 0_-|e^{-iH\tau}|0_-\rangle^{\mathbf{P}=0} = e^{-iE\tau}$, comparing with above equation we conclude that

$$E = \frac{i}{2}\int\frac{d\omega}{2\pi}\mathrm{Tr}\ln\mathbf{\Gamma}\mathbf{\Gamma}_0^{-1}. \tag{2.29}$$

This is the principal formula we will use for calculating the Casimir energy. It is worth noting that the total vacuum energy is given by the trace-log of the electric Green's dyadic only. While in the frequency domain, we place confidence in the so-called Euclidean postulate [87, 88], and switch to imaginary frequencies after a Euclidean rotation using $\omega \to i\zeta$. Correspondingly the dielectric function will be: $\varepsilon(\mathbf{x}, \omega) \to \varepsilon(\mathbf{x}, i\zeta)$. This leads to

$$E = -\frac{1}{2}\int \frac{d\zeta}{2\pi} \mathrm{Tr} \ln \mathbf{\Gamma}\mathbf{\Gamma}_0^{-1}. \tag{2.30}$$

2.1.2 Scalar case

We list the corresponding formula when the vacuum is assumed to be filled by single scalar field $\phi(x)$ without derivation. The scalar field interacting with a background potential is described by the Lagrangian

$$\mathcal{L}(\phi(x)) = -\frac{1}{2}(\partial_\mu \phi(x))^2 - \frac{1}{2}V(x)\phi(x)^2 \tag{2.31}$$

The vacuum energy can be written as

$$E = \frac{i}{2\tau} \mathrm{Tr} \ln G\, G_0^{-1}, \tag{2.32}$$

where $G(x, x')$ is the scalar Green's function in the presence of the boundary, which satisfies

$$-\Big[\partial^2 - V(x)\Big] G(x, x') = \delta^{(4)}(x - x'), \tag{2.33}$$

and $G_0(x, x')$ is the free scalar Green's function, which obeys

$$-\partial^2 G_0(x, x') = \delta^{(4)}(x - x'), \tag{2.34}$$

2.2 Multiple scattering formalism

The energy calculated using the formula given by Eq. (2.30) is divergent. These divergences arise due to the bulk contribution, self energy of the background potential, and curvature and corners of the boundaries. We require regularization and renormalization procedures to obtain a finite expression. However, in the presence of two non-overlapping boundaries it is possible to extract a finite energy for the interaction between two rigid boundaries using the multiple scattering (MS) formalism, which is all we need to define the Casimir force experienced by the boundaries. Multiple scattering techniques have been in use for a very long time (see introduction of [89] for a brief review of MS techniques). Notice that in Eq. (2.30) we have already subtracted the infinite bulk contribution given by

$$E_0 = -\frac{1}{2}\int \frac{d\zeta}{2\pi} \mathrm{Tr} \ln \mathbf{\Gamma}_0. \tag{2.35}$$

The free Green's dyadic $\mathbf{\Gamma}_0(\mathbf{x}, \mathbf{x}'; i\zeta)$ satisfies Eq. (2.20). Comparing Eqs. (2.10) and (2.20), it is suggestive to define a potential

$$\mathbf{V}(\mathbf{x}, i\zeta) = \mathbf{1}\Big[\varepsilon(\mathbf{x}, i\zeta) - 1\Big] \tag{2.36}$$

to rewrite Eq. (2.10) in the form

$$-\left[\frac{1}{\zeta^2}\boldsymbol{\nabla}\times\boldsymbol{\nabla}\times\ +\mathbf{1}+\mathbf{V}(\mathbf{x},i\zeta)\right]\cdot\boldsymbol{\Gamma}(\mathbf{x},\mathbf{x}';i\zeta)=\mathbf{1}\delta^{(3)}(\mathbf{x}-\mathbf{x}'). \tag{2.37}$$

This allows us to write the solution (in symbolic notation) for the Green's dyadic in the presence of a medium in terms of the free Green's dyadic, defined in Eq. (2.20) in the form

$$\boldsymbol{\Gamma}\cdot\boldsymbol{\Gamma}_0^{-1}=\Big[\mathbf{1}-\boldsymbol{\Gamma}_0\cdot\mathbf{V}\Big]^{-1}. \tag{2.38}$$

For a system described by two disjoint boundaries, the potential is given by

$$\mathbf{V}=\mathbf{V}_1+\mathbf{V}_2. \tag{2.39}$$

Using this in Eq. (2.38) we can write

$$\begin{aligned}\boldsymbol{\Gamma}\cdot\boldsymbol{\Gamma}_0^{-1}=&\boldsymbol{\Gamma}_2\cdot\boldsymbol{\Gamma}_0^{-1}\Big[\mathbf{1}-\boldsymbol{\Gamma}_1\cdot\mathbf{V}_1\cdot\boldsymbol{\Gamma}_2\cdot\mathbf{V}_2\Big]\boldsymbol{\Gamma}_1\cdot\boldsymbol{\Gamma}_0^{-1}\\ =&\Big[\mathbf{1}-\boldsymbol{\Gamma}_0\cdot\mathbf{V}_2\Big]^{-1}\Big[\mathbf{1}-\boldsymbol{\Gamma}_1\cdot\mathbf{V}_1\cdot\boldsymbol{\Gamma}_2\cdot\mathbf{V}_2\Big]\Big[\mathbf{1}-\boldsymbol{\Gamma}_0\cdot\mathbf{V}_1\Big]^{-1}.\end{aligned} \tag{2.40}$$

Substituting this in Eq. (2.30) we get

$$E=E_1+E_2+E_{12}, \tag{2.41}$$

where the self energy contributions of the individual potentials E_i are given by

$$E_i=-\frac{1}{2}\int\frac{d\zeta}{2\pi}\mathrm{Tr}\ln\Big[\mathbf{1}-\boldsymbol{\Gamma}_0\cdot\mathbf{V}_i\Big]^{-1},\qquad i=1,2, \tag{2.42}$$

which in general are divergent. The remaining part of the energy is the interaction term E_{12} between two disjoint boundaries and is given by

$$E_{12} = \frac{1}{2}\int \frac{d\zeta}{2\pi} \mathrm{Tr} \ln \Big[\mathbf{1} - \mathbf{\Gamma}_1 \cdot \mathbf{V}_1 \cdot \mathbf{\Gamma}_2 \cdot \mathbf{V}_2\Big]. \tag{2.43}$$

V_i refers to the potential describing single boundary and $\mathbf{\Gamma}_i$ refers to the Green's dyadic when only one boundary is present. It is written in terms of the free Green's dyadic as

$$\mathbf{\Gamma}_i = \Big[\mathbf{1} - \mathbf{\Gamma}_0 \cdot \mathbf{V}_i\Big]^{-1} \mathbf{\Gamma}_0. \tag{2.44}$$

We can define the $\mathbf{T}$-matrix as

$$\mathbf{T}_i = \mathbf{V}_i \Big[\mathbf{1} - \mathbf{\Gamma}_0 \cdot \mathbf{V}_i\Big]^{-1}, \tag{2.45}$$

The interaction energy can be written in terms of $\mathbf{T}$-matrix as

$$E_{12} = \frac{1}{2}\int \frac{d\zeta}{2\pi} \mathrm{Tr} \ln \Big[\mathbf{1} - \mathbf{\Gamma}_0 \cdot \mathbf{T}_1 \cdot \mathbf{\Gamma}_0 \cdot \mathbf{T}_2\Big]. \tag{2.46}$$

The two expressions of the interaction energy given by Eq. (2.43) and Eq. (2.46) are equivalent. It is interesting to pause and think about the two forms. The Green's dyadic $\mathbf{\Gamma}_i$ describes the electromagnetic propagator in presence of the i-th boundary, which according to Eq. (2.44) is essentially the modification of the free propagator $\mathbf{\Gamma}_0$ due to the existing boundary. These modified propagators mediate between the two boundaries $\mathbf{V}_1$ and $\mathbf{V}_2$ causing interaction. On the other hand, the $\mathbf{T}_i$-matrix describes the modification of the potential $\mathbf{V}_i$ due to its own fluctuations. The information from one boundary is mediated to other boundary by free propagators causing

interaction. The former approach is what describes the fluctuating fields interacting with static bodies viewpoint as mentioned in Section 1.1.2, while the later approach describes the interaction of the fluctuating bodies (molecules) viewpoint presented in Section 1.1.1.

In this thesis we will be considering the two disjoint background potentials and use Eq. (2.43) form of the interaction energy for evaluation of the Casimir energy. Writing out the explicit space dependence we have

$$E_{12} = \frac{1}{2}\int_{-\infty}^{\infty}\frac{d\zeta}{2\pi}\int d^3x\,\mathrm{tr}\ln\Big[\mathbf{1} - \mathbf{\Gamma}_1(\mathbf{x},\mathbf{x}')\cdot\mathbf{V}_1(\mathbf{x}')\cdot\mathbf{\Gamma}_2(\mathbf{x}',\mathbf{x})\cdot\mathbf{V}_2(\mathbf{x})\Big], \tag{2.47}$$

where trace is now only on the dyadic indices. This allows us to subtract off the divergent bulk contribution as well as the self energy contributions from the individual potential from the onset.

2.3 Green's dyadic

In the previous section we obtained the central formula given by Eq. (2.30) for evaluating the vacuum energy, which requires us to solve for the corresponding Green's dyadic for a given system. The Green's dyadic, as the name suggests, is a second rank tensor quantity having nine scalar components, which are coupled. The formal Green's function technique can be found in standard mathematical texts, for example, Chapter 7 of Morse and Feshbach [90]. This thesis concentrates on parallel plate geometry for the electromagnetic case and cylindrical geometry for the scalar case. Therefore, in this Section we outline the procedure for obtaining Green's dyadic for the parallel geometry. We will present the scalar Green's function for the cylindrical

case in the next chapter.

2.3.1 Free Green's dyadic

We start with the free Green's dyadic $\mathbf{\Gamma}_0$ that satisfies Eq. (2.20). Taking the divergence of Eq. (2.20) we have

$$\boldsymbol{\nabla} \cdot \mathbf{\Gamma}_0(\mathbf{x}, \mathbf{x}'; i\zeta) = \boldsymbol{\nabla} \delta^{(3)}(\mathbf{x} - \mathbf{x}'). \tag{2.48}$$

Using this in conjunction with the identity

$$\boldsymbol{\nabla} \times (\boldsymbol{\nabla} \times \mathbf{\Gamma}_0) = (\boldsymbol{\nabla}\boldsymbol{\nabla} - \mathbf{1}\nabla^2) \cdot \mathbf{\Gamma}_0, \tag{2.49}$$

we can write Eq. (2.20) as

$$-[\nabla^2 - \zeta^2]\mathbf{\Gamma}_0(\mathbf{x}, \mathbf{x}'; i\zeta) = -\zeta^2 \mathbf{1} \delta^{(3)}(\mathbf{x} - \mathbf{x}') + \boldsymbol{\nabla}\boldsymbol{\nabla} \delta^{(3)}(\mathbf{x} - \mathbf{x}'). \tag{2.50}$$

Consider the scalar Green's function G_0, which satisfies Eq. (2.34). In the frequency space that equation can be written as

$$-[\nabla^2 - \zeta^2] G_0(\mathbf{x}, \mathbf{x}'; i\zeta) = \delta^{(3)}(\mathbf{x} - \mathbf{x}'). \tag{2.51}$$

The free Green's dyadic now has the formal solution in terms of free Green's scalar as

$$\mathbf{\Gamma}_0(\mathbf{x}, \mathbf{x}'; i\zeta) = [\boldsymbol{\nabla}\boldsymbol{\nabla} - \zeta^2 \mathbf{1}] G_0(\mathbf{x}, \mathbf{x}'; i\zeta). \tag{2.52}$$

We will write an explicit form for this in the next chapter.

2.3.2 Green's dyadic equations

Next we turn our attention to the general Green's dyadic in in the presence of restrictive boundaries. For a non-magnetic, linear, isotropic, dispersive medium we wrote the differential equation satisfied by $\mathbf{\Gamma}$ in Eq. (2.37)

$$-\left[\frac{1}{\zeta^2}\boldsymbol{\nabla}\times\boldsymbol{\nabla}\times\ +\mathbf{1}+\mathbf{V}(\mathbf{x},i\zeta)\right]\cdot\mathbf{\Gamma}(\mathbf{x},\mathbf{x}';i\zeta)=\mathbf{1}\delta^{(3)}(\mathbf{x}-\mathbf{x}'), \tag{2.53}$$

which is related to the electric field and the polarization source as

$$\mathbf{E}(\mathbf{x},i\zeta)=\int d^3x'\,\mathbf{\Gamma}(\mathbf{x},\mathbf{x}';i\zeta)\cdot\mathbf{P}(\mathbf{x}',i\zeta). \tag{2.54}$$

Eq. (2.53) is a second order differential equation coupling the scalar components of the Green's dyadic. Using the free Green's dyadic Eq. (2.20) we can formally write the solution for the Green's dyadic as given in Eq. (2.44)

$$\mathbf{\Gamma}=\left[\mathbf{1}-\mathbf{\Gamma}_0\cdot\mathbf{V}\right]^{-1}\mathbf{\Gamma}_0. \tag{2.55}$$

This can be written as an infinite series and getting an explicit solution for the Green's dyadic depends on the potential describing the boundary and in turn on the boundary conditions imposed by it. As it turns out, it is not a trivial task. Even for the simple case of a step function potential re-summing the series is very difficult. In order to proceed further and keeping our goal of solving for the parallel geometry in mind we use technique given in [91] and define the corresponding magnetic Green's dyadic $\mathbf{\Phi}(\mathbf{x},\mathbf{x}';i\zeta)$

$$\mathbf{H}(\mathbf{x},i\zeta)=\int d^3x'\,\mathbf{\Phi}(\mathbf{x},\mathbf{x}';i\zeta)\cdot\mathbf{P}(\mathbf{x}',i\zeta). \tag{2.56}$$

In terms of the electric and magnetic Green's dyadic, defined in Eqs. (2.54) and (2.56), the Maxwell's equations given by Eqs. (2.8) are contained in

$$-\boldsymbol{\nabla} \times \boldsymbol{\Gamma}(\mathbf{x}, \mathbf{x}'; i\zeta) = \zeta \boldsymbol{\Phi}(\mathbf{x}, \mathbf{x}'; i\zeta), \tag{2.57a}$$

$$\boldsymbol{\nabla} \times \boldsymbol{\Phi}(\mathbf{x}, \mathbf{x}'; i\zeta) = \zeta \Big[\varepsilon(\mathbf{x}, i\zeta) \boldsymbol{\Gamma}(\mathbf{x}, \mathbf{x}'; i\zeta) + \mathbf{1} \delta^{(3)}(\mathbf{x} - \mathbf{x}') \Big]. \tag{2.57b}$$

This is illustrated by taking the dot-product of Eqs. (2.57) with $\mathbf{P}$ on the right and taking the integral over x', which reproduces the expressions in Eqs. (2.8). The homogeneous equations given by Eq. (2.7) can be obtained, similarly, by taking divergence from the left. Using Eq. (2.57a) in Eq. (2.57b) gives the second order differential equation for the Green's dyadic given in Eq. (2.10). The above equations are coupled first order differential equations. This doesn't reduce the amount of work; however, it provides a framework for solving the Green's dyadic for the case of a step potential (parallel geometry) as we shall see in next section.

2.4 Solution to the Green's dyadic for translationally symmetric potential in $x - y$ directions

Consider the physical situations involving translational symmetry in the x-y directions. We begin by writing the Green's dyadic and the unit operator in terms of basis vectors

$$\boldsymbol{\Gamma} = \boldsymbol{\Gamma}_x \hat{\mathbf{x}} + \boldsymbol{\Gamma}_y \hat{\mathbf{y}} + \boldsymbol{\Gamma}_z \hat{\mathbf{z}}, \tag{2.58a}$$

$$\boldsymbol{\Phi} = \boldsymbol{\Phi}_x \hat{\mathbf{x}} + \boldsymbol{\Phi}_y \hat{\mathbf{y}} + \boldsymbol{\Phi}_z \hat{\mathbf{z}}, \tag{2.58b}$$

$$\mathbf{1} = \hat{\mathbf{x}}\,\hat{\mathbf{x}} + \hat{\mathbf{y}}\,\hat{\mathbf{y}} + \hat{\mathbf{z}}\,\hat{\mathbf{z}}. \tag{2.58c}$$

In this case the potential given by Eq. (2.36) depends on the z-coordinate

$$V(z) = [\varepsilon(z) - 1]. \tag{2.59}$$

Using a Fourier transform in x-y directions we can define the dimensionally reduced dyadic

$$\mathbf{\Gamma}(\mathbf{x}, \mathbf{x}'; i\zeta) = \int \frac{d^2k}{(2\pi)^2}\, e^{i\mathbf{k}_\perp \cdot (\mathbf{x}-\mathbf{x}')_\perp} \boldsymbol{\gamma}(z, z'; i\zeta, k), \tag{2.60a}$$

$$\mathbf{\Phi}(\mathbf{x}, \mathbf{x}'; i\zeta) = \int \frac{d^2k}{(2\pi)^2}\, e^{i\mathbf{k}_\perp \cdot (\mathbf{x}-\mathbf{x}')_\perp} \boldsymbol{\phi}(z, z'; i\zeta, k), \tag{2.60b}$$

where $\mathbf{k}_\perp^2 = k_x^2 + k_y^2 = k^2$. Due to rotational symmetry in the x-y directions we can choose $k_y = 0, k_x = k$, without any loss of generality. Using Eqs. (2.58) and (2.60) in Eq. (2.57) we have

$$\boldsymbol{\phi}_x = \frac{1}{\zeta}\frac{\partial}{\partial z}\boldsymbol{\gamma}_y, \tag{2.61a}$$

$$\boldsymbol{\phi}_y = -\frac{1}{\zeta}\frac{\partial}{\partial z}\boldsymbol{\gamma}_x + i\frac{k}{\zeta}\boldsymbol{\gamma}_z, \tag{2.61b}$$

$$\boldsymbol{\phi}_z = -i\frac{k}{\zeta}\boldsymbol{\gamma}_y. \tag{2.61c}$$

and

$$\boldsymbol{\gamma}_x = \frac{1}{\zeta}\frac{1}{\varepsilon(z)}\frac{\partial}{\partial z}\boldsymbol{\phi}_y - \frac{\delta(z-z')}{\varepsilon(z)}\hat{\mathbf{x}}, \tag{2.62a}$$

$$\boldsymbol{\gamma}_y = \frac{1}{\zeta}\frac{1}{\varepsilon(z)}\frac{\partial}{\partial z}\boldsymbol{\phi}_x - i\frac{k}{\zeta}\frac{1}{\varepsilon(z)}\boldsymbol{\phi}_z - \frac{\delta(z-z')}{\varepsilon(z)}\hat{\mathbf{y}}, \tag{2.62b}$$

$$\boldsymbol{\gamma}_z = i\frac{k}{\zeta}\frac{1}{\varepsilon(z)}\boldsymbol{\phi}_y - \frac{\delta(z-z')}{\varepsilon(z)}\hat{\mathbf{z}}. \tag{2.62c}$$

Using Eqs. (2.61a) and (2.61c) in Eq. (2.62b) we obtain the differential equation for γ_y to be

$$-\left[\frac{\partial^2}{\partial z^2} - k^2 - \zeta^2\varepsilon(z)\right]\boldsymbol{\gamma}_y(z,z';i\zeta,k) = -\zeta^2\,\hat{\mathbf{y}}\,\delta(z-z'). \tag{2.63}$$

Similarly using Eqs. (2.62a) and (2.62c) in Eq. (2.61b) we have

$$-\left[\frac{\partial}{\partial z}\frac{1}{\varepsilon(z)}\frac{\partial}{\partial z} - \frac{k^2}{\varepsilon(z)} - \zeta^2\right]\boldsymbol{\phi}_y(z,z';i\zeta,k) = -i\hat{\mathbf{z}}\,\frac{k\zeta}{\varepsilon(z)}\delta(z-z') + \hat{\mathbf{x}}\,\frac{\zeta}{\varepsilon(z)}\frac{\partial}{\partial z}\delta(z-z'). \tag{2.64}$$

Let us now define reduced electric $g^E(z,z')$ and magnetic $g^H(z,z')$ scalar Green's functions[1] which satisfy

$$-\left[\frac{\partial^2}{\partial z^2} - k^2 - \zeta^2\varepsilon(z)\right]g^E(z,z') = \delta(z-z'), \tag{2.65a}$$

$$-\left[\frac{\partial}{\partial z}\frac{1}{\varepsilon(z)}\frac{\partial}{\partial z} - \frac{k^2}{\varepsilon(z)} - \zeta^2\right]g^H(z,z') = \delta(z-z'). \tag{2.65b}$$

It is now straightforward to obtain $\boldsymbol{\gamma}_y$ and $\boldsymbol{\phi}_y$ in terms of g^E and g^H as

$$\boldsymbol{\gamma}_y(z,z';i\zeta,k) = -\hat{\mathbf{y}}\zeta^2 g^E(z,z'), \tag{2.66a}$$

$$\boldsymbol{\phi}_y(z,z';i\zeta,k) = -i\hat{\mathbf{z}}\,\frac{k\zeta}{\varepsilon(z')}g^H(z,z') - \hat{\mathbf{x}}\,\frac{\zeta}{\varepsilon(z')}\frac{\partial}{\partial z'}g^H(z,z'), \tag{2.66b}$$

where we integrated by parts to obtain the second term in the ϕ_y expression. The remaining components are completely given in terms of $\boldsymbol{\gamma}_y$ and $\boldsymbol{\phi}_y$ as

$$\boldsymbol{\phi}_x = \frac{1}{\zeta}\frac{\partial}{\partial z}\boldsymbol{\gamma}_y, \tag{2.67}$$

$$\boldsymbol{\phi}_z = -i\frac{k}{\zeta}\boldsymbol{\gamma}_y, \tag{2.68}$$

[1]Here we use the notation in Schwinger*et al* [91], which was reversed in many of Milton's publications, for example in Milton's book [15] and [92].

and

$$\boldsymbol{\gamma}_x = -\frac{1}{\zeta}\frac{1}{\varepsilon(z)}\frac{\partial}{\partial z}\boldsymbol{\phi}_y - \hat{\mathbf{x}}\frac{\delta(z-z')}{\varepsilon(z)}, \tag{2.69}$$

$$\boldsymbol{\gamma}_z = i\frac{k}{\zeta}\frac{1}{\varepsilon(z)}\boldsymbol{\phi}_y - \hat{\mathbf{z}}\frac{\delta(z-z')}{\varepsilon(z)}. \tag{2.70}$$

Using the above the electric and magnetic Green's dyadic are given in terms of the reduced Green's function as

$$\boldsymbol{\phi}(z,z';i\zeta,k) = \begin{bmatrix} 0 & -\zeta\frac{\partial}{\partial z}g^E(z,z') & 0 \\ -\frac{\zeta}{\varepsilon(z')}\frac{\partial}{\partial z'}g^H(z,z') & 0 & -\frac{ik\zeta}{\varepsilon(z')}g^H(z,z') \\ 0 & ik\zeta g^E(z,z') & 0 \end{bmatrix} \tag{2.71}$$

and

$$\begin{aligned}\boldsymbol{\gamma}(z,z';i\zeta,k) = &\begin{bmatrix} \frac{1}{\varepsilon(z)}\frac{\partial}{\partial z}\frac{1}{\varepsilon(z')}\frac{\partial}{\partial z'}g^H(z,z') & 0 & \frac{ik}{\varepsilon(z)}\frac{1}{\varepsilon(z')}\frac{\partial}{\partial z}g^H(z,z') \\ 0 & -\zeta^2 g^E(z,z') & 0 \\ -\frac{ik}{\varepsilon(z)}\frac{1}{\varepsilon(z')}\frac{\partial}{\partial z'}g^H(z,z') & 0 & \frac{k^2}{\varepsilon(z)\varepsilon(z')}g^H(z,z') \end{bmatrix} \\ &- \frac{\delta(z-z')}{\varepsilon(z)}\begin{bmatrix} 1 & 0 & 0 \\ 0 & 0 & 0 \\ 0 & 0 & 1 \end{bmatrix}.\end{aligned} \tag{2.72}$$

Thus for the physical situations involving translational symmetry in x and y directions and non-magnetic, linear, isotropic, dispersive medium the whole problem decouples to solving for two scalar transverse electric and transverse magnetic Green's function, which are subject to the boundary conditions imposed by the physical problem.

Chapter 3

Scalar Green's functions

In the previous Chapter, Section 2.3, we presented the formal solution for the free Green's dyadic and the Green's dyadic in presence of a translationally symmetric background potential in terms of two free scalar Green's function. In this chapter we collect solutions to these scalar Green's function for the configurations we will be dealing in this thesis.

3.1 Free scalar Green's function

In absence of any boundary the free Green's function $G_0(\mathbf{x}, \mathbf{x}'; i\zeta)$, which satisfies Eq. (2.51) has translational symmetry in all coordinates. Therefore it can depend only on $(\mathbf{x} - \mathbf{x}')$. In three dimensions the explicit solution is given by

$$G_0(\mathbf{x} - \mathbf{x}'; i\zeta) = \frac{e^{-|\zeta||\mathbf{x}-\mathbf{x}'|}}{4\pi|\mathbf{x} - \mathbf{x}'|}. \tag{3.1}$$

If we assume translational invariance in one dimension then we can Fourier transform one coordinate and write

$$G_0(\mathbf{x}-\mathbf{x}';i\zeta) = \int \frac{dk_z}{2\pi} e^{ik_z(z-z')} g_0(\mathbf{x}_\perp - \mathbf{x}'_\perp;\kappa), \tag{3.2}$$

where κ is defined by $\kappa^2 = \zeta^2 + k_z^2$. Then the two dimensional reduced Green's function $g_0(\mathbf{x}_\perp - \mathbf{x}'_\perp;\kappa)$ is written in terms of the modified Bessel function K_0 as

$$g_0(\mathbf{x}_\perp - \mathbf{x}'_\perp;\kappa) = \frac{1}{2\pi} K_0(\kappa|(\mathbf{x}_\perp - \mathbf{x}'_\perp|). \tag{3.3}$$

We can go ahead and assume translation symmetry in x-y directions and write

$$G_0(\mathbf{x}-\mathbf{x}';i\zeta) = \int \frac{d^2k}{(2\pi)^2}\, e^{i\mathbf{k}_\perp\cdot(\mathbf{x}-\mathbf{x}')_\perp} g_0(z-z';\kappa), \tag{3.4}$$

where now $\kappa^2 = \zeta^2 + k_\perp^2$. The one dimensional reduced Green's function $g_0(z-z';\kappa)$ has the solution

$$g_0(z-z';\kappa) = \frac{1}{2\kappa}\, \mathrm{e}^{-\kappa|z-z'|}. \tag{3.5}$$

We also note that when the complete space consists of a uniform dielectric medium then κ is replaced by $\kappa'^2 = \zeta^2\varepsilon + k_\perp^2$ in the above equation.

3.2 Transverse electric Green's function

Next we turn our attention to the solution of the transverse electric Green's function for the case of translational symmetry in x-y direction. The potential $\mathbf{V}(\mathbf{x}, i\zeta)$,

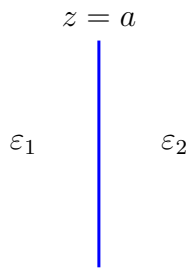

Figure 3.1: Two layered dielectric material.

described in Eq. (2.36), now has dependence on the z-coordinate only

$$V(z) = [\varepsilon(z) - 1]. \tag{3.6}$$

The differential equation for the electric Green's function in Eq. (2.65a) can be written as

$$-\left[\frac{\partial^2}{\partial z^2} - \kappa^2 - \zeta^2 V(z)\right] g^E(z, z'; \kappa) = \delta(z - z'), \tag{3.7}$$

where $\kappa^2 = \zeta^2 + k_\perp^2$.

3.2.1 Two layered dielectric medium

Consider two dielectric media of permittivity ε_1 and ε_2 separated by a plane surface located at $z = a$ shown in Figure 3.1. This physical situation can be described by

$$V(z) = (\varepsilon_1 - 1)\theta(a - z) + (\varepsilon_2 - 1)\theta(z - a), \tag{3.8}$$

where $\theta(z - a) = 0$ if $z < a$, and $\theta(z - a) = 1$ if $z > a$. Using the matching conditions, which are (a) g^E is continuous and (b) $\frac{d}{dz} g^E(z, z')$ is discontinuous across the boundary, we can solve the differential equation (2.65a). The solution for the

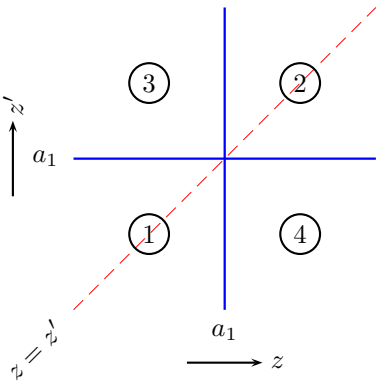

Figure 3.2: Regions for investigation of the Green's function for the step potential.

electric Green's function is

$$g^E(z,z') = \frac{s_n}{\kappa_z + \kappa_{z'}} e^{-\kappa_z|z-z'|} + \frac{t_n}{\kappa_z + \kappa_{z'}} e^{-\kappa_z|z-a_i|} e^{-\kappa_{z'}|z'-a_i|}, \tag{3.9}$$

where n represents regions 1 to 4 in Figure 3.2. Coefficients $s_n = 1$ if $n = 1, 2$, and zero otherwise. This basically represents the bulk term and is present only when z and z' are in the same region. In the above equations κ_z and $\kappa_{z'}$ take on values of κ_i based on the regions in which the respective z, z' are in. $\kappa_i^2 = k^2 + \zeta^2\varepsilon_i = \kappa^2 + \zeta^2(\varepsilon_i - 1)$ for $i = 1, 2$, and coefficients t_n are given in Table 3.1, where

$t_3 = 1$	$t_2 = -\alpha_{ji}$
$t_1 = \alpha_{ij}$	$t_4 = 1$

Table 3.1: Transition matrix coefficients for the two layered dielectric media.

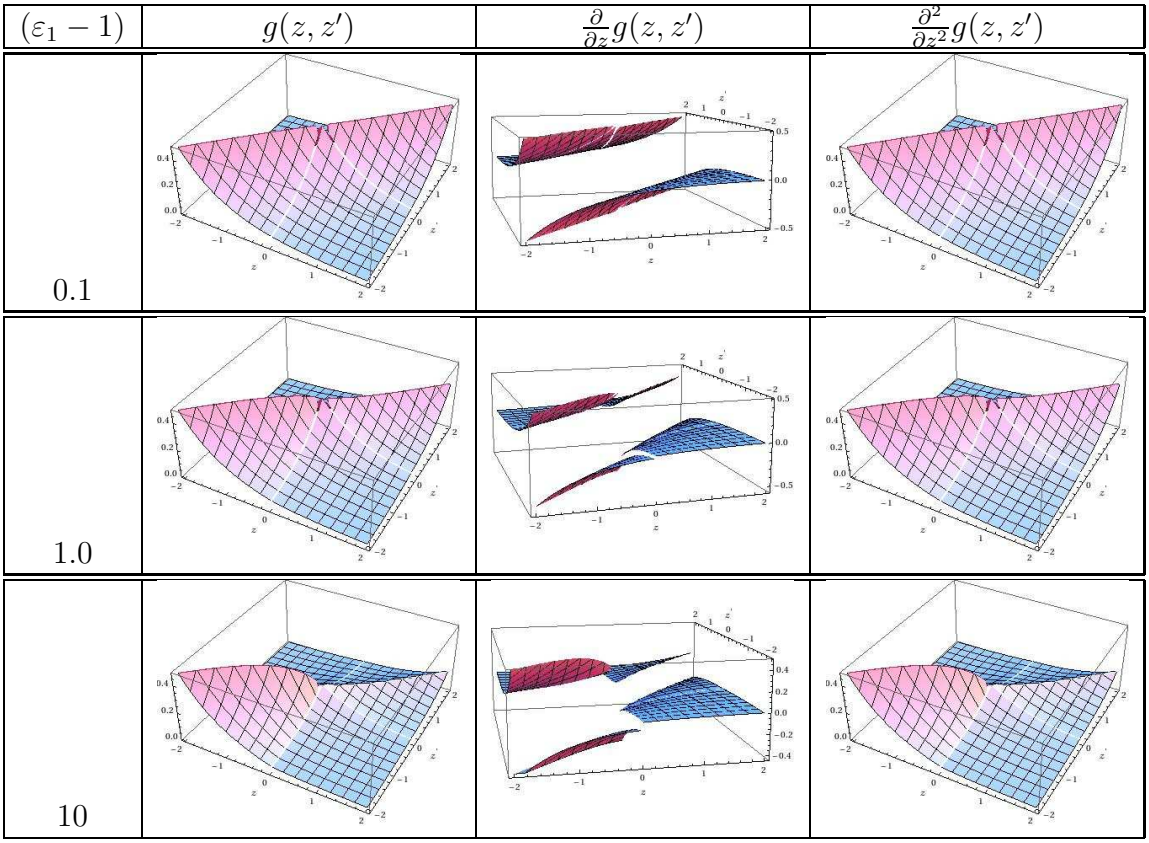

Figure 3.3: Electric Green's function for the infinite slab. ($a = 0$, $\kappa = 1$, $\zeta = 1$.)

$$\alpha_{ij} = \frac{\kappa_i - \kappa_j}{\kappa_i + \kappa_j}. \tag{3.10}$$

When one medium is vacuum, i.e. $\varepsilon \to 1$ for that medium, $\kappa' \to \kappa$ for that medium.

We plot the transverse electric Green's function g^E and its derivatives in Figure 3.3. The discontinuities along the slab surface is magnified for the higher value of dielectric permittivity. The discontinuity along the diagonal line corresponds to $z = z'$, which is the contribution from the δ-function on the right hand side of Eq. (3.7). This is a universal feature.

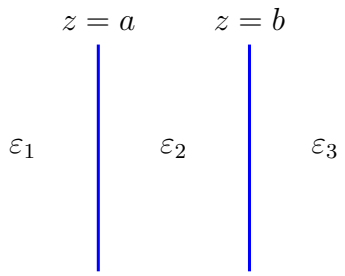

Figure 3.4: Three layered dielectric material.

3.2.2 Three layered dielectric medium

Next we consider three dielectric media separated by plane surfaces located at $z = a$ and $z = b$ as shown in Figure. 3.4, which can be described by the potential

$$V(z) = (\varepsilon_1 - 1)\theta(a - z) + (\varepsilon_2 - 1)\left[\theta(z - a) - \theta(b - z)\right] + (\varepsilon_3 - 1)\theta(z - b). \quad (3.11)$$

The middle slab has thickness $d = b - a$. The solution can be expressed in the form

$$g^E(z, z') = \frac{s_n}{\kappa_z + \kappa_{z'}} e^{-\kappa_z|z-z'|} + \mathbf{e}(z)^T \cdot \frac{1}{\Delta} \frac{\mathbf{t}_n}{\kappa_z + \kappa_{z'}} \cdot \mathbf{e}(z') \quad (3.12)$$

where n denotes regions from 1 to 9 in Figure 3.5. The coefficients $s_n = 1$, if $n = 1, 2, 3$, and zero otherwise. The vector $\mathbf{e}(z)$ is defined in terms of the free Green's function as

$$\mathbf{e}(z)^T = \left(e^{-\kappa_z|z-a_i|}, e^{-\kappa_z|z-b_i|}\right). \quad (3.13)$$

The determinant Δ is given by

$$\Delta = (1 - \alpha_{21}\alpha_{23}e^{-2\kappa_2 d}), \quad (3.14)$$

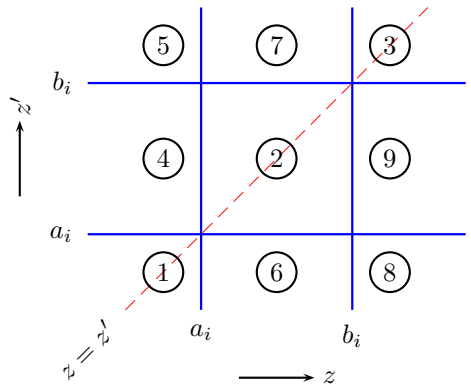

Figure 3.5: Regions for investigation of the Green's function for the slab potential.

where $\kappa_2^2 = \kappa^2 + \zeta^2(\varepsilon_2 - 1)$. The coefficients $\mathbf{t}_n$s are given in Table 3.4. For the specific

$\mathbf{t}_5 = \begin{bmatrix} 0 & (1-\alpha_{21}\alpha_{23})e^{-\kappa_2 d} \\ 0 & 0 \end{bmatrix}$	$\mathbf{t}_7 = \begin{bmatrix} 0 & \alpha_{21}e^{-\kappa_2 d} \\ 0 & 1 \end{bmatrix}$	$\mathbf{t}_3 = \begin{bmatrix} 0 & 0 \\ 0 & -(\alpha_{23} - \alpha_{21}e^{-\kappa_2 d}) \end{bmatrix}$
$\mathbf{t}_4 = \begin{bmatrix} 1 & alpha_{23}e^{-\kappa_2 d} \\ 0 & 0 \end{bmatrix}$	$\mathbf{t}_2 = \begin{bmatrix} \alpha_{21} & \alpha_{21}\alpha_{23}e^{-\kappa_2 d} \\ \alpha_{21}\alpha_{23}e^{-\kappa_2 d} & \alpha_{23} \end{bmatrix}$	$\mathbf{t}_9 = \begin{bmatrix} 0 & 0 \\ \alpha_{21}e^{-\kappa_i d_i} & 1 \end{bmatrix}$
$\mathbf{t}_1 = \begin{bmatrix} -(\alpha_{21} - \alpha_{23}e^{-\kappa_2 d}) & 0 \\ 0 & 0 \end{bmatrix}$	$\mathbf{t}_6 = \begin{bmatrix} 1 & 0 \\ \alpha_{23}e^{-\kappa_i d_i} & 0 \end{bmatrix}$	$\mathbf{t}_8 = \begin{bmatrix} 0 & 0 \\ (1-\alpha_{21}\alpha_{23})e^{-\kappa_2 d} & 0 \end{bmatrix}$

Table 3.2: Transition matrix coefficients for the three layered dielectric medium.

case when $\varepsilon_{1,3} = 1$ describes a dielectric slab. The solution can be obtained by setting $\kappa_{1,3} = \kappa$ in above equations. Subscript 2 used to identify the middle dielectric layer can be replaced by i to denote i-th slab.

3.2.3 Five layered dielectric medium

Let us now consider the potential

$$\begin{aligned} V(z) = \; & (\varepsilon_1 - 1)\theta(a_1 - z) + (\varepsilon_A - 1)\left[\theta(z - a_1) - \theta(z - b_1)\right] \\ & + (\varepsilon_2 - 1)\left[\theta(z - b_1) - \theta(z - a_2)\right] + (\varepsilon_B - 1)\left[\theta(z - a_2) - \theta(z - b_2)\right] \\ & + (\varepsilon_3 - 1)\theta(z - b_2), \end{aligned} \tag{3.15}$$

where $d_{1,2} = b_{1,2} - a_{1,2}$ and $a = a_2 - b_1$. The choice of subscript is governed by the fact that when $d_{1,2} \to 0$ we get potential described in the previous subsection. This is shown in Figure 3.6.

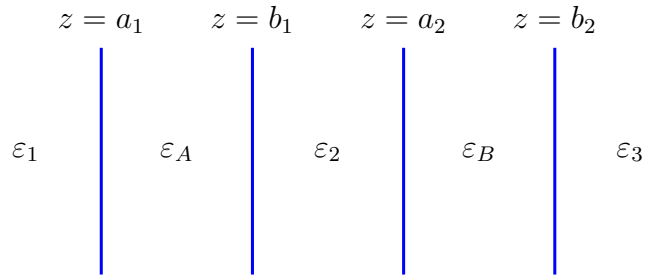

Figure 3.6: Five layered dielectric material.

The solution can be written as before

$$g^E(z, z') = \frac{s_n}{\kappa_z + \kappa_{z'}} e^{-\kappa_z |z - z'|} + \mathbf{e}(z)^T \cdot \frac{1}{\Delta} \frac{\mathbf{t}_n}{\kappa_z + \kappa_{z'}} \cdot \mathbf{e}(z') \tag{3.16}$$

where n denotes regions given in Figure 3.7. The coefficients $s_n = 1$, if $n = 1, 2, 3, A, B$, and zero otherwise. The vector $\mathbf{e}(z)$ is defined in terms of the free Green's function as

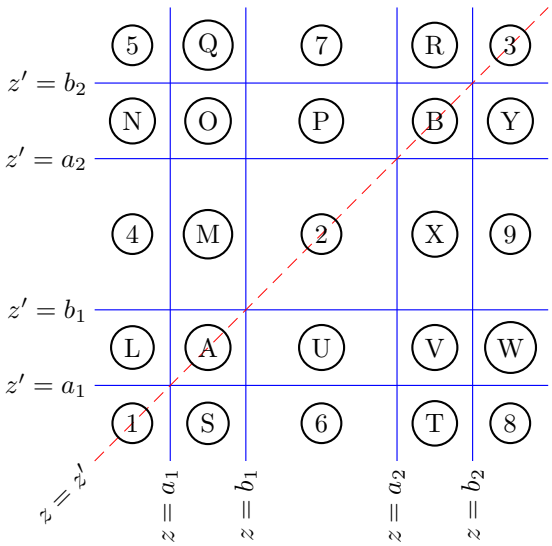

Figure 3.7: Regions for investigation of five region Green's function.

$$\mathbf{e}(z)^T = \left(e^{-\kappa_z|z-a_1|}, e^{-\kappa_z|z-b_1|}, e^{-\kappa_z|z-a_2|}, e^{-\kappa_z|z-b_2|}\right). \tag{3.17}$$

To save space we define

$$\delta_{11}=\alpha_{2A} + \alpha_{A1}e^{-2\kappa_A d_1} \tag{3.18a}$$

$$\delta_{12}=1 + \alpha_{2A}\alpha_{A1}e^{-2\kappa_A d_1} \tag{3.18b}$$

$$\delta_{21}=1 + \alpha_{2B}\alpha_{B3}e^{-2\kappa_B d_2} \tag{3.18c}$$

$$\delta_{22}=\alpha_{2B} + \alpha_{B3}e^{-2\kappa_B d_2} \tag{3.18d}$$

Using these notations the determinant Δ is given by

$$\Delta = \delta_{11}\delta_{22}e^{-\kappa_2 a} - \delta_{12}\delta_{21}e^{\kappa_2 a}. \tag{3.19}$$

In Tables 3.3 and 3.4 we give the non-vanishing components of the coefficients $\mathbf{t}_n$.

$\mathbf{t}_5^{a_1b_2}=\Big[(\alpha_{A1}+\alpha_{2A})(\alpha_{2B}+\alpha_{B3})$ $-(1+\alpha_{2A}\alpha_{A1})(1+\alpha_{2B}\alpha_{B3})\Big]e^{-\kappa_A d_1-\kappa_B d_2}$	$\mathbf{t}_Q^{b_1b_2}=-\Big[\,(1-\alpha_{2A}\alpha_{2B})+\alpha_{B3}\,(\alpha_{2B}-\alpha_{2A})\,\Big]e^{-\kappa_B d_2}$ $\mathbf{t}_Q^{a_1b_2}=\mathbf{t}_Q^{b_1b_2}\alpha_{A1}e^{-\kappa_A d_1}$	$\mathbf{t}_7^{b_1b_2}=-\,(1+\alpha_{2B}\alpha_{B3})\,\delta_{11}e^{-\kappa_B d_2}$ $\mathbf{t}_7^{a_2b_2}=-\,(1+\alpha_{2B}\alpha_{B3})\,\delta_{12}e^{-\kappa_B d_2}$
$\mathbf{t}_N^{a_1a_2}=-\Big[(1-\alpha_{2A}\alpha_{2B})+\alpha_{A1}\,(\alpha_{2A}-\alpha_{2B})\,\Big]e^{-\kappa_A d_1}$ $\mathbf{t}_N^{a_1b_2}=\mathbf{t}_N^{a_1a_2}\alpha_{B3}e^{-\kappa_B d_2}$	$\mathbf{t}_O^{a_1a_2}=-\alpha_{A1}\,(1-\alpha_{2A}\alpha_{2B})\,\Big]e^{-\kappa_A d_1}$ $\mathbf{t}_O^{a_1b_2}=\mathbf{t}_O^{a_1a_2}\alpha_{B3}e^{-\kappa_B d_2}$ $\mathbf{t}_O^{b_1a_2}=-\,(1-\alpha_{2A}\alpha_{2B})$ $\mathbf{t}_O^{b_1b_2}=\mathbf{t}_O^{b_1a_2}\alpha_{B3}e^{-\kappa_B d_2}$	$\mathbf{t}_P^{b_1a_2}=-\delta_{11}$ $\mathbf{t}_P^{b_1b_2}=\mathbf{t}_P^{b_1a_2}\alpha_{B3}e^{-\kappa_B d_2}$ $\mathbf{t}_P^{a_2a_2}=-\delta_{12}e^{-\kappa_2 a}$ $\mathbf{t}_P^{a_2b_2}=\mathbf{t}_P^{a_1a_2}\alpha_{B3}e^{-\kappa_B d_2}$
$\mathbf{t}_4^{a_1a_2}=-\,(1+\alpha_{2A}\alpha_{A1})\,\delta_{22}e^{-\kappa_A d_1}$ $\mathbf{t}_4^{a_1b_1}=-\,(1+\alpha_{2A}\alpha_{A1})\,\delta_{11}e^{-\kappa_A d_1}e^{\kappa_2 a}$	$\mathbf{t}_M^{b_1b_1}=-\delta_{12}e^{\kappa_2 a}$ $\mathbf{t}_M^{a_1b_1}=\mathbf{t}_M^{b_1b_2}\alpha_{A1}e^{-\kappa_A d_1}$ $\mathbf{t}_M^{b_1a_2}=-\delta_{22}$ $\mathbf{t}_M^{a_1a_2}=\mathbf{t}_M^{b_1a_2}\alpha_{A1}e^{-\kappa_A d_1}$	$\mathbf{t}_2^{b_1b_1}=-\delta_{11}\delta_{21}e^{\kappa_2 a}$ $\mathbf{t}_2^{b_1a_2}=-\delta_{11}\delta_{22}$ $\mathbf{t}_2^{a_2b_1}=\mathbf{t}_2^{b_1a_2}$ $\mathbf{t}_2^{a_2b_2}=-\delta_{22}\delta_{12}e^{\kappa_2 a}$
$\mathbf{t}_L^{a_1a_1}=\Big[\alpha_{2A}\delta_{22}e^{-\kappa_2 a}-\delta_{21}e^{\kappa_2 a}\Big]$ $\mathbf{t}_L^{a_1b_1}=\Big[\alpha_{2A}\delta_{21}e^{\kappa_2 a}-\delta_{22}e^{-\kappa_2 a}\Big]e^{-\kappa_A d_1}$	$\mathbf{t}_U^{b_1b_1}=\Big[\alpha_{2A}\delta_{21}e^{\kappa_2 a}-\delta_{22}e^{-\kappa_2 a}\Big]$ $\mathbf{t}_U^{a_1b_1}=\mathbf{t}_B^{b_1b_1}\alpha_{A1}e^{-\kappa_A d_1}$ $\mathbf{t}_U^{b_1a_1}=\mathbf{t}_B^{a_1b_1}$ $\mathbf{t}_U^{a_1a_1}=\Big[\alpha_{2A}\delta_{22}e^{-\kappa_2 a}-\delta_{21}e^{\kappa_2 a}\Big]\alpha_{A1}e^{-\kappa_A d_1}$	$\mathbf{t}_U^{b_1b_1}=-\delta_{12}e^{\kappa_2 a}$ $\mathbf{t}_U^{b_1a_1}=\mathbf{t}_U^{b_2b_1}\alpha_{A1}e^{-\kappa_A d_1}$ $\mathbf{t}_U^{a_2b_1}=-\delta_{22}$ $\mathbf{t}_U^{a_2a_1}=\mathbf{t}_U^{a_2b_1}\alpha_{A1}e^{-\kappa_A d_1}$
$\mathbf{t}_1^{a_1a_1}=\Big[\delta_{21}\delta_{11}e^{\kappa_2 a}-\delta_{22}\left(\alpha_{2A}\alpha_{A1}+e^{-2\kappa_A d_1}\right)e^{-\kappa_2 a}\Big]$	$\mathbf{t}_S^{a_1a_1}=\Big[\alpha_{2A}\delta_{22}e^{-\kappa_2 a}-\delta_{21}e^{\kappa_2 a}\Big]$ $\mathbf{t}_S^{b_1a_1}=\Big[\alpha_{2A}\delta_{21}e^{\kappa_2 a}-\delta_{22}e^{-\kappa_2 a}\Big]e^{-\kappa_A d_1}$	$\mathbf{t}_6^{a_2a_1}=-\,(1+\alpha_{2A}\alpha_{A1})\,\delta_{22}e^{-\kappa_A d_1}$ $\mathbf{t}_6^{b_1a_1}=-\,(1+\alpha_{2A}\alpha_{A1})\,\delta_{11}e^{-\kappa_A d_1}e^{\kappa_2 a}$

Table 3.3: Transition matrix components of five layered dielectric medium scalar electric Green's function–First three columns.

$\mathbf{t}_R^{a_2b_2} = \left[\alpha_{2B}\delta_{12}e^{\kappa_2 a} - \delta_{11}e^{-\kappa_2 a})\right]e^{-\kappa_B d_2}$ $\mathbf{t}_R^{b_2b_2} = \left[\alpha_{2B}\delta_{11}e^{\kappa_2 a} - \delta_{12}e^{\kappa_2 a}\right]$	$\mathbf{t}_3^{b_2b_2} = \left[\delta_{21}\delta_{12}e^{\kappa_2 a} - \delta_{11}(\alpha_{2B}\alpha_{B3} + e^{-\kappa_B d_2})e^{\kappa_2 a}\right]$
$\mathbf{t}_B^{a_2a_2} = \left[\alpha_{2B}\delta_{12}e^{\kappa_2 a} - \delta_{11}e^{-\kappa_2 a})\right]$ $\mathbf{t}_B^{a_2b_2} = \mathbf{t}_B^{a_2a_2}\alpha_{B3}e^{-\kappa_B d_2}$ $\mathbf{t}_B^{b_2a_2} = \mathbf{t}_B^{b_2a_2}$ $\mathbf{t}_B^{b_2b_2} = \left[\alpha_{2B}\delta_{11}e^{\kappa_2 a} - \delta_{12}e^{\kappa_2 a}\right]$	$\mathbf{t}_R^{b_2a_2} = \left[\alpha_{2B}\delta_{12}e^{\kappa_2 a} - \delta_{11}e^{-\kappa_2 a})\right]e^{-\kappa_B d_2}$ $\mathbf{t}_R^{b_2b_2} = \left[\alpha_{2B}\delta_{11}e^{\kappa_2 a} - \delta_{12}e^{\kappa_2 a}\right]$
$\mathbf{t}_X^{a_2b_1} = -\delta_{11}$ $\mathbf{t}_X^{b_2b_1} = \mathbf{t}_X^{a_2b_1}\alpha_{B3}e^{-\kappa_B d_2}$ $\mathbf{t}_X^{a_2a_2} = -\delta_{12}e^{\kappa_2 a}$ $\mathbf{t}_X^{b_2a_2} = \mathbf{t}_X^{a_2a_2}\alpha_{B3}e^{-\kappa_B d_2}$	$\mathbf{t}_9^{b_2b_1} = -\left(1 + \alpha_{2B}\alpha_{B3}\right)\delta_{11}e^{-\kappa_B d_2}$ $\mathbf{t}_9^{b_2a_2} = -\left(1 + \alpha_{2B}\alpha_{B3}\right)\delta_{12}e^{-\kappa_B d_2}$
$\mathbf{t}_V^{a_2a_1} = -\alpha_{A1}\left(1 - \alpha_{2A}\alpha_{2B}\right)\right]e^{-\kappa_A d_1}$ $\mathbf{t}_V^{b_2a_1} = \mathbf{t}_V^{a_2a_1}\alpha_{B3}e^{-\kappa_B d_2}$ $\mathbf{t}_V^{a_2b_1} = -\left(1 - \alpha_{2A}\alpha_{2B}\right)$ $\mathbf{t}_V^{b_2b_1} = \mathbf{t}_V^{a_2b_1}\alpha_{B3}e^{-\kappa_B d_2}$	$\mathbf{t}_W^{b_2b_1} = -\left[\left(1 - \alpha_{2A}\alpha_{2B}\right) + \alpha_{B3}\left(\alpha_{2B} - \alpha_{2A}\right)\right]e^{-\kappa_B d_2}$ $\mathbf{t}_W^{b_2a_1} = \mathbf{t}_W^{b_2b_1}\alpha_{A1}e^{-\kappa_A d_1}$
$\mathbf{t}_T^{a_2a_1} = -\left[(1 - \alpha_{2A}\alpha_{2B}) + \alpha_{A1}\left(\alpha_{2A} - \alpha_{2B}\right)\right]e^{-\kappa_A d_1}$ $\mathbf{t}_T^{a_1b_2} = \mathbf{t}_T^{a_2a_1}\alpha_{B3}e^{-\kappa_B d_2}$	$\mathbf{t}_8^{b_2a_1} = \left[(\alpha_{A1} + \alpha_{2A})(\alpha_{2B} + \alpha_{B3})\right.$ $\left.-(1 + \alpha_{A1}\alpha_{2A})(1 + \alpha_{2B}\alpha_{B3})\right]e^{-\kappa_A d_1 - \kappa_B d_2}$

Table 3.4: Transition matrix components of five layered dielectric medium scalar electric Green's function–last two columns.

3.2.4 Green's function for a single δ-function potential

For the sake of completeness we list the solution for the Green's function for a single semi-transparent δ-function potential, described by $V = \lambda\delta(z-a)$, which satisfies

$$-\Big[\frac{\partial^2}{\partial z^2} - \kappa^2 - \lambda\delta(z-a)\Big] g(z,z';\kappa) = \delta(z-z') \tag{3.20}$$

and has the solution

$$g(z,z';\kappa) = \frac{1}{2\kappa}\, e^{-\kappa|z-z'|} - \frac{1}{2\kappa}\frac{\lambda}{\lambda+2\kappa}\, e^{-\kappa|z-a|} e^{-\kappa|z'-a|}. \tag{3.21}$$

We plot the scalar Green's function $g(z,z')$ for semi-transparent δ-plate and its derivatives in Figure 3.8. The discontinuities along the plate surface increase as λ increases, which is a measure of increasing reflectivity of the plate. The discontinuity along the diagonal line corresponds to $z = z'$, which is there due to the δ-function on right hand side of Eq. (3.20). For comparable numbers the behavior of Green's function for both semi-transparent plate and infinite thickness slab is similar except for the qualitative behavior that for the slab transverse electric Green's function goes to zero in the slab region as permittivity increases while the scalar Green's function for the single semi-transparent δ-function potential goes to zero only on the plate surface as λ goes to infinity. This represents the Dirichlet boundary condition.

3.3 Transverse magnetic Green's function

Solving for the transverse magnetic Green's function requires imposing physical boundary conditions on the Green's function solutions since its not possible to get both

λ	$g(z,z')$	$\frac{\partial}{\partial z}g(z,z')$	$\frac{\partial^2}{\partial z^2}g(z,z')$
0.1	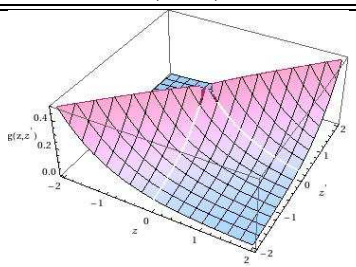	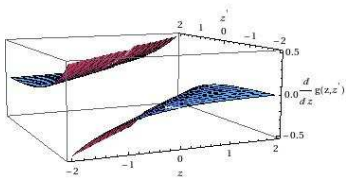	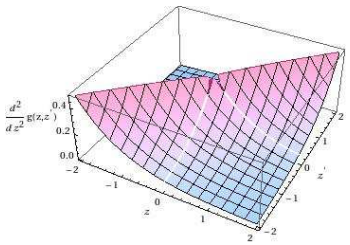
1.0	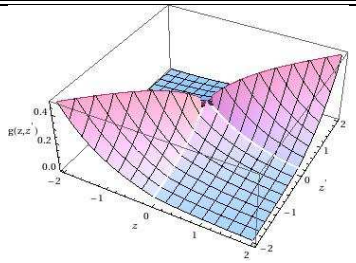	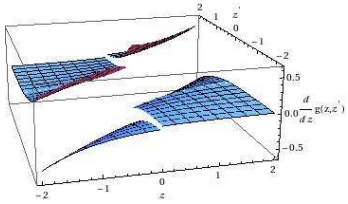	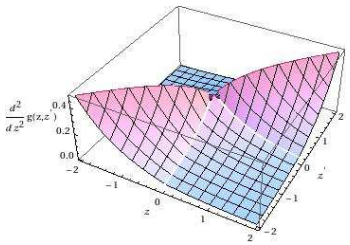
10	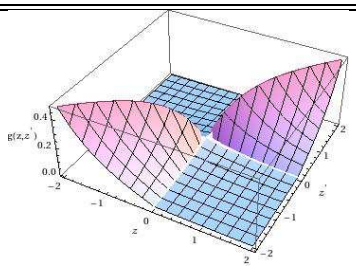	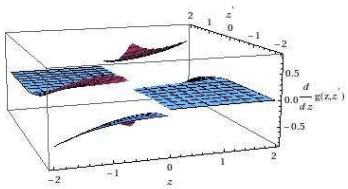	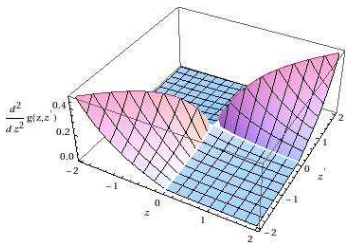

Figure 3.8: Green's function for single δ-plate. ($a = 0$, $\kappa = 1$.)

matching conditions on the boundary using Eq. (2.65b). Therefore, one condition needs to be fixed using the physical boundary conditions. For the electromagnetic field we know that $[\varepsilon \mathbf{E}]_3(z)$ is continuous on the boundary. Then using

$$\gamma_{33}(z, z') = \frac{1}{i}\langle \mathbf{E}_3(z)\mathbf{E}_3(z')\rangle, \tag{3.22}$$

and Eq. (2.72) and the continuity of $[\varepsilon \mathbf{E}]_3(z)$ we can conclude that $g^H(z, z')$ is continuous at the boundary of the two dielectric surfaces. This allows us to get the second condition from the Green's functions equation, which is

$$\left[-\frac{1}{\varepsilon(z)}\frac{\partial}{\partial z} g^H(z, z')\right]_{z=a-\epsilon}^{z=a+\epsilon} = 0. \tag{3.23}$$

The solution for the scalar magnetic Green's function for the two layered dielectric medium is

$$g^E(z, z') = \frac{s_n}{\overline{\kappa}_z + \overline{\kappa}_{z'}}\, e^{-\kappa_z|z-z'|} + \frac{t_n}{\overline{\kappa}_z + \overline{\kappa}_{z'}}\, e^{-\kappa_z|z-a_i|} e^{-\kappa_{z'}|z'-a_i|}, \tag{3.24}$$

where $\overline{\kappa}_z = \kappa_z/\varepsilon(z)$. This solution is similar to the scalar electric Green's function solution except that κ_zs are replaced by $\overline{\kappa}_z$s everywhere except in exponentials. This feature is generic for the θ-potential, so we will use solutions of the electric Green's function for the other case described in the previous section and let $\kappa_i \to \overline{\kappa}_i$ everywhere except in the exponential.

3.4 Cylindrical scalar Green's function

For the scalar field interacting with background potential, the Lagrangian density is given by Eq. (2.31) and corresponding Green's function obeys the differential equation given by Eq. (2.33). Consider two concentric semi-transparent cylinders described by the potential

$$V(r) = \lambda_1 \delta(r - a_1) + \lambda_2 \delta(r - a_2), \tag{3.25}$$

such that $a = a_2 - a_1 > 0$. Using translational symmetry in θ and z directions we can write

$$G^{(0)}(x, x') = \int \frac{d\omega}{2\pi} e^{-i\omega(t-t')} \int \frac{dk}{2\pi} e^{ik(z-z')} \sum_{m=-\infty}^{\infty} \frac{1}{2\pi} e^{im(\theta-\theta')} g_m^{(0)}(r, r'; \kappa), \tag{3.26}$$

where $\kappa^2 = k^2 - \omega^2$. The reduced Green's function, $g_m^{(0)}(r, r'; \kappa)$, satisfies the equation

$$-\left[\frac{1}{r}\frac{\partial}{\partial r} r \frac{\partial}{\partial r} - \frac{m^2}{r^2} - \kappa^2 - \lambda_1 \delta(r - a_1) - \lambda_2 \delta(r - a_2)\right] g_m^{(0)}(r, r'; \kappa) = \frac{\delta(r - r')}{r}. \tag{3.27}$$

The solution for $g_m^{(0)}(r, r'; \kappa)$ in the above equation can be written in a form similar to the parallel plate case as

$$g_m^{(0)}(r, r'; \kappa) = s_n I_m(\kappa r_<) K_m(\kappa r_>) + \mathbf{e}(z)^T \cdot \frac{1}{\Delta} \mathbf{t}_n \cdot \mathbf{e}(z'), \tag{3.28}$$

where as in three layered dielectric case n denotes regions from 1 to 9 in Figure (3.5). Coefficients $s_n = 1$, if $n = 1, 2, 3$, and zero otherwise. The vector $\mathbf{e}(z)$ is defined in terms of the free Green's function for the cylindrical case as

$$\mathbf{e}(z)^T = \Big(I_m(\kappa r),\ K_m(\kappa r) \Big). \tag{3.29}$$

the determinant Δ is

$$\Delta = 1 + \tilde{\lambda}_1 \, I_1 K_1 + \tilde{\lambda}_2 \, I_2 K_2 + \tilde{\lambda}_1 \tilde{\lambda}_2 \, I_1 K_2 \Big(I_2 K_1 - I_1 K_2 \Big). \tag{3.30}$$

We have used the notation $\tilde{\lambda}_i \equiv \lambda_i a_i$, $I_i \equiv I_m(\kappa a_i)$ and $K_i \equiv K_m(\kappa a_i)$ for $i = 1, 2$. The coefficients $\mathbf{t}_n$s are given in Table 3.4.

$\mathbf{t}_5 = \begin{bmatrix} 0 & 1 \\ 0 & 0 \end{bmatrix}$	$\mathbf{t}_7 = \begin{bmatrix} 0 & 1+\tilde{\lambda}_1 I_1 K_1 \\ 0 & \tilde{\lambda}_1 I_1^2 \end{bmatrix}$	$\mathbf{t}_3 = \begin{bmatrix} 0 & 0 \\ 0 & -\big[\tilde{\lambda}_1\tilde{\lambda}_2 I_1 I_2 \big(I_2 K_1 - I_1 K_2\big) \\ & +\tilde{\lambda}_1 I_1^2 + \tilde{\lambda}_2 I_2^2\big] \end{bmatrix}$
$\mathbf{t}_4 = \begin{bmatrix} \tilde{\lambda}_2 K_2^2 & 1+\tilde{\lambda}_2 I_2 K_2 \\ 0 & 0 \end{bmatrix}$	$\mathbf{t}_2 = \begin{bmatrix} -\tilde{\lambda}_2 K_2^2\big(1+\lambda_1 a_1 I_1 K_1\big) & \tilde{\lambda}_1\tilde{\lambda}_2 I_1^2 K_2^2 \\ \tilde{\lambda}_1\tilde{\lambda}_2 I_1^2 K_2^2\big(1+\tilde{\lambda}_2 I_2 K_2\big) & -\tilde{\lambda}_1 I_1^2 \end{bmatrix}$	$\mathbf{t}_9 = \begin{bmatrix} 0 & 0 \\ 1+\tilde{\lambda}_1 I_1 K_1 & \tilde{\lambda}_1 I_1^2 \end{bmatrix}$
$\mathbf{t}_1 = \begin{bmatrix} -\big[\tilde{\lambda}_1\tilde{\lambda}_2 K_1 K_2\big(I_2 K_1 - I_1 K_2\big) & 0 \\ +\tilde{\lambda}_1 K_1^2 + \tilde{\lambda}_2 K_2^2\big] & \\ 0 & 0 \end{bmatrix}$	$\mathbf{t}_6 = \begin{bmatrix} \tilde{\lambda}_2 K_2^2 & 0 \\ 1+\tilde{\lambda}_2 I_2 K_2 & 0 \end{bmatrix}$	$\mathbf{t}_8 = \begin{bmatrix} 0 & 0 \\ 1 & 0 \end{bmatrix}$

Table 3.5: Transition matrix amplitude for the Greens function of two concentric cylinders.

Chapter 4

Lifshitz energy for thick and thin materials

With the necessary mathematical tools in our bag we can now proceed to apply them to study the Casimir effect in planar and cylindrical geometries. In this chapter we apply the multiple scattering formalism to real materials with planar configuration. We shall start by considering the interaction energy between two dielectric slabs of finite thickness and obtain the standard Lifshitz energy between infinite dielectric semi-spaces and the Casimir energy between two perfectly conducting plates separated by the vacuum from the general expression. We shall next consider infinitesimally thin plates, which could be considered as idealized δ-function plates and verify the standard Casimir result for the perfectly conducting plates. We also present the case of an atom in front of a thick slab and thin plate for both the dielectric material and the perfect conductor and obtain the standard Casimir-Polder result.

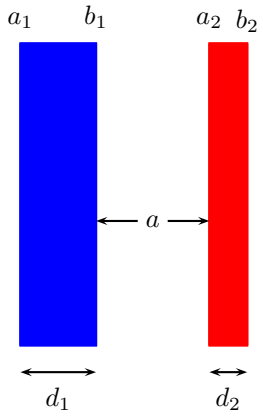

Figure 4.1: Two dielectric slabs of different finite thickness separated by a distance a.

4.1 Interaction energy of two slabs

When the background potential depends only on one co-ordinate, then we can solve the Green's dyadic in terms of the reduced Green's dyadic as shown in Section 2.4. The interaction energy between two disjoint bodies is given by Eq. (2.43). Consider two parallel dielectric slabs separated by the vacuum, which are described by the potentials

$$V_i(z) = (\varepsilon_i - 1)\left[\theta(z - a_i) - \theta(z - b_i)\right], \tag{4.1}$$

where $b_i - a_i = d_i$ for $i = 1, 2$ are the thickness of slabs, and $a_2 - b_1 = a$ is the distance between the slabs (see Figure 4.1). ε_i are the dielectric permittivities of the slabs, which are constant. Using translational symmetry we can write the Casimir energy per unit area for parallel slabs in the form

$$\mathcal{E}(a, d_i, \varepsilon_i - 1) = \frac{E_{12}}{L_x L_y} = \frac{1}{2}\int_{-\infty}^{\infty}\frac{d\zeta}{2\pi}\int\frac{d^2k}{(2\pi)^2}\,\mathrm{tr}\ln\Big[1 - \mathbf{K}(i\zeta, k)\Big], \tag{4.2}$$

where the trace is now only over the dyadic indices. The dyadic $\mathbf{K}(i\zeta,k)$ is given in terms of the reduced Green's dyadic in Eq. (2.72) as

$$\mathbf{K}(i\zeta,k)=(\varepsilon_1-1)(\varepsilon_2-1)\int_{a_1}^{b_1}dz\int_{a_2}^{b_2}dz'\boldsymbol{\gamma}_{1⑨}(z',z;i\zeta,k)\cdot\boldsymbol{\gamma}_{2④}(z,z';i\zeta,k), \quad (4.3)$$

where the circled number in the subscript denotes the region in Figure 3.5 in which the dyadic is to be evaluated. The reduced Green's dyadic is given in terms of the electric and magnetic Green's functions in Eqs. (2.65a) and (2.65b) whose solutions for parallel slabs described by the potentials in Eq. (4.1) are given in Eq. (3.12). The region of evaluation is unambiguously specified by the integration regions. The solution for the Green's dyadic for an individual plate is unaware of the presence of the other plate. Thus the meshed regions in Figure 4.2 belongs to the solid (blue) lines, which according to Figure 3.5 corresponds to region 9 for the first slab and region 4 for the second slab. The solution to the reduced electric Green's dyadic is given by Eq. (2.72). Notice that we can omit the δ-function term since z and z' are never evaluated at the same point. Using the equivalence of the trace-log and log-det we can decompose the interaction energy into the transverse electric and transverse magnetic parts as

$$\mathcal{E}(a,d_i,\varepsilon_i-1)=\frac{1}{2}\int_{-\infty}^{\infty}\frac{d\zeta}{2\pi}\int\frac{d^2k}{(2\pi)^2}\left\{\ln\left[1-K^E(i\zeta,k)\right]+\mathrm{tr}\ln\left[1-\mathbf{K}^H(i\zeta,k)\right]\right\}, \quad (4.4)$$

where

$$K^E(i\zeta,k)=(\varepsilon_1-1)(\varepsilon_2-1)\zeta^4\int_{a_1}^{b_1}dz\int_{a_2}^{b_2}dz'\,g^E_{1⑨}(z',z;i\zeta,k)g^E_{2④}(z,z';i\zeta,k), \quad (4.5)$$

$$\mathbf{K}^H(i\zeta,k)=(\varepsilon_1-1)(\varepsilon_2-1)\int_{a_1}^{b_1}dz\int_{a_2}^{b_2}dz'\,\boldsymbol{\gamma}^H_{1⑨}(z',z;i\zeta,k)\cdot\boldsymbol{\gamma}^H_{2④}(z,z';i\zeta,k). \quad (4.6)$$

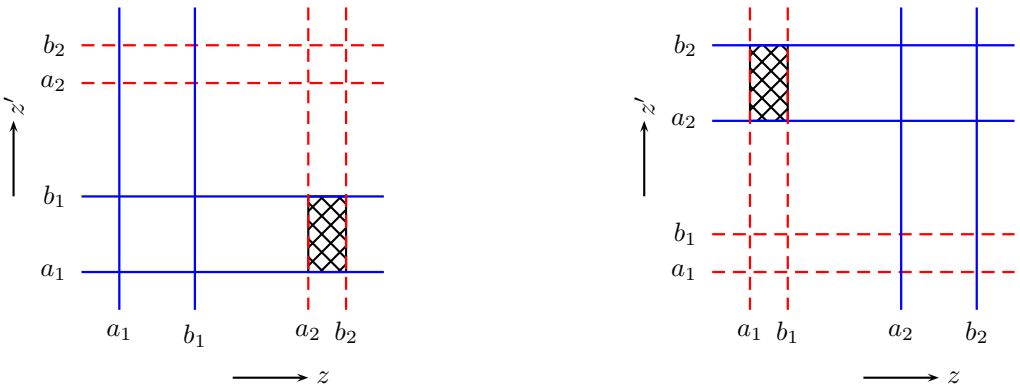

Figure 4.2: Region of integration for $\boldsymbol{\gamma}_1(z,z')$ (left) and $\boldsymbol{\gamma}_2(z,z')$ (right) in Eq. (4.3) shown as crosshatched.

The dimensionally reduced Green's dyadics are

$$\boldsymbol{\gamma}^H_{1⑨}(z',z;i\zeta,k) = \frac{1}{\varepsilon_1}\begin{bmatrix} \frac{\partial}{\partial z'}\frac{\partial}{\partial z}g^H_{1⑨}(z',z) & ik\frac{\partial}{\partial z'}g^H_{1⑨}(z',z) \\ -ik\frac{\partial}{\partial z}g^H_{1⑨}(z',z) & k^2 g^H_{1⑨}(z',z) \end{bmatrix}, \tag{4.7}$$

where we have used the fact that in region 9 (see Figure 3.5 and Figure 4.2)

$$\varepsilon_1(z) \to \varepsilon_1, \qquad \varepsilon_1(z') \to 1. \tag{4.8}$$

Similarly

$$\boldsymbol{\gamma}^H_{2④}(z,z';i\zeta,k) = \frac{1}{\varepsilon_2}\begin{bmatrix} \frac{\partial}{\partial z}\frac{\partial}{\partial z'}g^H_{2④}(z,z') & ik\frac{\partial}{\partial z}g^H_{2④}(z,z') \\ -ik\frac{\partial}{\partial z'}g^H_{2④}(z,z') & k^2 g^H_{2④}(z,z') \end{bmatrix} \tag{4.9}$$

where in region 4 (see Figure 3.5 and Figure 4.2)

$$\varepsilon_2(z) \to 1, \qquad \varepsilon_2(z') \to \varepsilon_2. \tag{4.10}$$

Using Eqs. (4.8) and (4.10) in the equation for the magnetic Green's function given by Eq. (2.65b) we have

$$\frac{\partial}{\partial z'} g^H_{1\textcircled{9}}(z',z) = -\kappa g^H_{1\textcircled{9}}(z',z), \qquad \frac{\partial^2}{\partial z'^2} g^H_{1\textcircled{9}}(z',z) = \kappa^2 g^H_{1\textcircled{9}}(z',z), \tag{4.11a}$$

$$\frac{\partial}{\partial z} g^H_{2\textcircled{4}}(z,z') = -\kappa g^H_{2\textcircled{4}}(z,z'), \qquad \frac{\partial^2}{\partial z^2} g^H_{2\textcircled{4}}(z,z') = \kappa^2 g^H_{2\textcircled{4}}(z,z'). \tag{4.11b}$$

Multiplying the two dyadics, and using Eqs. (4.11) to simplify the resulting expression, we obtain

$$\mathbf{K}^H(i\zeta,k) = \begin{bmatrix} K^H_{11}(i\zeta,k)K^H_{13}(i\zeta,k) \\ K^H_{31}(i\zeta,k)K^H_{33}(i\zeta,k) \end{bmatrix}, \tag{4.12}$$

whose components are

$$K^H_{11}(i\zeta,k) = \hat{\varepsilon}_1\hat{\varepsilon}_2 \int_{a_1}^{b_1} dz \int_{a_2}^{b_2} dz' \left[\kappa^2\zeta^2 - \kappa^3\frac{\partial}{\partial z} + \kappa\zeta^2\frac{\partial}{\partial z'} - \kappa^2\frac{\partial}{\partial z}\frac{\partial}{\partial z'}\right] g^H_{12}, \tag{4.13a}$$

$$K^H_{33}(i\zeta,k) = \hat{\varepsilon}_1\hat{\varepsilon}_2 \int_{a_1}^{b_1} dz \int_{a_2}^{b_2} dz' \left[-k^2\zeta^2 + k^2\kappa\frac{\partial}{\partial z}\right] g^H_{12}, \tag{4.13b}$$

$$K^H_{13}(i\zeta,k) = -\frac{(ik\kappa)}{k^2}\, K^H_{33}(i\zeta,k), \tag{4.13c}$$

$$K^H_{31}(i\zeta,k) = \frac{(ik\kappa)}{\kappa^2}\, K^H_{11}(i\zeta,k), \tag{4.13d}$$

where we have defined shorthand notations $\hat{\varepsilon}_i = (\varepsilon_i - 1)/\varepsilon_i$ for $i = 1, 2$ and $g^H_{12} = g^H_{1\textcircled{9}}(z',z)g^H_{2\textcircled{4}}(z,z')$ to save typographic space. We can now show that

$$\det \mathbf{K}^H(i\zeta,k) = K^H_{11}(i\zeta,k)K^H_{33}(i\zeta,k) - K^H_{13}(i\zeta,k)K^H_{31}(i\zeta,k) = 0, \tag{4.14}$$

which implies

$$\text{tr } \ln\Big[1 - \mathbf{K}^H(i\zeta,k)\Big] = \ln\Big[1 - \text{tr}\,\mathbf{K}^H(i\zeta,k)\Big]. \tag{4.15}$$

Further,

$$\operatorname{tr}\mathbf{K}^H(i\zeta,k)=\hat{\varepsilon}_1\hat{\varepsilon}_2\int_{a_1}^{b_1}dz\int_{a_2}^{b_2}dz'\left(1-\frac{\kappa}{\zeta^2}\frac{\partial}{\partial z}\right)\left(1+\frac{\kappa}{\zeta^2}\frac{\partial}{\partial z'}\right)g_{12}^H(z,z'). \tag{4.16}$$

4.1.1 Evaluation

Using Subsection (3.2.2) for the specific case of the slab where the permittivity $\varepsilon_{1,3}=1$ and $\varepsilon_2\to\varepsilon_i$ corresponding to the i-th slab we can obtain the relevant region-specific Green's functions

$$g_{1\textcircled{9}}^E(z_2,z_1;i\zeta,k)=\frac{e^{-\kappa(z_2-b_1)}}{(\kappa_1+\kappa)}\frac{\left[e^{-\kappa_1(b_1-z_1)}+\alpha_1e^{-\kappa_1d_1}e^{-\kappa_1(z_1-a_1)}\right]}{(1-\alpha_1^2e^{-2\kappa_1d_1})}, \tag{4.17a}$$

$$g_{2\textcircled{4}}^E(z_1,z_2;i\zeta,k)=\frac{e^{-\kappa(a_2-z_1)}}{(\kappa_2+\kappa)}\frac{\left[e^{-\kappa_2(z_2-a_2)}+\alpha_2e^{-\kappa_2d_2}e^{-\kappa_2(b_2-z_2)}\right]}{(1-\alpha_2^2e^{-2\kappa_2d_2})}, \tag{4.17b}$$

where the single interface reflection coefficients α_i's are defined as

$$\alpha_i=\frac{\kappa_i-\kappa}{\kappa_i+\kappa}. \tag{4.18}$$

We again introduce shorthand notation to keep track of the structure of the terms we are evaluating

$$K^E(i\zeta,k)=t_1^E(i\zeta,k)\,t_2^E(i\zeta,k)\,e^{-2\kappa a}, \tag{4.19a}$$

$$\operatorname{tr}\mathbf{K}^H(i\zeta,k)=t_1^H(i\zeta,k)\,t_2^H(i\zeta,k)\,e^{-2\kappa a}, \tag{4.19b}$$

where

$$t_i^E(i\zeta,k)=\frac{e^{\kappa a}}{(1-\alpha_i^2e^{-2\kappa_i d_i})}\frac{(\varepsilon_i-1)\zeta^2}{(\kappa_i+\kappa)}\int_{a_i}^{b_i}dz\,u_i^E(z), \tag{4.20a}$$

$$t_i^H(i\zeta,k)=\frac{e^{\kappa a}}{(1-\bar{\alpha}_i^2e^{-2\kappa_i d_i})}\frac{(\varepsilon_i-1)\zeta^2}{\varepsilon_i(\bar{\kappa}_i+\kappa)}\int_{a_i}^{b_i}dz\left[1+(-1)^i\frac{\kappa}{\zeta^2}\frac{\partial}{\partial z}\right]u_i^H(z), \tag{4.20b}$$

where

$$u_1^E(z)=e^{-\kappa(a_2-z)}\left[e^{-\kappa_1(b_1-z)}+\alpha_1e^{-\kappa_1 d_1}e^{-\kappa_1(z-a_1)}\right], \tag{4.21a}$$

$$u_2^E(z)=e^{-\kappa(z-b_1)}\left[e^{-\kappa_2(z-a_2)}+\alpha_2e^{-\kappa_2 d_2}e^{-\kappa_2(b_2-z)}\right], \tag{4.21b}$$

and the corresponding magnetic functions $u_i^H(z)$ are obtained by changing respective barred quantities. Completing the z-integral in Eq. (4.20a) and using the definition of κ_i before Table 3.1 to replace $(\varepsilon_i-1)\zeta^2$ we derive

$$t_i^E(i\zeta,k)=\frac{\alpha_i}{\Delta_i^N},\qquad i=1,2, \tag{4.22}$$

where the determinants Δ_i^N's are

$$\frac{1}{\Delta_i^N}=\frac{(1-e^{-2\kappa_i d_i})}{\Delta_i}=\frac{(1-e^{-2\kappa_i d_i})}{(1-\alpha_i^2e^{-2\kappa_i d_i})}, \tag{4.23}$$

Repeating the procedure in Eq. (4.20b) and using the identity

$$k^2\pm\kappa\kappa_i=-\zeta^2\varepsilon_i\frac{(\bar{\kappa}_i\mp\kappa)}{(\kappa_i\mp\kappa)}, \tag{4.24}$$

we derive

$$t_i^H(i\zeta,k)=\frac{\bar{\alpha}_i}{\bar{\Delta}_i^N},\qquad i=1,2, \tag{4.25}$$

where the barred quantities are obtained by replacing $\kappa_i \to \kappa_i/\varepsilon_i$ everywhere except in the exponentials. Thus we have the Casimir interaction energy between parallel slabs to be

$$\mathcal{E}(a, d_i, \varepsilon_i - 1) = \frac{1}{2}\int_{-\infty}^{\infty}\frac{d\zeta}{2\pi}\int\frac{d^2k}{(2\pi)^2}\left\{\ln\left[1 - t_1^E(i\zeta,k)\,t_2^E(i\zeta,k)\,e^{-2\kappa a}\right] + \ln\left[1 - t_1^H(i\zeta,k)\,t_2^H(i\zeta,k)\,e^{-2\kappa a}\right]\right\}. \tag{4.26}$$

It is instructive to note that the dependence in the properties of the individual plates is inside t_i^E and t_i^H. More explicitly we have

$$t_i^{E,H}(i\zeta,k) \to t_i^{E,H}(i\zeta,k;d_i,\varepsilon_i - 1). \tag{4.27}$$

4.1.2 Lifshitz energy for two infinite dielectric semi-spaces

We can obtain the standard Lifshitz result [12] by taking the thick-plate limit ($d_i \to \infty$). In this case we have $\Delta_i^N \to 1$ and $\bar{\Delta}_i^N \to 1$. Thus

$$t_i^E(i\zeta,k;\infty,\varepsilon_i - 1) = \alpha_i, \qquad t_i^H(i\zeta,k;\infty,\varepsilon_i - 1) = \bar{\alpha}_i. \tag{4.28}$$

Using this in Eq. (4.26) we get

$$\mathcal{E}(a,\infty,\varepsilon_i - 1) = \frac{1}{2}\int_{-\infty}^{\infty}\frac{d\zeta}{2\pi}\int\frac{d^2k}{(2\pi)^2}\left\{\ln\left[1 - \alpha_1\,\alpha_2\,e^{-2\kappa a}\right] + \ln\left[1 - \bar{\alpha}_1\,\bar{\alpha}_2\,e^{-2\kappa a}\right]\right\}. \tag{4.29}$$

Here α_i and $\bar{\alpha}_i$ are the reflection coefficients r_{TE} and r_{TM} used in the literature.

4.1.3 Casimir energy for two perfectly conducting plates

It is straightforward to obtain the classic Casimir energy for the two perfectly conducting plates from either Eq. (4.28) or Eq. (4.29). For a perfect conductor we take the limit ($\varepsilon_i \to \infty$), for which we have $\alpha_i \to 1$, $\bar{\alpha}_i \to -1$, $\Delta_i^N \to 1$ and $\bar{\Delta}_i^N \to 1$,

$$t_i^E(i\zeta, k; d_i, \infty) = 1, \qquad t_i^H(i\zeta, k; d_i, \infty) = -1. \tag{4.30}$$

This leads to

$$\begin{aligned}\mathcal{E}(a, d_i, \infty) =& \frac{1}{2}\int_{-\infty}^{\infty}\frac{d\zeta}{2\pi}\int\frac{d^2k}{(2\pi)^2}\,2\,\ln\left[1-e^{-2\kappa a}\right] \\ =& \frac{1}{2\pi^2}\int_0^{\infty}\kappa^2 d\kappa\,\ln\left[1-e^{-2\kappa a}\right] \\ =& -\frac{\pi^2}{720\,a^3}.\end{aligned} \tag{4.31a}$$

The above result is true without necessarily taking the thick-plate limit, which amounts to saying that in the perfect conductor limit the only region of interest is the space in between the slabs since the fields are zero inside the perfect conductor.

4.1.4 van der Waals interaction energy between two slabs

In the dilute dielectric limit ($\varepsilon_i - 1 \ll 1$), which is also the van der Waals limit, we have

$$\begin{aligned}t_i^E(i\zeta, k; d_i, \varepsilon_i - 1) &\sim (\varepsilon_i - 1)(1 - e^{-2\kappa d_i})\frac{\zeta^2}{4\kappa^2}, \\ t_i^H(i\zeta, k; d_i, \varepsilon_i - 1) &\sim (\varepsilon_i - 1)(1 - e^{-2\kappa d_i})\frac{(\zeta^2 - 2\kappa^2)}{4\kappa^2}.\end{aligned} \tag{4.32}$$

This leads to van der Waals energy between two slabs given by

$$\begin{aligned}\mathcal{E}(a,d_i,\varepsilon_i-1)\sim&-\frac{(\varepsilon_1-1)(\varepsilon_2-1)}{256\,\pi^3}\int_{-\infty}^{\infty}\frac{d\zeta}{2\pi}\int_{-\infty}^{\infty}\frac{dk_x}{2\pi}\int_{-\infty}^{\infty}\frac{dk_y}{2\pi}(1-e^{-2\kappa d_1})(1-e^{-2\kappa d_2})\\&\times e^{-2\kappa a}\left[\frac{\zeta^4}{\kappa^4}+\frac{(\zeta^2-2\kappa^2)^2}{\kappa^2}\right]\\=&-\frac{1}{3}\frac{23\,(\varepsilon_1-1)(\varepsilon_2-1)}{1920\,\pi^2}\frac{1}{2}\frac{\partial^3}{\partial a^3}\ln\left[\frac{a(a+d_1+d_2)}{(a+d_1)(a+d_2)}\right].\end{aligned}\tag{4.33}$$

In the thick plate limit the above expression leads to the classic van der Waals interaction energy between two thick slabs as

$$\mathcal{E}(a,\infty,\varepsilon_i-1)\sim-\frac{1}{3}\frac{23\,(\varepsilon_1-1)(\varepsilon_2-1)}{640\,\pi^2\,a^3}.\tag{4.34}$$

4.2 Plasma model for a thin-plate

The permittivity for a real material is described by classical models like Drude and plasma models. These models are described for the bulk material, which do not take into account the finite thickness of the material. We are interested in taking the thickness of the slabs described in the previous section to zero. Naively this will lead to vanishing interaction energy between two infinitesimally thin plates. In this section we describe a simple model for the dielectric permittivity, which allows us to take the thickness going to zero limit without giving a vanishing result. In particular we want to reproduce the δ-function potential starting from Eq. (4.1), for which we need $(\varepsilon_i-1)\propto d_i^{-1}$.

The Drude model for the dielectric permittivity uses the Maxwell-Boltzmann distribution for the electrons, which leads to the classical number density of electrons,

$n_e(\infty)$. However, electrons obey the Fermi-Dirac statistics. Sommerfeld revised the Drude model by using the Fermi-Dirac distribution for electrons to calculate the electron number density in metals, n_e. Sommerfeld's revision has been further extended, but our discussion will be restricted to Sommerfeld's model, which is sufficient for our case where we do not ascribe detailed quantum structure to the background potential.

We start with the plasma model, in which a conductor is described by

$$\varepsilon - 1 = -\frac{\omega_p^2}{\omega^2}. \tag{4.35}$$

The above equation seems to indicate $\varepsilon_i < 1$, which might naively lead to violate causality, but we refer to chapter 7 of [79] for a discussion on how Eq. (4.35) is compatible with causality. The plasma frequency for a metal in the non-quantum regime is defined as

$$[\omega_p(\infty)]^2 = \frac{e^2}{m^*} n_e(\infty), \tag{4.36}$$

where e is the charge of electron and m^* is the effective mass of the electron. The ∞ in the parenthesis denote the non-quantum regime, and the parameter representing the transition from classical to quantum will be introduced in the following subsection.

4.2.1 Number density

In the Sommerfeld model the electrons inside a metal are modeled as a gas. The electrons are assumed to be not interacting with each other. To describe the electrons in the electron gas, we consider the energy states of a slab of thickness d which is

infinite in extent in the x-y directions using the Schrödinger equation as

$$E_n(k_x, k_y) = \frac{\hbar^2}{2m^*}\left[k_x^2 + k_y^2 + \frac{n^2\pi^2}{d^2}\right], \qquad n = 0, 1, 2, \ldots. \tag{4.37}$$

The energy states are required to satisfy Neumann boundary conditions because the flux of electrons through the walls is zero. This translates into $n = 0$ also corresponding to an energy state. The total number of electrons in the slab is equal to twice the sum of occupied energy levels. In terms of the maximum occupied energy level, called the Fermi energy E_F, we can thus write

$$n_e = \frac{n_{\text{tot}}(E_F)}{L_x L_y d} = 2\,\frac{1}{d}\sum_{n=0}^{\infty}\int_{-\infty}^{\infty}\frac{dk_x}{2\pi}\int_{-\infty}^{\infty}\frac{dk_y}{2\pi}\,\theta(E_F - E_n(k_x, k_y)), \tag{4.38}$$

where the factor of 2 accommodates two electrons in each state. The k-integrals are evaluated trivially to yield

$$n_e = \frac{\pi}{2d^3}\sum_{n=0}^{[N]}(N^2 - n^2) = \frac{\pi}{2d^3}\left[\left([N]N^2 - \frac{1}{3}[N]^3\right) + \left(N^2 - \frac{1}{2}[N]^2\right) - \frac{1}{6}[N]\right], \tag{4.39}$$

where $[N]$ is the integer part of N, which is defined as

$$N = \sqrt{\frac{2m^* E_F d^2}{\hbar^2\pi^2}} = \frac{k_F d}{\pi} = \frac{2d}{\lambda_F}, \tag{4.40}$$

and expressed in terms of Fermi wave-vector, k_F, and Fermi wavelength, λ_F, defined for suitable insight. For metals described by the Drude-Sommerfeld's model the Fermi wavelength ranges between 0.3 nm - 1 nm. Notice that the limit $\hbar \to 0$ limit is

equivalent to taking $k_F \to \infty$ ($N \to \infty$). The number density in the limit $N \to \infty$ is

$$n_e(\infty) = \frac{\pi}{2d^3}\frac{2}{3}N^3 = \frac{k_F^3}{3\pi^2}, \tag{4.41}$$

Using Eq. (4.41) in Eq. (4.39) we have

$$n_e(N) = n_e(\infty)\nu(x), \tag{4.42}$$

where

$$\nu(x)=n_e(\infty)\left[\frac{3}{2}\left(x-\frac{1}{3}x^3\right)+\frac{3}{2N}\left(1-\frac{1}{2}x^2\right)-\frac{1}{4N^2}x\right], \qquad x=\frac{[N]}{N}. \tag{4.43}$$

We note the limiting cases (see Figure 4.3)

$$x = \frac{[N]}{N} \to \begin{cases} 0 & \text{if} \quad N < 1, \\ 1 & \text{if} \quad N \to \infty. \end{cases} \tag{4.44}$$

Convergence of x to unity is very slow. In particular we make an error of 1% in replacing $x \to 1$ even for N=100. The limiting cases for $\nu(x)$ in Eq. (4.43) are:

$$\nu(x) \to \begin{cases} \frac{3\pi}{2k_F d} & \text{if} \quad N < 1, \\ 1 & \text{if} \quad N \to \infty. \end{cases} \tag{4.45}$$

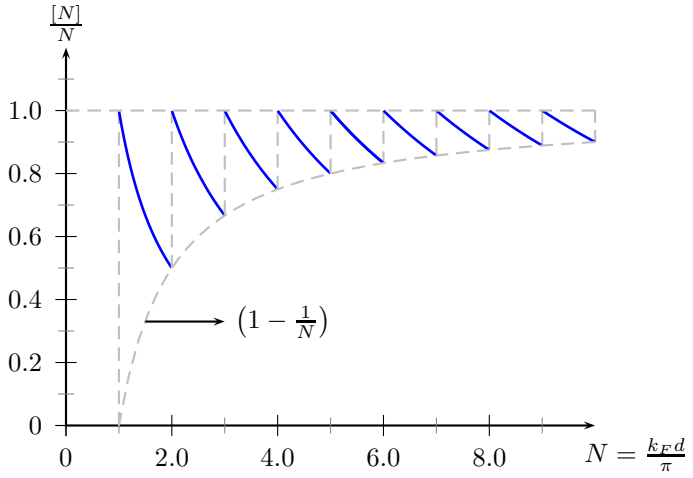

Figure 4.3: Fractional Floor function $\frac{[N]}{N}$ plotted with respect to N.

Using Eq. (4.45) we have the following limiting expressions for the number density in Eq. (4.42):

$$n_e(N) \to n_e(\infty) \begin{cases} \frac{3}{2N} & \text{if} \quad N < 1 \ (2d < \lambda_F), \\ 1 & \text{if} \quad N \to \infty \ (2d \gg \lambda_F). \end{cases} \tag{4.46}$$

For the first case corresponding to the thin-plate regime, we see the explicit dependence on the thickness of the plate. This is expected in the sense that we can intuitively get this dependence by a dimensional argument.

4.2.2 de-Haas–van Alphen effect

The third term inside the square bracket on the right hand side of Eq. (4.37) exhibits the discretization of the Fourier modes due to confinement. The energy of a charged particle in the presence of a magnetic field also involves an analogous discretization

$$E_n^{\text{mag}}(k_x, k_y) = \frac{\hbar^2}{2m^*}\left[k_x^2 + k_y^2 + n^2\frac{2eB}{\hbar c}\right], \qquad n = 0, 1, 2, \ldots, \tag{4.47}$$

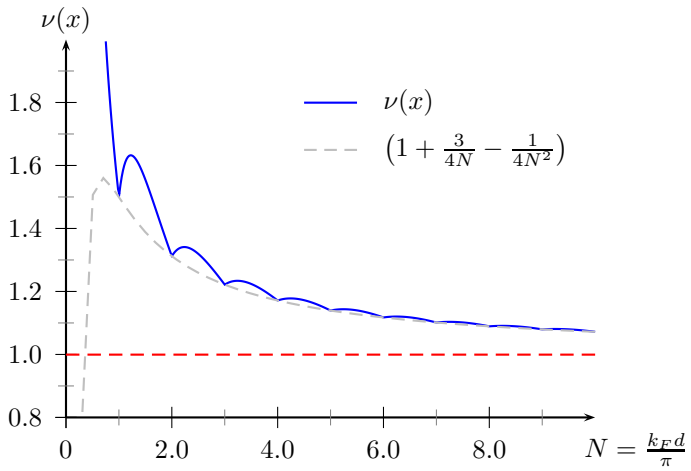

Figure 4.4: Plot of $\nu(x)$ versus N.

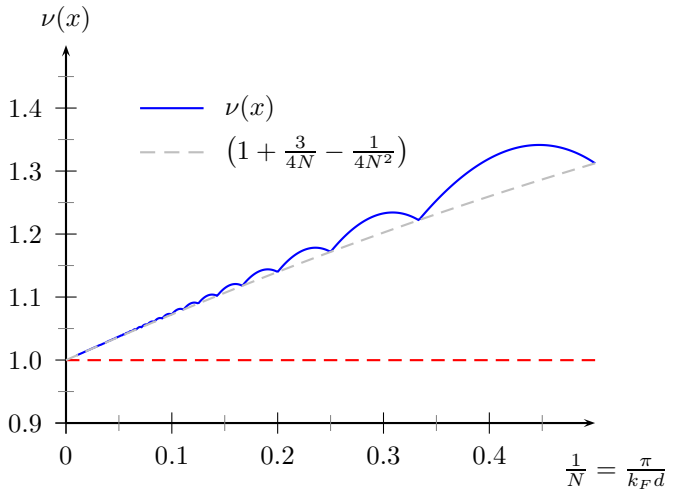

Figure 4.5: Plot of $\nu(x)$ versus $\frac{1}{N}$.

which is the famous Landau quantization. Comparison of Eqs. (4.37) and (4.47) suggests the following correspondence between quantum thin plate effects and the quantization effects due to the presence of the magnetic field:

$$\frac{d^2}{\pi^2} \leftrightarrow \frac{\hbar c}{2eB}. \tag{4.48}$$

de-Haas and van-Alphen in 1930 experimentally measured the magnetization of a sample of bismuth as a function of high magnetic field at relatively low temperatures, and found oscillations in the plot. The interpretation of these oscillations was given by Onsager in 1952. These oscillations were earlier predicted in 1930 by Landau [93], who was unaware of the experimental result. This phenomenon which is a signature of a purely quantum effect has been observed in measurements of various other physical quantities [94]. The de-Haas–van Alphen effect is used to probe the Fermi surface of a material and to measure the number density.

The oscillations in the function $\nu(x)$, see Eq. (4.43), plotted in Figures 4.4 and 4.5, are the source of the de-Haas–van Alphen oscillations. For comparison refer to Figure 14.3 in [94].

4.2.3 Plasma frequency

Using Eq. (4.46) in Eq. (4.36) we have the quantum correction to the plasma frequency due to finite thickness of the plate to be

$$[\omega_p(N)]^2 = [\omega_p(\infty)]^2 \nu(x) \to [\omega_p(\infty)]^2 \begin{cases} \frac{3}{2N} & \text{if} \quad N < 1 \ (2d < \lambda_F), \\ 1 & \text{if} \quad N \to \infty \ (2d \gg \lambda_F), \end{cases} \tag{4.49}$$

where $\omega_p(\infty)$ was introduced in Eq. (4.36) and can be written in the form (using Eq. (4.41))

$$[\omega_p(\infty)]^2 = \frac{(ck_F)^3}{\omega_0}. \tag{4.50}$$

We introduced

$$\frac{1}{\omega_0} = \frac{e^2}{3\pi^2 m^*}. \tag{4.51}$$

Typical numbers for metals that are described well by Drude-Sommerfeld's model of free electron gas are:

$$\omega_p(\infty)=(1-7)\times 10^{15}\frac{\text{rad}}{\text{s}} \qquad \text{for typical thick metals,} \tag{4.52}$$

$$ck_F=(1-6)\times 10^{18}\frac{\text{rad}}{\text{s}} \qquad \text{for typical thick metals,} \tag{4.53}$$

$$\omega_0=3.2\times 10^{24}\frac{\text{rad}}{\text{s}} \qquad \text{for } m^*=m_e. \tag{4.54}$$

Using the above we obtain that for materials described by Drude-Sommerfeld's model we have

$$\frac{\omega_p(\infty)}{ck_F} \sim 10^{-3}. \tag{4.55}$$

4.3 Casimir energy for materials described by Drude-Sommerfeld model

The plasma model is described by Eq. (4.35),

$$(\varepsilon_i - 1)\zeta^2 = [\zeta_{pi}(\infty)]^2, \tag{4.56}$$

where $\zeta_{pi}(\infty)$ is the classical plasma frequency of the i-th plate, after Euclidean rotation. We shall limit our discussion to plasma models because Casimir energies are relatively easier to analyze in this regime. The Casimir energy between slabs described by plasma model is given by Eq. (4.26) in conjunction with Eq. (4.56),

$$\mathcal{E}(a, d_i, \varepsilon_i - 1) \to \mathcal{E}_L(a, d_i; \zeta_{pi}(\infty)), \tag{4.57}$$

where the subscript stands for Lifshitz even though the above expression is generalized to be applicable for slabs of finite thickness. We have restricted ourselves by choosing the plasma model for simplicity, which is emphasized by the use of arrow instead of equal. $\zeta_{pi}(\infty)$ thus represents a parameter that describes the dielectric constant $(\varepsilon_i - 1)$.

The Drude-Sommerfeld model is obtained in the model by the replacement

$$\omega_p(\infty) \to \omega_p(N) \tag{4.58}$$

in Eq. (4.57) using Eq. (4.49), which leads to the expression for the Casimir energy between slabs described by Drude-Sommerfeld's model as

$$\mathcal{E}_L(a, d_i; \zeta_{pi}(\infty)) \to \mathcal{E}_P(a, d_i; \zeta_{pi}(N)), \tag{4.59}$$

where the subscript 'P' now stands for 'Plates'.

Use of the Fermi energy introduces a model dependent scale in the problem. In the Drude-Sommerfeld model we have the relation between the $\omega_p(\infty)$ and k_F given

by Eq. (4.50). We shall prefer to keep them independent though and replace

$$\mathcal{E}_P(a, d_i; \zeta_{pi}(N)) \to \mathcal{E}_P(a, d_i; \zeta_{pi}(\infty), k_{Fi}), \tag{4.60}$$

with the understanding that a particular model provides the relation between $\zeta_p(\infty)$ and k_F. Since $\omega_p(N) \to \omega_p(\infty)$ in the limit $k_F \to \infty$, we conclude that the expression for the Casimir energy between two slabs given by $\mathcal{E}_L(a, d_i; \zeta_{pi}(\infty))$ is obtained by taking $k_F \to \infty$ in the generalized expression. Thus we have the relation

$$\mathcal{E}_P(a, d_i; \zeta_{pi}(\infty), \infty) = \mathcal{E}_L(a, d_i; \zeta_{pi}(\infty)). \tag{4.61}$$

We choose the Fermi momentum to set the scale in the problem by fixing $k_F = 1$. This leads to the following redefinition of the parameters

$$\mathcal{E}_P(a, d_i; \zeta_{pi}(\infty), k_{Fi}), \to \mathcal{E}_P(k_F a, N; \pi \frac{\zeta_{pi}(\infty)}{c k_{Fi}}, k_{Fi}). \tag{4.62}$$

Plots of $\mathcal{E}_P(k_F a, N; \pi \frac{\zeta_{pi}(\infty)}{c k_{Fi}}, k_{Fi})$ for various values of $\frac{\zeta_{pi}(\infty)}{c k_{Fi}}$ have been generated in Figures 4.6. For $\frac{\zeta_{pi}(\infty)}{c k_{Fi}} \ll 1$ the percentage deviations relative to the corresponding Lifshitz formula are about 20%. However, the Casimir energy itself is relatively small for $\frac{\zeta_{pi}(\infty)}{c k_{Fi}} \ll 1$. The most remarkable deviation is in the modified expression for the Casimir energy between two slabs having a non-zero limit as the thickness of one of the slabs goes to zero, $d \to 0$.

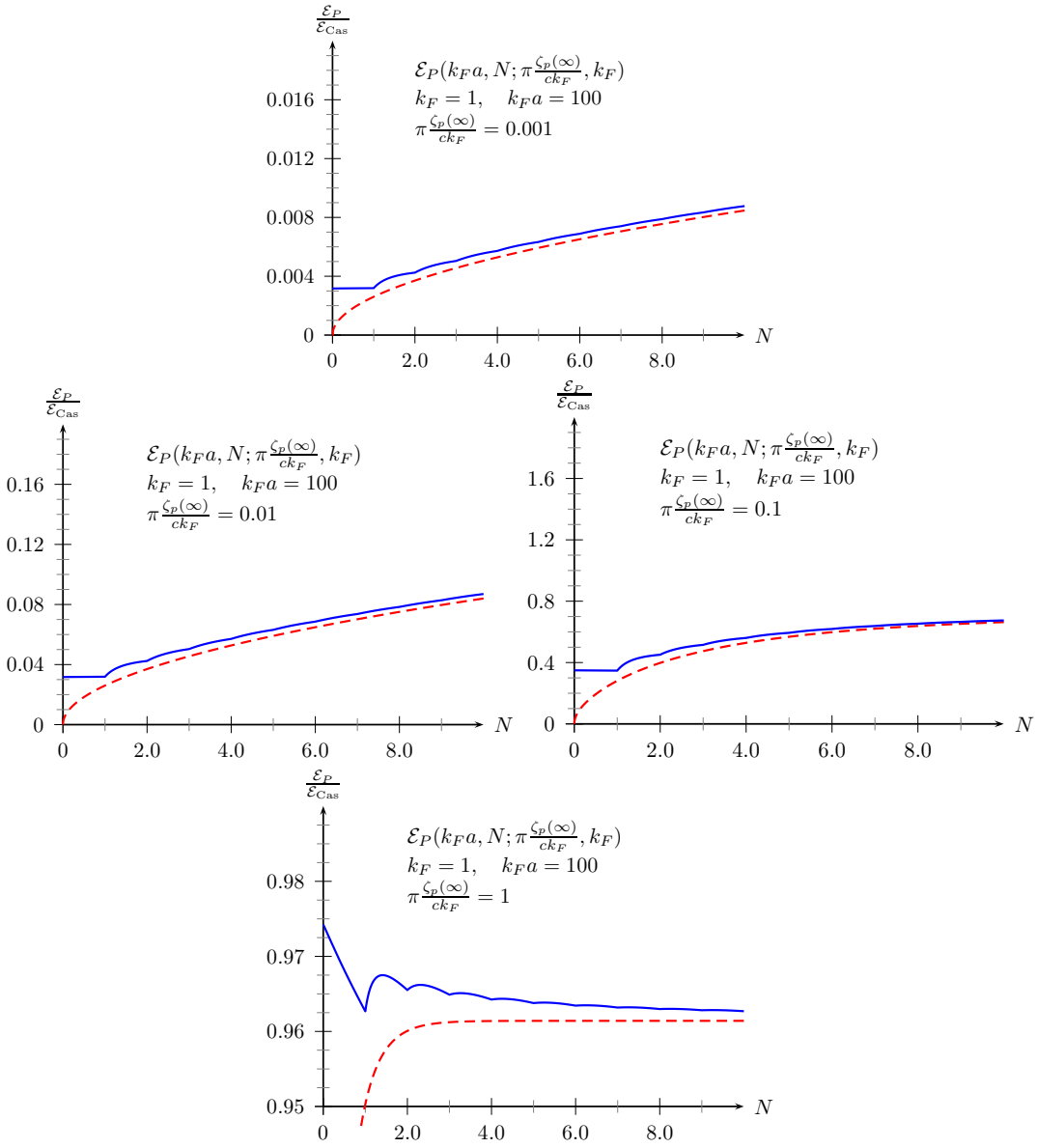

Figure 4.6: Plot of $\mathcal{E}_P(k_Fa, N; \pi\frac{\zeta_{pi}(\infty)}{ck_{Fi}}, k_{Fi})$ for $k_fa = 100$. The Drude-Sommerfeld model for metals is realized for $\frac{\zeta_{pi}(\infty)}{ck_{Fi}} = 0.001$.

4.4 Semi-transparent δ-function conducting thin-plates

Using Eq. (4.49) which generalized the definition of the plasma frequency as a guiding principle we claim that an infinitesimally thin conducting slab will always be described by the model

$$(\varepsilon_i - 1)\zeta^2 = \frac{\lambda_i}{d_i}, \tag{4.63}$$

where λ_i is a parameter with dimensions of inverse length. ($\lambda_i \to \lambda_i c^2,\ c = 1.$)

Restricting ourselves to frequencies and wavelength of the order

$$\zeta^2 \ll \frac{\lambda_i}{d_i}, \qquad k^2 \ll \frac{\lambda_i}{d_i}, \tag{4.64}$$

which are good approximations for a thin plate, we make the following leading-order replacements:

$$\varepsilon_i \sim \frac{\lambda_i}{d_i \zeta^2}\left[1 + \mathcal{O}\left(\zeta^2 \frac{d_i}{\lambda_i}\right)\right], \tag{4.65a}$$

$$\kappa_i \sim \sqrt{\frac{\lambda_i}{d_i}}\left[1 + \mathcal{O}\left(\zeta^2 \frac{d_i}{\lambda_i}, \kappa^2 \frac{d_i}{\lambda_i}\right)\right]. \tag{4.65b}$$

Using the above approximations to calculate the Casimir energy between two slabs of finite thickness translates to bounding the limits of integrations in Eq. (4.26) as

$$\mathcal{E}(a, d_i; \varepsilon_i - 1) \to \mathcal{E}_{\mathrm{TP}}(a, d_i; \lambda_i) \sim \frac{1}{2}\int_{-\sqrt{\frac{\lambda_i}{d_i}}}^{\sqrt{\frac{\lambda_i}{d_i}}} \frac{d\zeta}{2\pi}\left[\int_{-\sqrt{\frac{\lambda_i}{d_i}}}^{\sqrt{\frac{\lambda_i}{d_i}}} \frac{dk}{2\pi}\right]^2 \Big\{ \cdots \Big\}, \tag{4.66}$$

where 'TP' denotes thin plate, and the curly bracket represents the corresponding term in Eq. (4.26). Rescaling the integral parameters with a then tells us that the

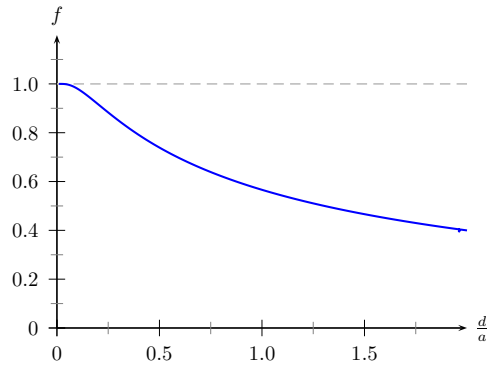

Figure 4.7: Fractional error in Casimir energy due to thin plate approximation as a function of d/a for $\lambda a = 1$.

thin plate approximation gives a good estimate of Casimir energy in the regime

$$\frac{d_i}{a} \ll \lambda_i a. \tag{4.67}$$

This has been illustrated in Figure 4.7 where we plot the the ratio of Casimir energy with the cutoff limits over the complete integral limits. The approximation contributes to less than 10% error for $\frac{d}{a} < 10\,\lambda a$.

Using the leading-order replacements in Eq. (4.65) we can further derive

$$\alpha_i \sim 1, \qquad \bar{\alpha}_i \sim -1, \qquad \frac{1}{\Delta_i} \sim \frac{\lambda_i}{\lambda_i + 2\kappa}, \qquad \frac{1}{\bar{\Delta}_i} \sim \frac{\lambda_i}{\lambda_i + 2\frac{\zeta^2}{\kappa}}. \tag{4.68}$$

The above thin plate approximations when substituted in Eq. (4.26) leads to a non-zero contribution to the Casimir energy given as

$$\mathcal{E}_{\rm TP}(a,\lambda_i) = \frac{1}{2}\int_{-\infty}^{\infty}\frac{d\zeta}{2\pi}\int\frac{d^2k}{(2\pi)^2}\left\{\ln\left[1-t_1(\kappa)t_2(\kappa)\,e^{-2\kappa a}\right]+\ln\left[1-t_1\left(\tfrac{\zeta^2}{\kappa}\right)t_2\left(\tfrac{\zeta^2}{\kappa}\right)\,e^{-2\kappa a}\right]\right\}, \tag{4.69}$$

where

$$t_i(\kappa) = \frac{\lambda_i}{\lambda_i + 2\kappa}. \tag{4.70}$$

We note the feature that the magnetic contribution to the Casimir energy in the thin plate limit is obtained by the replacement

$$\kappa \to \frac{\zeta^2}{\kappa} \tag{4.71}$$

inside the transition coefficients of the electric contribution. This was observed in the calulation of the lateral Casimir force between corrugated thin plates (see Chapter 6) and thus seems to be a generic feature in the thin plate limit.

Taking thin-plate limit first

It is of interest to ask if infinitesimally thin plates can be described using δ-function potentials. To answer this assertively we begin by replacing the potentials in Eq. (4.1) with its δ-function limits after introducing d_i's in the expression. Thus, we consider

$$V(z) = \frac{\lambda_1}{\zeta^2}\,\delta(z - b_1) + \frac{\lambda_2}{\zeta^2}\,\delta(z - a_2). \tag{4.72}$$

Most of the discussion in Section 4.1 remains the same with the change appearing in the following expression

$$\mathbf{K}(i\zeta, k) = \lambda_1\,\lambda_2 \left[\boldsymbol{\gamma}^{\mathrm{TP}}_{1⑨}(z', z; i\zeta, k) \cdot \boldsymbol{\gamma}^{\mathrm{TP}}_{2④}(z, z'; i\zeta, k)\right]_{\substack{z=b_1 \\ z'=a_2}}, \tag{4.73}$$

where the reduced Green's dyadic with superscript TP are now for the thin plates. The difference now is that we are taking the thin plate limit before carrying out the z

and z' integration while in the earlier part of the section it was done other way. The expressions for K^E and K^H now read as

$$\begin{aligned} K^E_{d_i\to 0}(i\zeta,k) &= \lambda_1\lambda_2\Big[g^E_{1⑨}(z',z;i\zeta,k)g^E_{2④}(z,z';i\zeta,k)\Big]_{\substack{z=b_1\\ z'=a_2}} \\ &= \mu^E_{1,d_1\to 0}(i\zeta,k)\mu^E_{2,d_2\to 0}(i\zeta,k), \end{aligned} \tag{4.74}$$

$$\begin{aligned} \operatorname{tr}\mathbf{K}^H_{d_i\to 0}(i\zeta,k) &= \frac{\lambda_1}{\varepsilon_1}\frac{\lambda_2}{\varepsilon_2}\left[\left(1-\frac{\kappa}{\zeta^2}\frac{\partial}{\partial z}\right)\left(1+\frac{\kappa}{\zeta^2}\frac{\partial}{\partial z'}\right)g^H_{1⑨}(z',z)g^H_{2④}(z,z')\right]_{\substack{z=b_1\\ z'=a_2}} \\ &= \mu^H_{1,d_1\to 0}(i\zeta,k)\mu^H_{2,d_2\to 0}(i\zeta,k), \end{aligned} \tag{4.75}$$

where $d_i \to 0$ represents the thin plate result. Using

$$\begin{aligned} \mu^E_{i,d_i\to 0}(i\zeta,k) &= \frac{\lambda_i}{\lambda_i+2\kappa}\frac{1}{2}u^E_{i,d_i\to 0}(a_i) \\ &= \frac{\lambda_i}{\lambda_i+2\kappa}\,e^{-\kappa a}, \end{aligned} \tag{4.76}$$

$$\begin{aligned} \mu^H_{i,d_i\to 0}(i\zeta,k) &= -\frac{\lambda_i}{\lambda_i+2\frac{\zeta^2}{\kappa}}\frac{1}{2}\sqrt{\frac{d_i}{\lambda_i}}\left[\frac{\partial}{\partial z}u^H_{i,d_i\to 0}(z)\right]_{z=a_i} \\ &= -\frac{\lambda_i}{\lambda_i+2\frac{\zeta^2}{\kappa}}\,e^{-\kappa a}, \end{aligned} \tag{4.77}$$

which leads to the same result as we obtained earlier in Eq. (4.69).

Taking $\lambda_i \to \infty$ limit leads to the standard Casimir energy between two perfectly conducting plates. This agrees with the results given in [95] for the Casimir energy for the two perfectly conducting thin plates.

4.5 Casimir-Polder energy for thick and thin conductors

In [95] Bordag found that the Casimir-Polder force for the infinitesimally thin perfect conductor is 13% less than the standard value while for a thick conductor it is unchanged. It is therefore relevant to check these results using our method for taking the thin plate limit. In this Section we present the Casimir-Polder energy for an atom in front of a thick dielectric slab and thin conducting plate. We take the perfect conductor limit in both cases to obtain the standard Casimir-Polder result.

4.5.1 Atom in front of a thick dielectric slab

Let us consider the physical situation of an atom in front of a dielectric slab shown in Figure 4.8. The background potential for this system is described by

$$\begin{aligned} V(\mathbf{x};i\zeta) &= V_1(\mathbf{x};i\zeta) + V_1(\mathbf{x};i\zeta) \\ &= (\varepsilon_1(i\zeta)-1)\left[\theta(z-a)-\theta(z-b)\right] + 4\pi\boldsymbol{\alpha}_P(i\zeta)\delta^{(3)}(\mathbf{x}-\mathbf{x}_0). \end{aligned} \tag{4.78}$$

where $\boldsymbol{\alpha}_P(i\zeta)$ is the polarizability tensor of the atom, which is located at $\mathbf{x}_0 = (0,0,a_2)$. We have kept the frequency dependence of the permittivity to keep expressions general. Since the atom interacts weakly with the slab, only the single scattering term from the expansion of the multiple scattering formula given by Eq. (2.43)

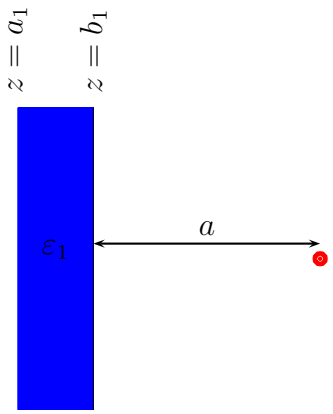

Figure 4.8: Atom in front of a finite size dielectric slab.

is important. Thus the interaction energy is given by

$$\begin{aligned} E_{12}^{CP} =& -\frac{1}{2}\int_{-\infty}^{\infty}\frac{d\zeta}{2\pi}\,\mathrm{Tr}\,\mathbf{\Gamma}_1\cdot\mathbf{V}_1\cdot\mathbf{\Gamma}_0\cdot\mathbf{V}_2 \\ =& -\frac{1}{2}\int_{-\infty}^{\infty}\frac{d\zeta}{2\pi}\left[4\pi\boldsymbol{\alpha}_P(i\zeta)\right]\cdot\int d^3x\,\mathbf{\Gamma}_1(\mathbf{x}_0,\mathbf{x})\cdot\mathbf{V}_1(\mathbf{x})\cdot\mathbf{\Gamma}_0(\mathbf{x},\mathbf{x}_0) \\ =& -\frac{1}{2}\int_{-\infty}^{\infty}\frac{d\zeta}{2\pi}\left[4\pi\boldsymbol{\alpha}_P(i\zeta)\right]\cdot\left[\mathbf{\Gamma}_1-\mathbf{\Gamma}_0\right]. \end{aligned} \tag{4.79}$$

For an isotropic polarizable atom we have

$$E_{12}^{CP} = \frac{1}{2}\int_{-\infty}^{\infty}\frac{d\zeta}{2\pi}\int_{-\infty}^{\infty}\frac{d^2k}{2\pi}\left[4\pi\alpha_P(i\zeta)\right](\varepsilon_1(i\zeta)-1)K(k,\zeta;a,d_1), \tag{4.80}$$

where

$$K(k,\zeta;a,d_1) = \int_{a_1}^{b_1} dz\,\mathrm{tr}\,\boldsymbol{\gamma}_1(a_2,z;k,\zeta)\cdot\boldsymbol{\gamma}_0(z,a_2;k,\zeta). \tag{4.81}$$

Using Eqs. (2.52),(3.4), and (3.5) we can write the explicit form for the reduced free Green's dyadic as

$$\boldsymbol{\gamma}_0(z,z';i\zeta,k)=\begin{bmatrix} -\kappa^2 & 0 & -ik\kappa\,\eta(z-z') \\ 0 & \zeta^2 & 0 \\ -ik\kappa\,\eta(z-z') & 0 & k^2 \end{bmatrix}\frac{1}{2\kappa}\,e^{-\kappa|z-z'|}, \tag{4.82}$$

where $\eta(z)=1$ if $z>1$, and $\eta(z)=-1$ if $z<1$. Using this and Eq. (2.72) we have the result

$$E_{12}^{CP}=-\frac{1}{2}\int_{-\infty}^{\infty}\frac{d\zeta}{2\pi}[4\pi\alpha_P(i\zeta)]\int\frac{d^2k}{(2\pi)^2}\,e^{-2\kappa a}\left[\frac{(\kappa^2-k^2)}{2\kappa}\frac{\alpha_1}{\Delta_1}-\frac{(\kappa^2+k^2)}{2\kappa}\frac{\bar{\alpha}_1}{\bar{\Delta}_1}\right], \tag{4.83}$$

which is the expected result found in the literature [15]. In the thick-plate limit $d\to\infty$ we have

$$E_{12}^{CP(d\to\infty)}=-\frac{1}{2}\int_{-\infty}^{\infty}\frac{d\zeta}{2\pi}[4\pi\alpha_P(i\zeta)]\int\frac{d^2k}{(2\pi)^2}\,e^{-2\kappa a}\left[\frac{(\kappa^2-k^2)}{2\kappa}\alpha_1-\frac{(\kappa^2+k^2)}{2\kappa}\bar{\alpha}_1\right]. \tag{4.84}$$

If the polarizability is independent of the frequency then taking the perfect conductor limit $\varepsilon_1\to\infty$ we reproduce the standard Casimir-Polder energy

$$E_{12}^{CP(\varepsilon_1\to\infty)}=-\frac{3\alpha_P}{8\pi a^4}. \tag{4.85}$$

4.5.2 Atom in front of a δ-function conducting plate

We can take the thin-plate limit $d \to 0$ in Eq. (4.83) described in Sections 4.2 and 4.4

$$E_{12}^{CP(d\to 0)} = -\frac{1}{2}\int_{-\infty}^{\infty}\frac{d\zeta}{2\pi}[4\pi\alpha_P(i\zeta)]\int_{-\infty}^{\infty}\frac{d^2k}{(2\pi)^2}\,e^{-2\kappa a}\Big[\frac{(\kappa^2-k^2)}{2\kappa}\frac{\lambda_1}{\lambda_1+2\kappa} + \frac{(\kappa^2+k^2)}{2\kappa}\frac{\lambda_1}{\lambda_1+2\frac{\zeta^2}{\kappa}}\Big]. \tag{4.86}$$

In the perfect conductor limit $\lambda_1 \to \infty$

$$E_{12}^{CP(\lambda_1\to\infty)} = -\frac{1}{2}\int_{-\infty}^{\infty}\frac{d\zeta}{2\pi}[4\pi\alpha_P(i\zeta)]\int_{-\infty}^{\infty}\frac{d^2k}{(2\pi)^2}\,e^{-2\kappa a}\kappa, \tag{4.87}$$

which when $\alpha_P(i\zeta)$ is independent of frequency gives the standard Casimir Polder result

$$E_{12}^{CP(\varepsilon_1\to\infty)} = -\frac{3\alpha_P}{8\pi a^4}. \tag{4.88}$$

Thus a δ-function perfectly conducting thin-plate interacting with an atom reproduces the Casimir-Polder energy exactly, which we believe is the correct result. For a perfect conductor the field goes to zero at the surface and the skin depth of the material is zero as well. Therefore the region beyond the slab or plate does not contribute to the energy. We believe that the thickness of the material should not affect the perfect conductor results.

4.5.3 Discussion

As we see in previous subsection our result does not agree with Bordag's claim of reduction of 13% in the Casimir Polder energy for an atom in front of a thin conductor [95]. He attributes the origin of this discrepancy to the freedom in choice of the

boundary condition for the normal component of the electric field $E_\perp$. For a perfect conductor the required boundary conditions are $E_\parallel = H_\perp = 0$. This, according to him leaves room to impose different boundary conditions on the normal component of the electric field in different cases. However, notice that if the boundary conditions for perfect conductor are used in conjunction with the Maxwell's equation ($\boldsymbol{\nabla} \cdot \mathbf{E} = 0$) for a charge–and current-less space then the condition on the third component is unambiguously fixed. This according to him is the case for the thick material, while for the thin material the third component remains free. He shows the calculation for the energy, for the two cases, by calculating propagator for the photon field. We can easily check that the electric field obtained from both the forms are same, which indicates that the energy obtained from the two forms should also be the same. This seems to be a puzzling result, which we intend to discuss with him personally.

In this context we should also point out previous work by Fetter in [96], where he considers the motion of an electron in the vicinity of a thin-plate modeled by the electron gas in presence of neutralizing background and shows that the dynamics of the electron is different in this case from the bulk material. He, however, considers only real conductors and is not considering quantum vacuum effects.

Chapter 5

Casimir torque: Cylindrical non-contact gears

In the previous chapter we concentrated on the planar background potential, which depends only on one length parameter. Thus the Casimir energy per unit area also depends on one parameter. If we define the Casimir force as the change in the Casimir energy with respect to the separation parameter, we get the force acting normal to the planar surface. However, ideally material surfaces are not smooth and have surface roughness and corrugations. In such a case the potential would be two or three dimensional and we can expect the presence of a force lateral to the surface in addition to the normal force [97, 98]. On one hand it is very interesting as it leads to possibilities of designing nano-gears [99, 100, 101]. On the other hand solving the problem analytically gets difficult as the potential is no longer separable. Theoretical analysis of the lateral Casimir force has been done using the proximity force approximation, piecewise summation, the perturbative approximation, and exact numerical calculations. Experimentally it has been verified to very good accuracy recently [102, 103, 104].

In this chapter we present the perturbative approach towards calculating the lateral Casimir force for the case of two concentric corrugated cylinders [105], which in this case would be the Casimir torque. The Casimir torque between two material bodies, which is the rotational analog of the Casimir force, was studied for the first time in 1973 [106]. The Casimir torque between two uni-axial birefringent dielectric plates was studied in [107]. A non-contact rack and pinion arrangement was first proposed by Ashourvan *et al* [100] and discussed in the proximity force approximation (PFA) limit. This proposal was generalized to the design of a non-contact gear consisting of two corrugated concentric cylinders in [108, 109] to discuss possible experimental arrangements.

5.1 Casimir torque

Let us consider two concentric corrugated cylinders described by the semi-transparent δ-function potentials,

$$V_i(r,\theta) = \lambda_i\,\delta(r - a_i - h_i(\theta)), \tag{5.1}$$

where $i = 1, 2$ refer to the individual cylinders. The mean distance between the cylinders is $a = a_2 - a_1 > 0$, and the functions $h_i(\theta)$ describe the profile of the corrugations associated with the individual cylinders. We define the function

$$a(\theta) = a + h_2(\theta) - h_1(\theta), \tag{5.2}$$

which measures the relative corrugations between the cylinders. The corrugations $h_i(\theta)$ are chosen in a way such that the mean of the relative corrugations evaluates

to a over a period,

$$\frac{1}{2\pi}\int_0^{2\pi} d\theta \left[h_2(\theta) - h_1(\theta)\right] = 0. \tag{5.3}$$

Rotation of one cylinder with respect to the other changes the geometric configuration of the background potential leading to the change in the total energy. This will give rise to a torque between the cylinders, which is given by

$$\mathcal{T} = -\frac{\partial E}{\partial \theta_0}, \tag{5.4}$$

where E is the total Casimir energy associated with the two concentric corrugated cylinders, including the divergent contributions associated with the single cylinders. Angular rotation, θ_0, describes the shift of the corrugations on the inner cylinder as $h_1(\theta + \theta_0)$.

When both the cylinders are uncorrugated or when either one of the cylinders is uncorrugated, rotation of one cylinder with respect to the other does not change the geometric configuration of the system. Hence, there are no torques in these cases. Using this fact we can now write the total energy as

$$E = E^{(0)}(a) + E_1(a, h_1) + E_2(a, h_2) + E_{12}(a, h_1, h_2, \theta_0), \tag{5.5}$$

where, $E^{(0)}$ is the energy of the configuration when both the cylinders are uncorrugated, E_i is the additional contribution to the Casimir energy when one of the cylinders is uncorrugated, and E_{12} is the contribution to the energy which is present only when both cylinders are corrugated. Thus E_i is expected to go to zero if the corrugations $h_i(\theta)$ goes to zero. Similarly, the interaction energy E_{12} goes to zero when either of the corrugations h_i is zero. The interaction energy does not change

when the angular rotation is in multiples of 2π. Thus, E_{12} is the interaction energy due to the presence of corrugation, and only this term in Eq. (5.5) contributes to the torque between the cylinders. We treat the uncorrugated cylindrical configuration as a background whose potential is

$$V_i^{(0)}(r) = \lambda_i \delta(r - a_i), \qquad i = 1, 2, \tag{5.6}$$

which has no angular dependence. We can further write

$$\Delta E = E - E^{(0)} = E_1 + E_2 + E_{12}, \tag{5.7}$$

where we suppress the dependencies of the various terms. Δ represents the deviation of the quantity from the background. Thus we can define the potential of the corrugated cylinders as

$$V_i = V_i^{(0)} + \Delta V_i, \qquad i = 1, 2. \tag{5.8}$$

5.1.1 Casimir energy contributing to the lateral force

Using the formula Eq. (2.32) to evaluate the change in the total energy from the background energy given by Eq. (5.7), we have

$$\Delta E = E - E^{(0)} = \frac{i}{2\tau} \operatorname{Tr} \ln G G_0^{-1} - \frac{i}{2\tau} \operatorname{Tr} \ln G^{(0)} G_0^{-1} = \frac{i}{2\tau} \operatorname{Tr} \ln G {G^{(0)}}^{-1}, \tag{5.9}$$

where G_0 is the free Green's function, which satisfies Eq. (2.34). Note that G_0 cancels in the above expression and the reference now is with respect to the uncorrugated surfaces. The Green's function G satisfies Eq. (2.33). The potentials in our case are

disjoint so we can symbolically write the Green's function equation as

$$\Big[-\partial^2 + V_1 + V_2 \Big] G = 1. \tag{5.10}$$

Similarly the Green's function associated with the background satisfies the differential equation,

$$\Big[-\partial^2 + V_1^{(0)} + V_2^{(0)} \Big] G^{(0)} = 1. \tag{5.11}$$

Then using above two equations and Eq. (5.8) we obtain

$$G {G^{(0)}}^{-1} = \Big[1 + G^{(0)} \Delta V_1 + G^{(0)} \Delta V_2 \Big]^{-1}. \tag{5.12}$$

Following steps in section 2.2 we can get the interaction energy term as

$$E_{12} = -\frac{i}{2\tau} \operatorname{Tr} \ln \Big[1 - G_1 \Delta V_1 G_2 \Delta V_2 \Big], \tag{5.13}$$

where G_i $(i = 1, 2)$ are the Green's functions for the configuration when only one of the cylinder has corrugations on it and it satisfies

$$\Big[-\partial^2 + V_1^{(0)} + V_2^{(0)} + \Delta V_i \Big] G_i = 1. \tag{5.14}$$

Using Eq. (5.11) we observe that

$$G_i {G^{(0)}}^{-1} = (1 + G^{(0)} \Delta V_i)^{-1} = 1 - G^{(0)} \Delta V_i (1 + G^{(0)} \Delta V_i)^{-1} = 1 - (1 + G^{(0)} \Delta V_i)^{-1} G^{(0)} \Delta V_i. \tag{5.15}$$

The interaction energy given by Eq. (5.13) is similar to the expression given by Eq. (2.43) except that now the background energy associated with the uncorrugated

cylinders has been subtracted out as evident from the ΔV_i terms.

5.1.2 Formal series expansion

Using Eq. (5.15) to expand $G_i \Delta V_i$ in terms of $G^{(0)} \Delta V_i$ we can write

$$G_i \Delta V_i = (-1)^n \sum_{n=1}^{\infty} \left(G^{(0)} \Delta V_i \right)^n . \tag{5.16}$$

We can now formally expand the logarithm given in Eq. (5.13) as a series in terms of background Green's function only

$$E_{12} = \frac{i}{2\tau} \operatorname{Tr} \sum_{m=1}^{\infty} \frac{1}{m} \left[\sum_{n_1=1}^{\infty} \sum_{n_2=1}^{\infty} (-1)^{n_1} (-1)^{n_2} \left\{ G^{(0)} \Delta V_1 \right\}^{n_1} \left\{ G^{(0)} \Delta V_2 \right\}^{n_2} \right]^m . \tag{5.17}$$

Our potentials in Eq. (5.1) can be formally expanded in powers of h_i as

$$\Delta V_i(r,\theta) = \sum_{n=1}^{\infty} V_i^{(n)}(r,\theta) = \sum_{n=1}^{\infty} \frac{[-h_i(\theta)]^n}{n!} \frac{\partial^n}{\partial r^n} V_i^{(0)}(r) = \lambda_i \left[e^{-h_i(\theta)\frac{\partial}{\partial r}} - 1 \right] \delta(z - a_i), \tag{5.18}$$

so we can further write the series expansion as

$$E_{12} = \frac{i}{2\tau} \operatorname{Tr} \sum_{m=1}^{\infty} \frac{1}{m} \left[\sum_{n_1=1}^{\infty} \sum_{n_2=1}^{\infty} (-\lambda_1)^{n_1} (-\lambda_2)^{n_2} \left\{ G^{(0)} \left[e^{-h_1 \partial} - 1 \right] \delta_1 \right\}^{n_1} \times \left\{ G^{(0)} \left[e^{-h_2 \partial} - 1 \right] \delta_2 \right\}^{n_2} \right]^m , \tag{5.19}$$

where we again use symbolic notation and suppress the variable dependence in h_i, ∂, and the delta functions. This expansion allows us to do calculations perturbatively in terms of background Green's functions, which has the advantage of solving them in the one-dimensional case.

5.2 Second order perturbation in Casimir energy due to corrugations

When the corrugations can be treated as small perturbations we can approximate the potentials by keeping a few terms in the expansion in Eq. (5.17). Thus, to the leading order the interaction energy of the corrugations in Eq. (5.17) is given by

$$E_{12}^{(2)} = \frac{i}{2\tau}\,\mathrm{Tr}\Big[G^{(0)}\Delta V_1^{(1)} G^{(0)}\Delta V_2^{(1)}\Big], \tag{5.20}$$

where the superscripts (2) represents the second order perturbation in a quantity, which here is the corrugation amplitude. In the leading order the potentials is

$$\Delta V_i(r,\theta) \approx V_i^{(1)}(r,\theta) = h_i(\theta)\frac{\partial}{\partial r}V_i^{(0)}(r), \tag{5.21}$$

where we have used the superscript (1) to represent the first order perturbation in the quantity.

5.2.1 Interaction energy

We presented the solution to the scalar Green's function for the two concentric cylinders in terms of the reduced Green's function in Section 3.4. Using the reduced Green's function defined in Eq. (3.26) we can write the interaction energy, to the leading order, in Eq. (5.20) as

$$\frac{E_{12}^{(2)}}{L_z} = \frac{1}{(2\pi)^2}\sum_{m=-\infty}^{\infty}\sum_{n=-\infty}^{\infty}(\tilde{h}_1)_{m-n}(\tilde{h}_2)_{n-m}\,L_{mn}^{(2)}, \tag{5.22}$$

where $(\tilde{h}_i)_m$ are the Fourier transforms of the functions describing the corrugations $h_i(\theta)$

$$(\tilde{h}_i)_m = \int_0^{2\pi} d\theta \, e^{-im\theta} \, h_i(\theta). \tag{5.23}$$

The kernel $L^{(2)}_{mn}$ in Eq. (5.22) can be written as

$$L^{(2)}_{mn} = -\frac{1}{4\pi} \int_0^{\infty} \kappa \, d\kappa \, I^{(2)}_{mn}(a_1, a_2; \kappa), \tag{5.24}$$

where $\kappa^2 = k_z^2 - \omega^2 = k_z^2 + \zeta^2$, after switching to imaginary frequencies by a Euclidean rotation, $\omega \to i\zeta$. The related matrix $I^{(2)}_{mn}(a_1, a_2; \kappa)$ is expressed as derivatives of the reduced Green's function in the form

$$I^{(2)}_{mn}(a_1, a_2; \kappa) = \lambda_1 \lambda_2 \frac{\partial}{\partial r} \frac{\partial}{\partial \bar{r}} \Big[r \, \bar{r} \, g^{(0)}_m(r, \bar{r}; \kappa) \, g^{(0)}_n(\bar{r}, r; \kappa) \Big] \Big|_{\bar{r}=a_1, r=a_2}. \tag{5.25}$$

The reciprocal symmetry in the Green's function leads to the following symmetry in the above kernel:

$$I^{(2)}_{mn}(a_1, a_2; \kappa) = I^{(2)}_{nm}(a_2, a_1; \kappa). \tag{5.26}$$

Thus we need to evaluate the reduced Green's functions and their derivatives at the point $\bar{r} = a_1, r = a_2$. Using Section 3.4 we can evaluate

$$g^{(0)}_m(a_1, a_2; \kappa) = \frac{1}{\Delta} \, I_1 K_2. \tag{5.27}$$

The relevant first derivatives are evaluated using the averaging prescription described in the appendix A of [110],which is not necessary in either the Dirichlet or weak limit,

as

$$\left\{\frac{\partial}{\partial r} g_m^{(0)}(r,r';\kappa)\right\}_{\substack{r=a_1\\ r'=a_2}} = \frac{\kappa}{\Delta}\left[I_1' K_2 + \frac{\lambda_1}{2\kappa} I_1 K_2\right], \tag{5.28a}$$

$$\left\{\frac{\partial}{\partial r} g_m^{(0)}(r,r';\kappa)\right\}_{\substack{r=a_1\\ r'=a_2}} = \frac{\kappa}{\Delta}\left[I_1 K_2' - \frac{\lambda_2}{2\kappa} I_1 K_2\right], \tag{5.28b}$$

where we have used a prime to denote the derivative of the modified Bessel function with respect to the argument. The derivatives acting on the second variable in the Green's function can be deduced using the symmetry of the Green's function. The relevant second derivatives are evaluated to be

$$\left\{\frac{\partial}{\partial r}\frac{\partial}{\partial r'} g_m^{(0)}(r,r';\kappa)\right\}_{\substack{r=a_1\\ r'=a_2}} = \frac{\kappa^2}{\Delta}\left[I_1' K_2' + \frac{\lambda_1}{2\kappa} I_1 K_2' - \frac{\lambda_2}{2\kappa} I_1' K_2 - \frac{\lambda_1}{2\kappa}\frac{\lambda_2}{2\kappa} I_1 K_2\right]. \tag{5.29}$$

The above evaluations used the Wronskian,

$$[I_m(x) K_m'(x) - I_m'(x) K_m(x)] = -\frac{1}{x}, \tag{5.30}$$

satisfied by the modified Bessel functions.

The expression in Eq. (5.25) is evaluated using Eqs. (5.27),

$$
\begin{aligned}
I^{(2)}_{mn}(a_1,a_2;\kappa)=\frac{\lambda_1\lambda_2}{\Delta\tilde{\Delta}}\Bigg[& I_1K_2\,\tilde{I}_1\tilde{K}_2 \\
& +\kappa a_1\, I_1K_2\left(\tilde{I}_1'\tilde{K}_2+\frac{\lambda_1}{2\kappa}\,\tilde{I}_1\tilde{K}_2\right)+\kappa a_1\left(I_1'K_2+\frac{\lambda_1}{2\kappa}\,I_1K_2\right)\tilde{I}_1\tilde{K}_2 \\
& +\kappa a_2\, I_1K_2\left(\tilde{I}_1\tilde{K}_2'-\frac{\lambda_2}{2\kappa}\,\tilde{I}_1\tilde{K}_2\right)+\kappa a_2\left(I_1K_2'-\frac{\lambda_2}{2\kappa}\,I_1K_2\right)\tilde{I}_1\tilde{K}_2 \\
& +\kappa a_1\kappa a_2\left(I_1K_2'-\frac{\lambda_2}{2\kappa}\,I_1K_2\right)\left(\tilde{I}_1'\tilde{K}_2+\frac{\lambda_2}{2\kappa}\,\tilde{I}_1\tilde{K}_2\right) \\
& +\kappa a_1\kappa a_2\left(I_1'K_2+\frac{\lambda_1}{2\kappa}\,I_1K_2\right)\left(\tilde{I}_1\tilde{K}_2'-\frac{\lambda_2}{2\kappa}\,\tilde{I}_1\tilde{K}_2\right) \\
& +\kappa a_1\kappa a_2\left(I_1'K_2'+\frac{\lambda_1}{2\kappa}\,I_1K_2'-\frac{\lambda_2}{2\kappa}\,I_1'K_2-\frac{\lambda_1}{2\kappa}\frac{\lambda_2}{2\kappa}\,I_1K_2\right)\tilde{I}_1\tilde{K}_2 \\
& +\kappa a_1\kappa a_2\, I_1K_2\left(\tilde{I}_1'\tilde{K}_2'+\frac{\lambda_1}{2\kappa}\,\tilde{I}_1\tilde{K}_2'-\frac{\lambda_2}{2\kappa}\,\tilde{I}_1'\tilde{K}_2-\frac{\lambda_1}{2\kappa}\frac{\lambda_2}{2\kappa}\,\tilde{I}_1\tilde{K}_2\right)\Bigg],
\end{aligned}
\tag{5.31}
$$

where we have used the notation in which the modified Bessel function with a tilde on it is of order n and that without a tilde is of order m. The tilde on Δ means that we use the corresponding modified Bessel functions in Eq. (3.30). Using this along with Eqs. (5.24) and (5.22) gives the interaction energy between two corrugated concentric cylinders. Notice that we still have an integration and two sums to perform. We shall analyze this result for two limiting cases—the Dirichlet (strong coupling) and the weak coupling limit.

5.2.2 Dirichlet limit

For the case of the Dirichlet limit ($a\lambda_{1,2} \gg 1$) the expression in Eq. (5.31) takes the relatively simple form

$$\begin{aligned} I_{mn}^{(2)D}(a_1, a_2; \kappa) &= -\frac{1}{a_1 a_2} \frac{1}{[I_2 K_1 - I_1 K_2]} \frac{1}{[\tilde{I}_2 \tilde{K}_1 - \tilde{I}_1 \tilde{K}_2]} \\ &= -\frac{1}{a_1 a_2} \frac{1}{D_m(\alpha; \kappa R)} \frac{1}{D_n(\alpha; \kappa R)} \end{aligned} \tag{5.32}$$

where the superscript D stands for Dirichlet, and we have introduced the function

$$D_m(\alpha; x) = I_m\Big(x[1+\alpha]\Big) K_m\Big(x[1-\alpha]\Big) - I_m\Big(x[1-\alpha]\Big) K_m\Big(x[1+\alpha]\Big), \tag{5.33}$$

to save typographical space. $R = (a_1 + a_2)/2$ is the mean radius of the two cylinders under consideration, and $\alpha = a/2R$ is a related variable, which by definition is less than unity. We note that

$$\frac{a^2}{a_1 a_2} = \frac{4\,\alpha^2}{(1-\alpha^2)}. \tag{5.34}$$

Two cylinders with very large radius, such that $a_i \to \infty$ with a kept fixed, will simulate a parallel plate in the region of small variations in the angle ($\theta \to 0$). This corresponds to $m, n \to \infty$, such that m/R is finite and $\alpha \to 0$. These limits are compatible with the leading uniform asymptotic approximants to the modified Bessel functions for large orders, see for eg. [111],

$$I_m(mz) \sim \sqrt{\frac{t}{2\pi m}}\, e^{m\eta(z)} \qquad \text{and} \qquad K_m(mz) \sim \sqrt{\frac{\pi t}{2m}}\, e^{-m\eta(z)}, \qquad m \to \infty, \tag{5.35}$$

where

$$t = \frac{1}{\sqrt{1+z^2}} \qquad \text{and} \qquad \eta(z) = \sqrt{1+z^2} + \ln \frac{z}{1+\sqrt{1+z^2}}. \tag{5.36}$$

Using the above asymptotic behaviors and neglecting terms of order α we can deduce, for large order m,

$$\frac{4\,\alpha^2}{(1-\alpha^2)}\frac{1}{D_m(\alpha;\kappa R)}\frac{1}{D_n(\alpha;\kappa R)} \sim \frac{\kappa_m a}{\sinh\kappa_m a}\frac{\kappa_n a}{\sinh\kappa_n a}, \tag{5.37}$$

where we have denoted $\kappa_m^2 = \kappa^2 + (m/R)^2$ and $\kappa_n^2 = \kappa^2 + (n/R)^2$. Using the above limiting form in Eq. (5.32), and after interpreting $m/R \to k$ as the Fourier transform of the coordinate containing the corrugations on the plates, we reproduce the expression derived for the corrugated plates in [110].

Using Eq. (5.32) in Eq. (5.24) the L-matrix in the Dirichlet limit takes the form

$$L_{mn}^{(2)D} = \frac{1}{a^2}\frac{1}{4\pi}\int_0^\infty \kappa\, d\kappa \frac{a^2}{a_1 a_2}\frac{1}{D_m(\alpha;\kappa R)}\frac{1}{D_n(\alpha;\kappa R)}, \tag{5.38}$$

which also leads to the corresponding result for the corrugated plates.

5.2.3 Weak coupling limit

For the case of the weak coupling limit ($a\lambda_{1,2} \ll 1$) the expression in Eq. (5.31) takes the form

$$I_{mn}^{(2)W}(a_1,a_2;\kappa) = \lambda_1\lambda_2\frac{\partial}{\partial a_1}a_1\frac{\partial}{\partial a_2}a_2\Big[I_m(\kappa a_1)K_m(\kappa a_2)I_n(\kappa a_1)K_n(\kappa a_2)\Big], \tag{5.39}$$

where W stands for weak coupling limit. Using the above expression for the I-matrix in Eq. (5.24) we can write the L-matrix in the weak coupling limit as

$$L_{mn}^{(2)W} = -\frac{\lambda_1\lambda_2}{4\pi}\frac{\partial}{\partial a_1}a_1\frac{\partial}{\partial a_2}\frac{1}{a_2}\,F_{mn}\Big(\frac{a_1}{a_2}\Big), \tag{5.40}$$

where we have introduced the function

$$F_{mn}(\beta) = \int_0^\infty x\, dx\, K_m(x) K_n(x) I_m(\beta x) I_n(\beta x). \tag{5.41}$$

Taking the uniform asymptotic approximants of the modified Bessel functions, see Eq. (5.35), in the above expression, we can reproduce the corresponding result for the corrugated plates in [110].

It is possible to convert the above integral into a single sum using the technique described in [89]. We replace those modified Bessel functions which are well defined at the origin, I_m, with their power series expansions, then perform the integral using

$$\int_0^\infty x\, dx\, x^{m+n+2k} K_m(x) K_n(x) = \frac{1}{2}\, \frac{2^{m+n+2k}(m+n+2k+1)!}{k!(k+m)!(k+n)!(k+m+n)!}, \tag{5.42}$$

for $m \geq 0, n \geq 0, k \geq 0$, which leaves Eq. (5.41) in terms of two sums. One of the sums can be performed after regrouping the terms, and leads to

$$\begin{aligned} F_{mn}(\beta) =& \frac{1}{2}\beta^{m+n} \sum_{k=0}^{\infty} \beta^{2k} \frac{1}{(m+n+2k+1)!} \sum_{k'=0}^{k} \frac{k!(k+m)!(k+n)!(k+m+n)!}{k'!(k'+m)!(k-k')!(k-k'+n)!} \\ =& \frac{1}{2} \sum_{k=0}^{\infty} \frac{\beta^{2k+m+n}}{(2k+m+n+1)}, \qquad m \geq 0, n \geq 0. \end{aligned} \tag{5.43}$$

Substituting the above expression into Eq. (5.40), and taking the derivatives with respect to a_1 and a_2, we immediately perform the sum, leading to

$$\begin{aligned} L_{mn}^{(2)W} &= \frac{\lambda_1 \lambda_2}{8\pi} \frac{1}{a_2^2} \frac{\partial}{\partial \beta} \left[\frac{\beta^{m+n+1}}{1-\beta^2} \right] \\ &= -\frac{\lambda_1 \lambda_2}{16\pi} \frac{1}{a^2}\, \alpha^2 \frac{\partial}{\partial \alpha} \left[\frac{1}{\alpha} \left(\frac{1-\alpha}{1+\alpha} \right)^{m+n} (1-\alpha^2) \right], \qquad m \geq 0, n \geq 0, \end{aligned} \tag{5.44}$$

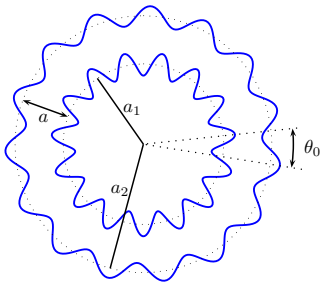

Figure 5.1: Non-contact gears: Concentric corrugated cylinders with the same corrugation frequency, $\nu = 15$, on each cylinder. θ_0 is the angular shift between the gears.

where we have denoted $\beta = a_1/a_2$ for convenience. Interpreting $m/R \to k_1$ and $n/R \to k_2$, and taking the limit $m \to \infty$, $n \to \infty$, while keeping $k_{1,2}$ fixed, we obtain the expression for the L-kernel for corrugated plates in the weak limit [110].

5.3 Sinusoidal corrugations

Next we consider the particular case of sinusoidal corrugations, as described in Figure 5.1, so that we will have

$$h_1(\theta) = h_1 \sin[\nu(\theta + \theta_0)], \tag{5.45a}$$

$$h_2(\theta) = h_2 \sin[\nu\theta], \tag{5.45b}$$

where $h_{1,2}$ are the corrugation amplitudes and ν is the frequency associated with the corrugations. Necessarily, ν must be a positive integer. The Fourier transforms, $(\tilde{h}_i)_m$, corresponding to the above corrugations are

$$(\tilde{h}_1)_m = h_1 \frac{2\pi}{2i}\Big[e^{i\nu\theta_0}\delta_{m,\nu} - e^{-i\nu\theta_0}\delta_{m,-\nu}\Big]. \tag{5.46}$$

In general the corrugation frequencies of the two cylinders can be different. However, we note that, to the leading order, the interaction energy gets contributions only when both cylinders have the same frequency.

Using the above expression in Eq. (5.22) and using the symmetry property of $I^{(2)}_{mn}$ in Eq. (5.26), which further lets us deduce $L^{(2)}_{mn} = L^{(2)}_{nm}$, we can write

$$\frac{E^{(2)}_{12}}{L_z} = \cos(\nu\theta_0)\,\frac{h_1 h_2}{2}\sum_{m=-\infty}^{\infty} L^{(2)}_{m,m+\nu} = -\cos(\nu\theta_0)\,\frac{h_1 h_2}{8\pi}\sum_{m=-\infty}^{\infty}\int_0^\infty \kappa\, d\kappa\, I^{(2)}_{m,m+\nu}(a_1, a_2; \kappa), \tag{5.47}$$

where the kernel has been explicitly evaluated in Eq. (5.31).

5.3.1 Dirichlet limit

In the Dirichlet limit the interaction energy in Eq. (5.47) can be expressed in the form

$$\frac{E^{(2)}_{12}}{2\pi R\, L_z} = \cos(\nu\theta_0)\,\frac{\pi^2}{240\, a^3}\,\frac{h_1}{a}\frac{h_2}{a}\,B^{(2)D}_{\nu}(\alpha) \tag{5.48}$$

where we have divided by a factor of $2\pi R$, which is the mean circumference in the direction of corrugations. We have also defined a suitable function $B^{(2)}_{\nu}(\alpha)$ to make it convenient to compare our results with those obtained in the PFA limit and with those for corrugated plates in the appropriate limits. We define

$$B^{(2)D}_{\nu}(\alpha) = \frac{15}{\pi^4}\sum_{m=-\infty}^{\infty} 8\alpha^3 \int_0^\infty x\, dx \frac{4\,\alpha^2}{(1-\alpha^2)}\frac{1}{D_m(\alpha; x)}\frac{1}{D_{m+\nu}(\alpha; x)}. \tag{5.49}$$

Using Eq. (5.37) it is straightforward to verify the corrugated plate limit of the above expression. The function $B^{(2)D}_{\nu}(\alpha)$ has been plotted with respect to $t_0 = 2\alpha\nu$ in figure 5.2. The redefined parameter helps us compare our results with the corrugated plates.

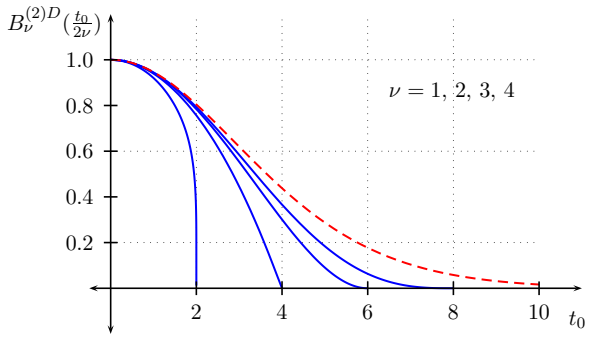

Figure 5.2: Dirichlet limit: Plots of $B_\nu^{(2)D}(\frac{t_0}{2\nu})$ versus t_0, for $t_0 < 2\nu$ and fixed ν. The dashed curve is the corresponding plot for corrugated plates which is approached by the corrugated cylinders for larger values of ν.

We note that for larger values of ν the plots approach the curve for the corrugated plates very quickly. We note that $B_\nu^{(2)D}(1) = 0$, because for $\alpha = 1$ the radius of the inner cylinder approaches zero. Thus, it is pointless to consider the regime $\alpha > 1$. We also note that $B_\nu^{(2)D}(0) = 1$, which then implies the PFA limit.

The Casimir torque per unit area, for the Dirichlet case, can thus be evaluated, using Eq. (5.48) in Eq. (5.4), to be

$$\frac{\mathcal{T}^{(2)D}}{2\pi R\, L_z} = \nu \sin(\nu\theta_0)\, \frac{\pi^2}{240\, a^3}\, \frac{h_1}{a}\frac{h_2}{a}\, B_\nu^{(2)D}(\alpha). \tag{5.50}$$

5.3.2 Weak coupling limit

The evaluation for the L-matrix in the weak limit in Eq. (5.44)is valid for positive indices only. Therefore, we begin by rewriting the expression for the interaction energy in Eq. (5.47) in the form

$$\frac{E_{12}^{(2)W}}{L_z} = \cos(\nu\theta_0)\, \frac{h_1 h_2}{2} \left[2 \sum_{m=0}^{\infty} L_{m,m+\nu}^{(2)W} + \sum_{m=1}^{\nu-1} L_{m,\nu-m}^{(2)W} \right], \tag{5.51}$$

where the finite sum is interpreted as zero when $\nu = 1$. We have used the symmetry property mentioned before Eq. (5.47), and further used $L^{(2)W}_{m,n} = L^{(2)W}_{-m,n} = L^{(2)W}_{m,-n} = L^{(2)W}_{-m,-n}$, which can be deduced from eq (5.39) using the Bessel function property $I_{-m}(x) = I_m(x)$ and $K_{-m}(x) = K_m(x)$. After substituting the L-matrix, derived in Eq. (5.44), into the above equation we can immediately perform the sums to yield

$$\frac{E^{(2)W}_{12}}{2\pi R\, L_z} = \cos(\nu\theta_0)\, \frac{\lambda_1\lambda_2}{32\pi^2\, a}\, \frac{h_1}{a}\frac{h_2}{a}\, B^{(2)W}_{\nu}(\alpha), \tag{5.52}$$

where we have defined the function

$$B^{(2)W}_{\nu}(\alpha) = -\frac{\alpha^3}{2}\frac{\partial}{\partial\alpha}\left[\frac{1}{\alpha^2}\left(\frac{1-\alpha}{1+\alpha}\right)^{\nu}(1-\alpha^2)(1+2\alpha\nu+\alpha^2)\right]. \tag{5.53}$$

The Casimir torque per unit area, for the weak coupling limit, can thus be evaluated, using Eq. (5.52) in Eq. (5.4), to be

$$\frac{\mathcal{T}^{(2)W}}{2\pi R\, L_z} = \nu\sin(\nu\theta_0)\, \frac{\lambda_1\lambda_2}{32\pi^2\, a}\, \frac{h_1}{a}\frac{h_2}{a}\, B^{(2)W}_{\nu}(\alpha). \tag{5.54}$$

We note that $B^{(2)W}_{\nu}(0) = 1$. This verifies that the above result satisfies the proximity force theorem. As in the Dirichlet case, we note that $B^{(2)W}_{\nu}(1) = 0$, because for $\alpha = 1$ the radius of the inner cylinder approaches zero. The above result should also yield the result for corrugated parallel plates in the limit $\nu \to \infty$, $a_{1,2} \to \infty$, $R \to \infty$, such that a and ν/R is finite. Also, in this limit $\alpha \to 0$. Recalling the corrugated plates parameter [110], $k_0 a \to \nu a/R = 2\nu\alpha \equiv t_0$, we note that the limit to corrugated plates is achieved by taking the limit $\nu \to \infty$ with t_0 kept fixed. To this end we rewrite

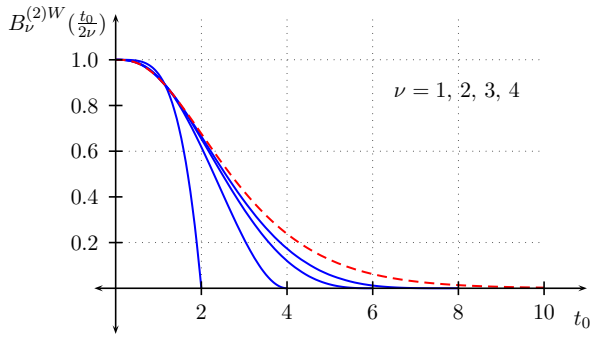

Figure 5.3: Weak coupling limit: Plots of $B_\nu^{(2)W}(\frac{t_0}{2\nu})$ versus t_0, for $t_0 < 2\nu$ and fixed ν. The dashed curve is the corresponding plot for corrugated plates which is approached by the corrugated cylinders for larger values of ν.

Eq. (5.53) in terms of t_0 as

$$B_\nu^{(2)W}\left(\frac{t_0}{2\nu}\right) = -\frac{t_0^3}{2}\frac{\partial}{\partial t_0}\left[\frac{1}{t_0^2}\left(1-\frac{t_0}{2\nu}\right)^\nu\left(1+\frac{t_0}{2\nu}\right)^{-\nu}\left(1-\frac{t_0^2}{4\nu^2}\right)\left(1+t_0+\frac{t_0^2}{4\nu^2}\right)\right] \tag{5.55}$$

in which the $\nu \to \infty$ limit can be immediately taken to yield

$$\lim_{\nu\to\infty} B_\nu^{(2)W}\left(\frac{t_0}{2\nu}\right) = -\frac{t_0^3}{2}\frac{\partial}{\partial t_0}\left[\frac{1}{t_0^2}(1+t_0)\,e^{-t_0}\right] = \frac{t_0^3}{2}\frac{\partial^2}{\partial t_0^2}\left[\frac{1}{t_0}\,e^{-t_0}\right], \tag{5.56}$$

which matches the result for the corrugated plates exactly. The function $B_\nu^{(2)W}(\alpha)$ has been plotted with respect to t_0 in figure 5.3. As in the case of Dirichlet case, we note that for larger values of ν the plots approach the plot for corrugated plates very quickly.

5.4 Summary

We have evaluated the Casimir torque between two concentric corrugated cylinders perturbatively in the corrugation amplitude for the scalar case and obtained explicit expressions for the case when the cylinders have sinusoidal corrugations. Nonzero contributions in the leading order requires the corrugation frequencies on the two cylinders to be identical. Our results for the Casimir torque reproduce the results for the lateral force on corrugated parallel plates in the limit of large radii and small corrugation wavelengths, which gives confidence in the calculational technique.

The amount of calculational complexity increases in analytic evaluation of the higher order, which was one of the achievements in our calculation for the parallel plate geometry. Since we could obtain the exact result for the weak case, comparison of the perturbative calculation when the next-to-leading order contribution is included matched remarkably well with the exact case. Thus doing a higher order calculation could be worth the effort. However, the scalar case is a toy model and for any practical purposes we need to consider the electromagnetic case, which we take up next for the parallel geometry. In addition new exact numerical techniques [74, 75] were proposed, which evaluates the Casimir energy for the arbitrary shapes and corrugation amplitudes by numerically evaluating the scattering matrix or the reflection matrix for a particular geometry. These, although requiring truncating the matrix at some order, are still very powerful techniques, which are very useful for experimental purposes. However, our approach will have the advantage of providing analytical expressions, which yields complementary insight and understanding of the subject.

Chapter 6

Lateral Casimir energy: Electromagnetic gears

In the previous chapter we talked about a design of a non-contact gear in a cylindrical geometry described by two concentric corrugated semi-transparent corrugated cylinders [105] and analyzed it in the presence of a scalar field. In the earlier work we calculated the contribution of the next-to-leading order to the lateral Casimir force between two corrugated semi-transparent δ-function plates interacting with a scalar field [110]. For anything practical we need to set up the problem for the real electromagnetic field. In this chapter we present our ongoing work on the evaluation of the lateral force between two corrugated dielectric (non-magnetic) slabs of finite thickness interacting through the electromagnetic field [112]. We can analyze the result for various limiting cases such as the perfect conductor limit and the dilute dielectric limit. Taking the thickness of the dielectric slabs to infinity leads us to the lateral force between dielectric slabs of infinite extent. Taking the thin-plate limit based on the model proposed in Chapter 4, Section 4.2, we have calculated the lateral force

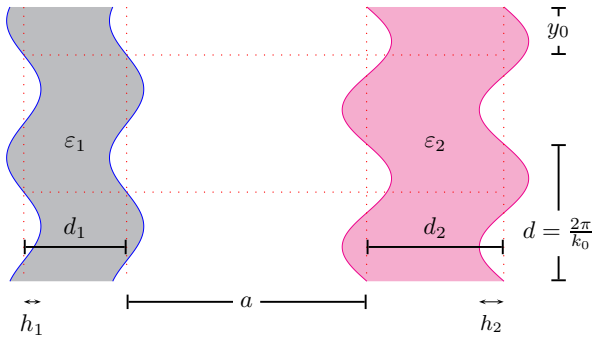

Figure 6.1: Parallel dielectric slabs with sinusoidal corrugations.

between corrugated thin plates.

6.1 Interaction energy between two corrugated dielectric (non-magnetic) slabs

We consider two dielectric slabs of infinite extent in x-y plane, which have corrugations in the y-direction, as described in Figure 6.1. We describe the dielectric slabs by the potentials

$$V_i(z, y) = (\varepsilon_i - 1)\,[\theta(z - a_i - h_i(y)) - \theta(z - b_i - h_i(y))]\,, \tag{6.1}$$

where $i = 1, 2$, designates the individual dielectric slabs. $\theta(z)$ is the Heaviside theta function defined previosly. $h_i(y)$ describes the corrugations on the surface of the slabs. We define the thickness of the individual slabs as $d_i = b_i - a_i$, such that $a = a_2 - b_1 > 0$ represents the distance between the slabs. The permittivities of the slabs are represented by ε_i. Following Subsection 5.1.1 and Section 5.2 in the previous chapter with the change that the scalar Green's function is now replaced with the

Green's dyadic we can obtain the contribution to the interaction energy between the two slabs in leading order in the corrugation amplitudes to be

$$E_{12}^{(2)} = -\frac{1}{2}\int \frac{d\zeta}{2\pi}\,\mathrm{Tr}\left[\mathbf{\Gamma}^{(0)}\Delta V_1^{(1)}\cdot\mathbf{\Gamma}^{(0)}\,\Delta V_2^{(1)}\right], \tag{6.2}$$

where $\Delta V_i^{(1)}$ are the leading order contributions in the potentials described by Eq. (6.1) due to the presence of corrugations given as

$$\Delta V_i^{(1)}(z,y) = -h_i(y)\,(\varepsilon_i - 1)\,[\delta(z-a_i) - \delta(z-b_i)]\,. \tag{6.3}$$

Note in particular that

$$V_i^{(0)}(z) = (\varepsilon_i - 1)\;[\theta(z-a_i) - \theta(z-b_i)]\,, \tag{6.4}$$

describes the potential for the case when the corrugations are absent and represents the background in the description of the lateral forces. $\mathbf{\Gamma}^{(0)} = \mathbf{\Gamma}^{(0)}(\boldsymbol{x},\boldsymbol{x}';i\zeta)$ is the Green's dyadic in the presence of background potential $V_i^{(0)}(z)$ and satisfies

$$\left[\frac{1}{\zeta^2}\boldsymbol{\nabla}\times\boldsymbol{\nabla}\times\;+\mathbf{1}+V_1^{(0)}+V_2^{(0)}\right]\cdot\mathbf{\Gamma}^{(0)}(\boldsymbol{x},\boldsymbol{x}';i\zeta) = -\mathbf{1}\delta^{(3)}(\boldsymbol{x}-\boldsymbol{x}'). \tag{6.5}$$

The corresponding reduced Green's dyadic $\boldsymbol{\gamma}^{(0)}(z,z';k_x,k_y,i\zeta)$ is defined by Fourier transforming in the transverse variables as

$$\mathbf{\Gamma}^{(0)}(\boldsymbol{x},\boldsymbol{x}';i\zeta) = \int \frac{dk_x}{2\pi}\frac{dk_y}{2\pi}\,e^{ik_x(x-x')}e^{ik_y(y-y')}\,\boldsymbol{\gamma}^{(0)}(z,z';k_x,k_y,i\zeta), \tag{6.6}$$

and it satisfies the differential equation

$$\begin{bmatrix} -\frac{\partial^2}{\partial z^2}+k^2+\zeta^2\varepsilon(z) & -k_xk_y & ik_x\frac{\partial}{\partial z} \\ -k_xk_y & -\frac{\partial^2}{\partial z^2}+k^2+\zeta^2\varepsilon(z) & ik_y\frac{\partial}{\partial z} \\ ik_x\frac{\partial}{\partial z} & ik_y\frac{\partial}{\partial z} & -\frac{\partial^2}{\partial z^2}+k^2+\zeta^2\varepsilon(z) \end{bmatrix} \cdot \boldsymbol{\gamma}^{(0)}(z,z';k_x,k_y,i\zeta) = -\zeta^2\delta(z-z'). \tag{6.7}$$

We have used the definitions $k^2 = k_x^2 + k_y^2$ and

$$\varepsilon(z) - 1 = V_1^{(0)}(z) + V_2^{(0)}(z). \tag{6.8}$$

The solution to $\boldsymbol{\gamma}^{(0)}$ is given in Eq. (2.72), which we can read out from the general solution for the case of five layered dielectric medium presented in Section 3.2.3 for the specific case of dielectric permittivities $\varepsilon_{1,2,3} = 1$. Using the fact that our system is translationally invariant in the x-direction, we can write

$$\frac{E_{12}^{(2)}}{L_x} = \int_{-\infty}^{\infty}\frac{dk_y}{2\pi}\int_{-\infty}^{\infty}\frac{dk_y'}{2\pi}\,\tilde{h}_1(k_y-k_y')\,\tilde{h}_2(k_y'-k_y)\,L^{(2)}(k_y,k_y'), \tag{6.9}$$

where L_x is the infinite length in the x-direction and $\tilde{h}_i(k_y)$ are the Fourier transforms of the functions $h_i(y)$ describing the corrugations. The z-integrals contributing to the trace in Eq. (6.2) is trivially evaluated due to δ-function form of the potential in Eq. (6.3). The kernel $L^{(2)}(k_y,k_y')$ is then given by

$$L^{(2)}(k_y,k_y') = -\frac{1}{2}\int\frac{d\zeta}{2\pi}\int\frac{dk_x}{2\pi}\,I^{(2)}(k_x,\zeta,k_y,k_y'), \tag{6.10}$$

where the $I^{(2)}$-kernel is given by

$$\begin{aligned} I^{(2)}(k_x, i\zeta, k_y, k_y') = (\varepsilon_a - 1)(\varepsilon_b - 1) \Big[& \boldsymbol{\gamma}^{(0)}_{\textcircled{T}}(a_2, a_1; k_x, k_y, i\zeta) \cdot \boldsymbol{\gamma}^{(0)}_{\textcircled{M}}(a_1, a_2; k_x, k_y', i\zeta) \\ & - \boldsymbol{\gamma}^{(0)}_{\textcircled{8}}(b_2, a_1; k_x, k_y, i\zeta) \cdot \boldsymbol{\gamma}^{(0)}_{\textcircled{O}}(a_1, b_2; k_x, k_y', i\zeta) \\ & - \boldsymbol{\gamma}^{(0)}_{\textcircled{V}}(a_2, b_1; k_x, k_y, i\zeta) \cdot \boldsymbol{\gamma}^{(0)}_{\textcircled{2}}(b_1, a_2; k_x, k_y', i\zeta) \\ & + \boldsymbol{\gamma}^{(0)}_{\textcircled{W}}(b_2, b_1; k_x, k_y, i\zeta) \cdot \boldsymbol{\gamma}^{(0)}_{\textcircled{P}}(b_1, b_2; k_x, k_y', i\zeta) \Big], \end{aligned} \tag{6.11}$$

where the reduced Green's dyadics are evaluated using solutions to Eq. (6.7). The circled quantities in subscripts refer to the regions of evaluation in Figure 3.7. We note that

$$\boldsymbol{\gamma}^{(0)}(z, z'; k_x, k_y, i\zeta) = \boldsymbol{\gamma}^{(0)\,\dagger}(z', z; k_x, k_y, i\zeta). \tag{6.12}$$

Our task thus reduces to evaluating the reduced Green's dyadic in the presence of the background, which are just the parallel slabs.

6.2 Evaluation of the reduced Green's dyadic

In Section 2.4 we obtained the solution to the Green's dyadic for the planar geometry. For simplicity we exploited the rotational symmetry of the problem to set the Fourier component $k_y = 0$ and $k_x = k$. However, the corrugated geometry does not have this symmetry and therefore $L^{(2)}$-kernel explicitly depends on k_y. We thus need to know the reduced Green's dyadic arbitrary k_y, which can be obtained easily by the rotation

$$\boldsymbol{\gamma}^{(0)}(z, z'; k_x, k_y, i\zeta) = \mathbf{R} \cdot \boldsymbol{\gamma}^{(0)}(z, z'; k, 0, i\zeta) \cdot \mathbf{R}^T, \tag{6.13}$$

where

$$\mathbf{R} = \frac{1}{k}\begin{bmatrix} k_x & -k_y & 0 \\ k_y & k_x & 0 \\ 0 & 0 & k \end{bmatrix}. \tag{6.14}$$

Using Eq. (2.72) in above equations we get

$$\boldsymbol{\gamma}^{(0)}(z,z';k_x,k_y,i\zeta) =$$

$$\begin{bmatrix} \frac{k_x^2}{k^2}\frac{1}{\varepsilon(z)}\frac{\partial}{\partial z}\frac{1}{\varepsilon(z')}\frac{\partial}{\partial z'}\,g^H - \zeta^2\frac{k_y^2}{k^2}\,g^E & \frac{k_xk_y}{k^2}\frac{1}{\varepsilon(z)}\frac{\partial}{\partial z}\frac{1}{\varepsilon(z')}\frac{\partial}{\partial z'}\,g^H + \zeta^2\frac{k_xk_y}{k^2}\,g^E & \frac{ik_x}{\varepsilon(z')}\frac{1}{\varepsilon(z)}\frac{\partial}{\partial z}\,g^H \\ \frac{k_xk_y}{k^2}\frac{1}{\varepsilon(z)}\frac{\partial}{\partial z}\frac{1}{\varepsilon(z')}\frac{\partial}{\partial z'}\,g^H + \zeta^2\frac{k_xk_y}{k^2}\,g^E & \frac{k_y^2}{k^2}\frac{1}{\varepsilon(z)}\frac{\partial}{\partial z}\frac{1}{\varepsilon(z')}\frac{\partial}{\partial z'}\,g^H - \zeta^2\frac{k_x^2}{k^2}\,g^E & \frac{ik_y}{\varepsilon(z')}\frac{1}{\varepsilon(z)}\frac{\partial}{\partial z}\,g^H \\ -\frac{ik_x}{\varepsilon(z)}\frac{1}{\varepsilon(z')}\frac{\partial}{\partial z'}\,g^H & -\frac{ik_y}{\varepsilon(z)}\frac{1}{\varepsilon(z')}\frac{\partial}{\partial z'}\,g^H & \frac{k^2}{\varepsilon(z)\varepsilon(z')}\,g^H \end{bmatrix}$$

$$-\frac{\delta(z-z')}{\varepsilon(z)}\frac{1}{k^2}\begin{bmatrix} k_x^2 & k_xk_y & 0 \\ k_xk_y & k_y^2 & 0 \\ 0 & 0 & k^2 \end{bmatrix}. \tag{6.15}$$

The δ-functions in Eq. (6.15) do not contribute in the evaluation of the $I^{(2)}$-kernel in Eq. (6.11) because they are evaluated at different points. We now need to evaluate the electric and magnetic scalar Green's functions g^E and g^H for the two parallel slab configuration, which as we mentioned in the previous section, can be read off using Section 3.2.3.

6.3 I-kernel for corrugated dielectric slabs

We evaluate $I^{(2)}(k_x, i\zeta, k_y, k'_y)$ in Eq. (6.11) as

$$
\begin{aligned}
I^{(2)}(k_x, i\zeta, k_y, k'_y) = \\
-\frac{1}{k^2}\frac{1}{k'^2}\frac{e^{-a(\kappa+\kappa')}}{2\kappa\, 2\kappa'}\Bigg[&\frac{1}{\Delta}\frac{1}{\Delta'}M(-\alpha_1,-\alpha'_1)M(-\alpha_2,-\alpha'_2)(k_x^2+k_yk'_y)^2\zeta^4 \\
&+\frac{1}{\Delta}\frac{1}{\bar{\Delta}'}M(-\alpha_1,\bar{\alpha}'_1)M(-\alpha_2,\bar{\alpha}'_2)k_x^2(k_y-k'_y)^2\zeta^2\kappa'^2 \\
&+\frac{1}{\bar{\Delta}}\frac{1}{\Delta'}M(\bar{\alpha}_1,-\alpha'_1)M(\bar{\alpha}_2,-\alpha'_2)k_x^2(k_y-k'_y)^2\zeta^2\kappa^2 \\
&+\frac{1}{\bar{\Delta}}\frac{1}{\bar{\Delta}'}\left\{M(\bar{\alpha}_1,\bar{\alpha}'_1)(k_x^2+k_yk'_y)\kappa\kappa'+M(-\bar{\alpha}_1,-\bar{\alpha}'_1)\frac{k^2k'^2}{\varepsilon_1}\right\} \\
&\qquad\times\left\{M(\bar{\alpha}_2,\bar{\alpha}'_2)(k_x^2+k_yk'_y)\kappa\kappa'+M(-\bar{\alpha}_2,-\bar{\alpha}'_2)\frac{k^2k'^2}{\varepsilon_2}\right\}\Bigg],
\end{aligned}
\tag{6.16}
$$

where

$$
\Delta = \Big[(1-\alpha_1^2\, e^{-2\kappa_1 d_1})(1-\alpha_2^2\, e^{-2\kappa_2 d_2})-\alpha_1\alpha_2(1-e^{-2\kappa_1 d_1})(1-e^{-2\kappa_2 d_2})\, e^{-2\kappa a}\Big], \tag{6.17}
$$

and

$$
\begin{aligned}
M(\alpha_i,\alpha'_i) = (\varepsilon_i-1)\Big[&(1-\alpha_i^2)\, e^{-\kappa_i d_i}(1-\alpha_i'^2)\, e^{-\kappa'_i d_i} \\
&-(1+\alpha_i)(1-\alpha_i\, e^{-2\kappa_i d_i})(1+\alpha'_i)(1-\alpha'_i\, e^{-2\kappa'_i d_i})\Big],
\end{aligned}
\tag{6.18}
$$

where various quantities are already defined in earlier chapters.

Substituting Eq. (6.16) in Eq. (6.10) and subsequently using it in Eq. (6.9) gives the interaction energy between the two corrugated dielectric slabs. The physical

parameters involved in the expression of energy are

$$E = E(a, d_i, (\varepsilon_i - 1); h_i, k_0, y_0) \tag{6.19}$$

We will consider the ideal (perfect) conductor limit, the dilute (weak) dielectric limit, the thick plate limit and the thin plate limit for the interaction energy. The approximations involved in these are:

$(\varepsilon_i - 1) \to \infty$	:	Ideal conductor limit.
$(\varepsilon_i - 1) \ll 1$	:	Dilute dielectric limit
$d_i \gg a$	:	Thick plate limit.
$(\varepsilon_i - 1)\zeta^2 = \frac{\lambda_i}{d_i}$, with $d_i \ll \lambda_i a^2$	:	Thin plate limit.
$E(k_0 a, (\varepsilon_i - 1), k_0 h_i, k_0 d_i, k_0 y_0)$	:	Exact dilute dielectric limit.
$E(0, (\varepsilon_i - 1), k_0 h_i, k_0 d_i, k_0 y_0)$	:	Dilute dielectric PFA.
$E(k_0 a, (\varepsilon_i - 1)^{(1)}, (k_0 h_i)^{(2)}, k_0 d_i, k_0 y_0)$	:	Dilute dielectric limit in perturbative leading order.

We have scaled the physical parameters with the wavevector k_0 to get dimensionless parameters.

6.3.1 Ideal conductor limit

In the ideal (perfect) conductor limit ($\varepsilon_i \to \infty$) we have the approximations:

$$\begin{aligned} &\varepsilon_i \to \infty, \quad \kappa_i \sim \zeta\sqrt{\varepsilon_i} \to \infty, \quad \bar{\kappa}_i \sim \frac{\zeta}{\sqrt{\varepsilon_i}} \to 0, \\ &\alpha \to 1, \quad \bar{\alpha}_i \to -1, \quad \Delta \to (1 - e^{-2\kappa a}). \end{aligned} \tag{6.20}$$

Using the above in Eq. (6.16) we have

$$
\begin{aligned}
I^{(2)}_{\varepsilon\to\infty}(\kappa,\kappa',k_y-k'_y) = & I^{(2)}_D(\kappa,\kappa')\Bigg[1-\frac{k_x^2(k_y-k'_y)^2}{\kappa^2\kappa'^2} \\
& \qquad +\frac{\zeta^2}{\kappa^2}\frac{\zeta^2}{\kappa'^2}\left[\frac{k_x^2(k_y-k'_y)^2}{k^2k'^2}+\left\{\frac{k_x^2+k_yk'_y}{kk'}+\frac{kk'}{\zeta^2}\right\}^2\right]\Bigg] \\
= & I^{(2)}_D(\kappa,\kappa')\left[2-\frac{k_x^2(k_y-k'_y)^2}{\kappa^2\kappa'^2}-\frac{\zeta^2(k_y-k'_y)^2}{\kappa^2\kappa'^2}\right] \\
= & I^{(2)}_D(\kappa,\kappa')\left[2-(k_x^2+\zeta^2)\,\frac{(k_y-k'_y)^2}{\kappa^2\kappa'^2}\right] \\
= & I^{(2)}_D(\kappa,\kappa')\left[1+\frac{\{\kappa^2+\kappa'^2-(k_y-k'_y)^2\}^2}{4\,\kappa^2\kappa'^2}\right], \qquad (6.21)
\end{aligned}
$$

where

$$
I^{(2)}_D(\kappa,\kappa') = -\frac{\kappa}{\sinh\kappa a}\frac{\kappa'}{\sinh\kappa' a}. \qquad (6.22)
$$

The contribution from 1 inside the square bracket in the above expression can be associated to the contribution from the Dirichlet mode in the scalar case [110]. It is worth pointing out that the total contribution is not two times the Dirichlet mode.

6.3.2 Thin plate limit

Using the thin plate approximations collected in Appendix A in Eq. (6.16) gives the thin plate limit for the $I^{(2)}$-kernel to be

$$\begin{aligned} I^{(2)}_{TP}(k_x,\zeta,k_y,k'_y) =& I^{(2)}_s(\kappa,\kappa') - \frac{k_x^2(k_y-k'_y)^2}{k^2k'^2}\Bigg[I^{(2)}_s(\kappa,\kappa') \\ &- I^{(2)}_s\left(\kappa,\frac{\zeta^2}{\kappa'}\right) - I^{(2)}_s\left(\frac{\zeta^2}{\kappa},\kappa'\right) + I^{(2)}_s\left(\frac{\zeta^2}{\kappa},\frac{\zeta^2}{\kappa'}\right)\Bigg] \\ &+ I^{(2)}_s\left(\frac{\zeta^2}{\kappa},\frac{\zeta^2}{\kappa'}\right)\left[\frac{\kappa^2}{\zeta^2}\frac{\kappa'^2}{\zeta^2} - \frac{(k_y-k'_y)^2}{\zeta^2}\right]. \end{aligned} \tag{6.23}$$

where

$$\begin{aligned} I^{(2)}_s(\kappa,\kappa') = -\frac{\lambda_1}{2\kappa}\frac{\lambda_2}{2\kappa'}\frac{e^{-a(\kappa+\kappa')}}{\Delta_s\Delta'_s}&\left[\kappa\left(1+\frac{\lambda_1}{2\kappa}\right)+\kappa'\left(1+\frac{\lambda_1}{2\kappa'}\right)\right] \\ &\times\left[\kappa\left(1+\frac{\lambda_2}{2\kappa}\right)+\kappa'\left(1+\frac{\lambda_2}{2\kappa'}\right)\right] \end{aligned} \tag{6.24}$$

is the $I^{(2)}$-kernel for the scalar case [see Eq. (49) in [110]], and Δ_s is given by

$$\Delta_s = \left(1+\frac{\lambda_1}{2\kappa}\right)\left(1+\frac{\lambda_2}{2\kappa}\right) - \frac{\lambda_1}{2\kappa}\frac{\lambda_2}{2\kappa}e^{-2\kappa a}, \tag{6.25}$$

which was defined [in Eq. (A2)] in [110].

Taking the perfect conductor limit of Eq. (6.23), i.e. taking $\lambda_i \to \infty$ we reproduce the result in Eq. (6.21), which is expected since thickness of the perfectly conducting

material body should be irrelevant. This involves

$$I_s^{(2)}((\kappa,\kappa')\to I_D^{(2)}(\kappa,\kappa') \tag{6.26}$$

$$I_s^{(2)}\left(\kappa,\frac{\zeta^2}{\kappa'}\right)\to\frac{\zeta^2}{\kappa'^2}I_D^{(2)}(\kappa,\kappa') \tag{6.27}$$

$$I_s^{(2)}\left(\frac{\zeta^2}{\kappa},\kappa'\right)\to\frac{\zeta^2}{\kappa^2}I_D^{(2)}(\kappa,\kappa') \tag{6.28}$$

$$I_s^{(2)}\left(\frac{\zeta^2}{\kappa},\frac{\zeta^2}{\kappa'}\right)\to\frac{\zeta^2}{\kappa^2}\frac{\zeta^2}{\kappa'^2}I_D^{(2)}(\kappa,\kappa') \tag{6.29}$$

where $I_D^{(2)}(\kappa,\kappa')$ was defined in Eq. (6.22).

6.3.3 Dilute dielectric limit

In the dilute dielectric limit, $(\varepsilon_i-1)\ll 1$, we have $\kappa_i,\bar{\kappa}_i\to\kappa$, and $\alpha_i,\bar{\alpha}_i\to 0$. Further,

$$\Delta\to\Delta_W=e^{\kappa a},\qquad\text{and}\qquad M_W(\alpha_i,\alpha_i')=M(0,0)=(\varepsilon_i-1)\Big[e^{-d_i(\kappa+\kappa')}-1\Big]. \tag{6.30}$$

Thus the $I^{(2)}$-kernel takes the form

$$\begin{aligned}I_W^{(2)}(i\zeta,\kappa,\kappa',k_y-k_y') = &-\frac{(\varepsilon_1-1)}{2\kappa}\frac{(\varepsilon_2-1)}{2\kappa'}\,e^{-a(\kappa+\kappa')}\\ &\Big[e^{-d_1(\kappa+\kappa')}-1\Big]\Big[e^{-d_2(\kappa+\kappa')}-1\Big]\zeta^4C_W^{(2)}(\zeta,\kappa,\kappa',k_y-k_y')\end{aligned} \tag{6.31}$$

where

$$C_W^{(2)}(i\zeta,\kappa,\kappa',k_y-k_y')=\frac{1}{\zeta^4}\frac{1}{k^2k'^2}\Big[(k_x^2+k_yk_y')^2\zeta^4+k_x^2(k_y-k_y')^2\zeta^2(\kappa^2+\kappa'^2) + \Big\{(k_x^2+k_yk_y')^2\kappa\kappa'+k^2k'^2\Big\}^2\Big] \tag{6.32}$$

$$=1+\frac{1}{\zeta^4}\Big[\kappa\kappa'+k_x^2+k_yk_y'\Big]^2 \tag{6.33}$$

$$=1+\frac{1}{4\zeta^4}\Big[(\kappa+\kappa')^2-(k_y-k_y')^2-2\zeta^2\Big]^2. \tag{6.34}$$

6.3.4 Thick plate limit

In the thick plate limit we have

$$\Delta\to(1-\alpha_1\alpha_2e^{-2\kappa a}) \qquad \text{and} \qquad M(\alpha_i,\alpha')\to-(\varepsilon_i-1)(1+\alpha_i)(1+\alpha_i'). \tag{6.35}$$

Using the following relations

$$(1-\alpha_i)\frac{\zeta}{2\kappa}\sqrt{\varepsilon_i-1}=\sqrt{\alpha_i}, \tag{6.36}$$

$$(1+\bar{\alpha}_i)\frac{\zeta}{2\kappa}\sqrt{\varepsilon_i-1}=\sqrt{\alpha_i}\frac{\zeta^2}{\kappa^2}\left(1-\frac{k^2}{\kappa\kappa_i}\right)^{-1}, \tag{6.37}$$

$$(1-\bar{\alpha}_i)\frac{\zeta}{2\kappa}\sqrt{\varepsilon_i-1}=\sqrt{\alpha_i}\sqrt{\varepsilon_i}\frac{\zeta}{\kappa}\left(1-\frac{k^2}{\kappa\kappa_i}\right)^{-1}\sqrt{1-\frac{k^2}{\kappa_i^2}}, \tag{6.38}$$

in Eq. (6.16) we derive

$$
\begin{aligned}
&I^{(2)}_{d_i\to\infty}(k_x,\zeta,k_y,k_y') = \\
&-\sqrt{\alpha_1\alpha_1'\alpha_2\alpha_2'}\left[\frac{2\kappa\, e^{-\kappa a}}{(1-\alpha_1\alpha_2 e^{-2\kappa a})}\,\frac{2\kappa'\, e^{-\kappa' a}}{(1-\alpha_1'\alpha_2' e^{-2\kappa' a})}\right. \\
&-\frac{k_x^2(k_y-k_y')^2}{k^2k'^2}\left\{\frac{2\kappa\, e^{-\kappa a}}{(1-\alpha_1\alpha_2 e^{-2\kappa a})}-\frac{2\kappa\, e^{-\kappa a}}{(1-\bar\alpha_1\bar\alpha_2 e^{-2\kappa a})}\frac{\zeta^2}{\kappa^2}\frac{1}{\left(1-\frac{k^2}{\kappa_1\kappa}\right)}\frac{1}{\left(1-\frac{k^2}{\kappa_2\kappa}\right)}\right\} \\
&\qquad\times\left\{\frac{2\kappa'\, e^{-\kappa' a}}{(1-\alpha_1'\alpha_2' e^{-2\kappa' a})}-\frac{2\kappa'\, e^{-\kappa' a}}{(1-\bar\alpha_1'\bar\alpha_2' e^{-2\kappa' a})}\frac{\zeta^2}{\kappa'^2}\frac{1}{\left(1-\frac{k'^2}{\kappa_1'\kappa'}\right)}\frac{1}{\left(1-\frac{k'^2}{\kappa_2'\kappa'}\right)}\right\} \\
&+\frac{2\kappa\, e^{-\kappa a}}{(1-\bar\alpha_1\bar\alpha_2 e^{-2\kappa a})}\frac{2\kappa'\, e^{-\kappa' a}}{(1-\bar\alpha_1'\bar\alpha_2' e^{-2\kappa' a})}\frac{\zeta^2}{\kappa^2}\frac{1}{\left(1-\frac{k^2}{\kappa_1\kappa}\right)}\frac{1}{\left(1-\frac{k^2}{\kappa_2\kappa}\right)}\frac{\zeta^2}{\kappa'^2}\frac{1}{\left(1-\frac{k'^2}{\kappa_1'\kappa'}\right)}\frac{1}{\left(1-\frac{k'^2}{\kappa_2'\kappa'}\right)} \\
&\times\left.\left[\frac{k_x^2(k_y-k_y')^2}{k^2k'^2}+\left\{\frac{k_x^2+k_yk_y'}{kk'}+\frac{kk'}{\zeta^2}\frac{\zeta^2\varepsilon_1}{\kappa_1\kappa_1'}\right\}\left\{\frac{k_x^2+k_yk_y'}{kk'}+\frac{kk'}{\zeta^2}\frac{\zeta^2\varepsilon_2}{\kappa_2\kappa_2'}\right\}\right]\right],
\end{aligned}
\tag{6.39}
$$

which probably can be factored into a simpler form.

6.4 Sinusoidal corrugations

We now consider sinusoidal corrugations described by

$$h_1(y)=h_1\sin[k_0(y+y_0)], \tag{6.40a}$$

$$h_2(y)=h_2\sin[k_0y]. \tag{6.40b}$$

where k_0 is the wavenumber corresponding to the corrugation wavelength. The Fourier transforms $\tilde h_i(k)$ for sinusoidal corrugations evaluates to

$$\tilde h_1(k) = h_1\frac{2\pi}{2i}\Big[e^{ik_0y_0}\delta(k-k_0)-e^{-ik_0y_0}\delta(k+k_0)\Big]. \tag{6.41}$$

Using the above expression in eq. (6.9), we write

$$\begin{aligned}\frac{E_{12}^{(2)}}{L_x L_y} &= \cos k_0 y_0 \, \frac{h_1 h_2}{4\pi} \int_{-\infty}^{\infty} dk \, L^{(2)}(k, k_+) \\ &= -\cos k_0 y_0 \, \frac{h_1 h_2}{16\pi^2} \int_{-\infty}^{\infty} dk \int_0^{\infty} \bar{\kappa} \, d\bar{\kappa} \, I^{(2)}(\kappa, \kappa_+),\end{aligned} \tag{6.42}$$

where we have treated $2\pi\delta(0) = L_y$ as the infinite length in the y direction. We have used the symmetry property in the $I^{(2)}$-kernel, and performed suitable rescaling in the integration variables. We define $k_\pm = k \pm k_0$, and $\kappa_\pm^2 = \bar{\kappa}^2 + k_\pm^2$.

6.4.1 Perfect conductor limit

Using the expression for the $I^{(2)}$-kernel given by Eq. (6.22) in Eq. (6.42) and taking derivative with respect to y_0 gives the lateral force per unit area in the conductor limit as

$$F_{\varepsilon\to\infty}^{(2)} = 2k_0 a \, \sin(k_0 y_0) \left| F_{\rm Cas}^{(0)} \right| \frac{h_1}{a} \frac{h_2}{a} A_{\varepsilon\to\infty}^{(1,1)}(k_0 a), \tag{6.43}$$

where

$$A_{\varepsilon\to\infty}^{(1,1)}(t_0) = \frac{15}{\pi^4} \int_{-\infty}^{\infty} dt \int_0^{\infty} \bar{s} d\bar{s} \frac{s}{\sinh s} \frac{s_+}{\sinh s_+} \left[\frac{1}{2} + \frac{(s^2 + s_+^2 - t_0^2)^2}{8 \, s^2 s_+^2} \right], \tag{6.44}$$

where $s^2 = \bar{s}^2 + t^2$ and $s_+^2 = \bar{s}^2 + (t + t_0)^2$. We note that $A_{\varepsilon\to\infty}^{(1,1)}(0) = 1$. See Figure 6.2 for the plot of $A_{\varepsilon\to\infty}^{(1,1)}(k_0 a)$ versus $k_0 a$. We observe that only in the PFA limit is the electromagnetic contribution twice that of the Dirichlet case, and in general the electromagnetic case is less than twice that of the Dirichlet case. Since the above expression involves a convolution of two functions we can evaluate one of the integrals

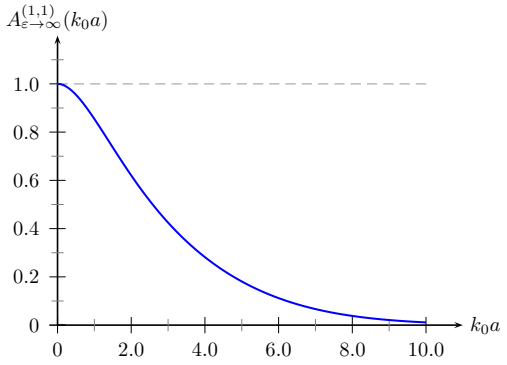

Figure 6.2: Plot of $A^{(1,1)}_{\varepsilon\to\infty}(k_0a)$ versus k_0a.

to get

$$A^{(1,1)}_{\varepsilon\to\infty}(t_0)=\frac{15}{4}\int_0^\infty du\,\frac{\sin(2t_0u/\pi)}{(2t_0u/\pi)}\left[\frac{\sinh^2 u}{\cosh^6 u}\left(\frac{7}{2}-\sinh^2 u\right)\right.$$
$$\left.-\frac{1}{2}\left(\frac{2t_0}{\pi}\right)^2\frac{\sinh^2 u}{\cosh^4 u}+\frac{1}{16}\left(\frac{2t_0}{\pi}\right)^4\frac{\sinh^2 u}{\cosh^2 u}\right] \tag{6.45}$$

which reproduces the result in Emig *et al* [113] apart from an overall factor of 2, which presumably is a typo in Emig *et al* [113]. Even though Eq. (6.45) involves only a single integral it turns out that the double integral representation in Eq. (6.44) is more useful for numerical evaluation because of the oscillatory nature of the function $\sin x/x$.

6.4.2 Dilute dielectric limit

For the dilute dielectric case, and assuming the dielectric constants to be independent of frequency, we can write the interaction energy as

$$\frac{E^{(2)W}_{12}}{L_xL_y}=\cos(k_0y_0)\frac{h_1}{a}\frac{h_2}{a}\frac{23(\varepsilon_1-1)(\varepsilon_2-1)}{320\pi^2a^3}A^{(1,1)}_W(k_0a,\bar{d}_i). \tag{6.46}$$

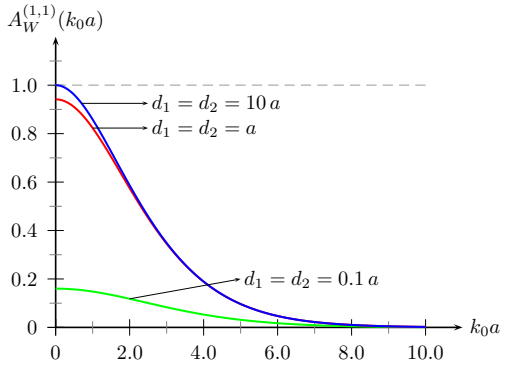

Figure 6.3: Plot of $A_W^{(1,1)}(k_0a)$ versus k_0a for different values of d_i/a when $d_1 = d_2$.

Differentiation with respect to y_0 gives the lateral Casimir force per unit area

$$F_{\varepsilon\to 1}^{(2)} = 2k_0a\,\sin(k_0y_0)\left|F_{\rm vdW}^{(0)}\right|\frac{h_1}{a}\frac{h_2}{a}A_{\varepsilon\to 1}^{(1,1)}(k_0a), \tag{6.47}$$

where the dielectric permittivity approaches 1 from above. $F_{\rm vdW}^{(0)}$ is the dilute limit to the Lifshitz formula or the force obtained using van der Waals (Casimir-Polder) interactions [114]. It is given by

$$F_{\rm vdW}^{(0)} = -\frac{23(\varepsilon_1-1)(\varepsilon_2-1)}{640\pi^2a^4}. \tag{6.48}$$

The coefficient $A_{\varepsilon\to 1}^{(1,1)}(k_0a)$ is given by

$$A_W^{(1,1)}(k_0a,\bar{d}_i) = \frac{5}{46}\int_{-\infty}^{\infty}dt\int_0^{\infty}\frac{\bar{s}\,d\bar{s}}{ss_+}\,e^{-(s+s_+)}\Big[e^{-\bar{d}_1(s+s_+)}-1\Big]\Big[e^{-\bar{d}_2(s+s_+)}-1\Big] \\ \Big[\bar{s}^4+\frac{1}{2}\Big\{\bar{s}^2+t_0^2-(s+s_+)^2\Big\}^2\Big], \tag{6.49}$$

where $\bar{d}_i = d_i/a$. We observe that

$$A_W^{(1,1)}(k_0a,\infty)=\frac{5}{46}\int_{-\infty}^{\infty}dt\int_0^{\infty}\frac{\bar{s}\,d\bar{s}}{ss_+}\,e^{-(s+s_+)}\Big[\bar{s}^4+\frac{1}{2}\left\{\bar{s}^2+t_0^2-(s+s_+)^2\right\}^2\Big],$$

$$\begin{aligned}A_W^{(1,1)}(0,\bar{d}_i)=&1-\frac{1}{(1+\bar{d}_1)^5}-\frac{1}{(1+\bar{d}_2)^5}+\frac{1}{(1+\bar{d}_1+\bar{d}_2)^5}\\ =&\frac{a^3}{2}\frac{\partial^3}{\partial a^3}\ln\left[\frac{a(a+d_1+d_2)}{(a+d_1)(a+d_2)}\right]\\ =&\frac{a^3}{2}\Big[1-e^{d_1\frac{\partial}{\partial a}}\Big]\Big[1-e^{d_2\frac{\partial}{\partial a}}\Big]\frac{\partial^2}{\partial a^2}\frac{1}{a},\end{aligned}\tag{6.50}$$

$$A_W^{(1,1)}(0,\infty)=1.\tag{6.51}$$

The above evaluations were achieved by going to spherical polar coordinates. The angular integrals are immediate and the radial integral involves gamma functions. In Figure 6.3 we plot $A_W^{(1,1)}(k_0a,\infty)$ with respect to k_0a for different values of $\bar{d}_i$ when both the thicknesses are same. We see that the lateral force in the dilute dielectric limit decreases with decreasing thickness of the slabs.

6.5 Proximity force approximation

We can verify that our results given in Section 6.4 in the proximity force approximation (PFA) matches the standard PFA result for the sinusoidal corrugations. The PFA limit is obtained by keeping h_i/a fixed while taking $k_0a\to 0$. We can write the distance between the corrugated slabs as

$$a(y)=a+h_2\sin[k_0y]-h_1\sin[k_0(y+y_0)].\tag{6.52}$$

In the PFA limit the two surfaces are very close such that the distance between them is small in comparison to the corrugation wavelength. Then we can approximate the

surface to be made out of small length sections which can be treated as parallel plates.

6.5.1 Perfect conductor limit

Using the expression for the Casimir force between parallel plates in the perfect conductor limit we can thus write

$$dE_D^{\rm PFA}(a(y)) = -L_x\, dy\, \frac{\pi^2}{720}\frac{1}{a(y)^3}, \tag{6.53}$$

where we interpret $L_x\, dy$ to be the area of the small section under consideration. Thus the total Casimir energy in this approximation, after interpreting $L_y = \lim_{N\to\infty} Nd$, will be

$$\begin{aligned}\frac{E_D^{\rm PFA}}{L_x L_y} &= -\frac{\pi^2}{720}\,\frac{1}{a^3}\,\frac{1}{2\pi}\int_{-\pi}^{\pi} d\theta \frac{1}{\left[1+\frac{h_2}{a}\sin\theta - \frac{h_1}{a}\sin(\theta+k_0y_0)\right]^3} \\ &= -\frac{\pi^2}{720}\,\frac{1}{a^3}\,\frac{1}{2\pi}\int_{-\pi}^{\pi} d\theta \frac{1}{\left[1-\frac{r}{a}\cos\theta\right]^3},\end{aligned} \tag{6.54}$$

where we have used the substitutions: $r\sin\alpha = h_2 - h_1\cos k_0y_0$, $r\cos\alpha = h_1\sin k_0y_0$, and used the periodicity property of the function to eliminate α. We note that $r^2 = h_1^2 + h_2^2 - 2h_1h_2\cos(k_0y_0)$.

We calculate the lateral Casimir force in the proximity force approximation, by taking derivative of the energy with respect to y_0, which is

$$F_{\varepsilon\to\infty}^{\rm PFA} = 2\,k_0a\,\sin(k_0y_0)\,\left|F_{\rm Cas}^{(0)}\right|\,\frac{h_1}{a}\frac{h_2}{a}\,\frac{1}{4}\left[\frac{5}{(1-\frac{r^2}{a^2})^{\frac{7}{2}}} - \frac{1}{(1-\frac{r^2}{a^2})^{\frac{5}{2}}}\right] \quad \text{for} \quad |h_1|+|h_2| < a. \tag{6.55}$$

It is easy to check that for $k_0a = 0$ the lateral force given by Eq. (6.43) matches exactly with the above equation for the leading order in h_1h_2.

6.5.2 Dilute dielectric limit

To calculate the dilute dielectric case in the PFA, we start with the van der Waals interaction energy for the parallel slabs in Eq. (4.34) and use Eq. (6.51) to write

$$\frac{E_{12W}^{\rm slabs}}{L_x L_y} = -\frac{23(\varepsilon_1-1)(\varepsilon_2-1)}{1920\pi^2 a^3} A_W^{(1,1)}(0,\bar{d}_i). \tag{6.56}$$

The PFA limit is constructed using the element

$$dE_{12W}^{\rm PFA} = -L_x dy \frac{23(\varepsilon_1-1)(\varepsilon_2-1)}{1920\pi^2}\Big[1-e^{d_1\frac{\partial}{\partial a}}\Big]\Big[1-e^{d_2\frac{\partial}{\partial a}}\Big]\frac{1}{2}\frac{\partial^2}{\partial a^2}\frac{1}{a(y)}, \tag{6.57}$$

where $a(y) = a + h_2\sin(k_0 y) - h_1 \sin k_0(y+y_0)$. Using Eq. (105) in [110] we can perform the y-integral to obtain

$$\frac{E_{12W}^{\rm PFA}}{L_x L_y} = -\frac{23(\varepsilon_1-1)(\varepsilon_2-1)}{1920\pi^2}\Big[1-e^{d_1\frac{\partial}{\partial a}}\Big]\Big[1-e^{d_2\frac{\partial}{\partial a}}\Big]\frac{1}{2}\frac{\partial^2}{\partial a^2}\frac{1}{\sqrt{a^2-r^2}}, \tag{6.58}$$

where $r^2 = h_1^2 + h_2^2 - 2h_1h_2\cos(k_0 y_0)$. As a consistency check one can evaluate the h_1h_2-term contribution from the above expression to obtain Eq. (6.46).

6.6 Non-perturbative dilute dielectric case

The dilute dielectric (weak) limit, though not very exiting experimentally, provides a good check for any approximate results as it can be solved exactly. To calculate the lateral force non-perturbatively in the dilute dielectric limit we start from the expression [115]

$$E_{12}^W = -\frac{23}{(4\pi)^3}\int d^3r \int d^3r' \frac{V_1(\mathbf{r})V_2(\mathbf{r}')}{|\mathbf{r}-\mathbf{r}'|^7}. \tag{6.59}$$

Using the potentials for our corrugations given by Eq. (6.1) and using the integral

$$\int_{\infty}^{\infty} dx \frac{1}{(x^2+a^2)^{\frac{7}{2}}} = \frac{16}{15a^6} \tag{6.60}$$

we have

$$\frac{E_{12}^W}{L_x} = -\frac{23}{(4\pi)^3}\frac{16}{15}\int_{\infty}^{\infty} dy \int_{\infty}^{\infty} dy' \int_{a_1+h_1(y)}^{b_1+h_1(y)} dz \int_{a_2+h_2(y')}^{b_2+h_2(y')} dz' \frac{(\varepsilon_1-1)(\varepsilon_2-1)}{[(y-y')^2+(z-z')^2]^3}. \tag{6.61}$$

Substituting $z_1 = z - b_1 - h_1(y)$, $z_2 = z' - a_2 - h_2(y')$, and then taking $z_1 \to -z_1$ we have

$$\begin{aligned}\frac{E_{12}^W}{L_x} = &-\frac{23(\varepsilon_1-1)(\varepsilon_2-1)}{60\pi^3} \\ &\times \int_{\infty}^{\infty} dy \int_{\infty}^{\infty} dy' \int_0^{d_1} dz_1 \int_0^{d_2} dz_2 \frac{1}{[(y-y')^2+\{z_1+z_2+a(y,y')\}^2]^3},\end{aligned} \tag{6.62}$$

where $a(y,y') = a - h_1(y) + h_2(y')$. Using the indefinite integral

$$\begin{aligned}\int dz_1 \int dz_2 \frac{1}{[b^2+(z_1+z_2+a)^2]^3} = &-\frac{1}{8b^2}\frac{1}{[b^2+(z_1+z_2+a)^2]} \\ &+ \frac{3(z_1+z_2+a)}{8b^5}\tan^{-1}\frac{(z_1+z_2+a)}{b},\end{aligned} \tag{6.63}$$

changing variables $y - y' \to y$, $y + y' \to 2\theta/k_0$, and using the substitutions after Eq. (6.54) we can write

$$\frac{E_{12}^W}{L_x L_y} = -\frac{23(\varepsilon_1-1)(\varepsilon_2-1)}{960\pi^4}\left[1-e^{d_1\frac{\partial}{\partial a}}\right]\left[1-e^{d_2\frac{\partial}{\partial a}}\right]\int_{\infty}^{\infty} dy \int_0^{2\pi} d\theta\, R(y,\theta;a), \tag{6.64}$$

where

$$R(y,\theta;a) = -\frac{1}{y^2}\frac{1}{(y^2+\bar{x}^2)} + \frac{3\bar{x}}{y^5}\tan^{-1}\left[\frac{\bar{x}}{y}\right], \qquad \bar{x} = a - r(k_0 y)\cos\theta, \tag{6.65}$$

where

$$r(k_0 y) = \sqrt{h_1^2 + h_2^2 - 2h_1 h_2 \cos(k_0 y + k_0 y_0)} \tag{6.66}$$

$$= 2h \sin\left(\frac{k_0 y + k_0 y_0}{2}\right) \qquad (\text{if} \quad h_1 = h_2 = h). \tag{6.67}$$

To investigate the pole structure of the function $R(y,\theta;x)$ we write

$$r(k_0 y)\cos\theta = r_0 + r_2 y^2 + r_4 y^4 + \mathcal{O}(y^6), \tag{6.68}$$

where $r_0 = r(0)$. We note that r_0, r_2, and r_4, are independent of a. Further using

$$\tan^{-1}\left[\frac{\bar{x}}{y}\right] = \frac{\pi}{2} - \frac{y}{\bar{x}} + \frac{1}{3}\frac{y^3}{\bar{x}^3} - \frac{1}{5}\frac{y^5}{\bar{x}^5} + \mathcal{O}(y^7), \tag{6.69}$$

we derive the pole structure of the function $R(y,\theta;a)$ to be

$$R(y,\theta;a) = \frac{3\pi}{2}\frac{(a-r_0)}{y^5} - \frac{3}{y^4} - \frac{3\pi}{2}\frac{r_2}{y^3} - \frac{3\pi}{2}\frac{r_4}{y} + \frac{2}{5}\frac{1}{(a-r_0)^4} + \mathcal{O}(y), \tag{6.70}$$

which has poles around $y = 0$. But, the pole terms are linear in a and thus they cancel in the four terms of the square brackets in Eq. (6.64) to yield

$$\left[1 - e^{d_1\frac{\partial}{\partial a}}\right]\left[1 - e^{d_2\frac{\partial}{\partial a}}\right]R(y,\theta;a) = \frac{2}{5}\left[1 - e^{d_1\frac{\partial}{\partial a}}\right]\left[1 - e^{d_2\frac{\partial}{\partial a}}\right]\frac{1}{(a-r_0)^4} + \mathcal{O}(y). \tag{6.71}$$

This assures us that the energy in Eq. (6.64) is well defined.

The θ-integrals can be carried out using

$$\frac{1}{2\pi}\int_0^{2\pi} d\theta \frac{1}{y^2+\bar{x}^2} = \frac{1}{y^2}\frac{2}{\tilde{r}}\,\mathrm{Im}\left[\mathbf{s}_- - \frac{1}{\mathbf{s}_-}\right]^{-1} \tag{6.72}$$

and

$$\frac{1}{2\pi}\int_0^{2\pi} d\theta\, \frac{\bar{x}}{y}\tan^{-1}\left[\frac{\bar{x}}{y}\right] = -\left(1+\frac{\pi}{2}\tilde{a}\right) - \mathrm{Im}\Big[\tilde{a}\ln \mathbf{s}_- - \frac{\tilde{r}}{4}\left(\mathbf{s}_- - \frac{1}{\mathbf{s}_-}\right)\Big], \tag{6.73}$$

where the the expressions on the right hand side have been expressed in terms of the complex numbers

$$\mathbf{s}_\pm = \frac{1}{\tilde{r}}\left[(\tilde{a}+i) \pm \sqrt{(\tilde{a}+i)^2-1}\right] = \exp\left[\pm i\cos^{-1}\left(\frac{\tilde{a}+i}{\tilde{r}}\right)\right], \tag{6.74}$$

which are roots of

$$z^2 - 2\frac{(\tilde{a}+i)}{\tilde{r}}z + 1 = 0. \tag{6.75}$$

We note that

$$\left.\begin{array}{l} |\mathbf{s}_+| > 1 \\ |\mathbf{s}_-| < 1 \end{array}\right\}, \qquad \text{if} \quad \frac{\tilde{a}}{\tilde{r}} > 0 \quad \text{and} \quad \frac{1}{\tilde{r}} \neq 0. \tag{6.76}$$

The evaluation of the second of the above integrals has been described in Appendix B. We also used the notation

$$\tilde{a} = \frac{a}{y}, \qquad \tilde{r} = \frac{r}{y}. \tag{6.77}$$

Using the above integrals in Eq. (6.64) and observing

$$\left[1 - e^{d_1\frac{\partial}{\partial a}}\right]\left[1 - e^{d_2\frac{\partial}{\partial a}}\right]\left(1+\frac{\pi}{2}\tilde{a}\right) = 0, \tag{6.78}$$

we obtain

$$\frac{E_{12}^{W}}{L_x L_y} = -\frac{23(\varepsilon_1 - 1)(\varepsilon_2 - 1)}{960\pi^4}\left[1 - e^{d_1 \frac{\partial}{\partial a}}\right]\left[1 - e^{d_2 \frac{\partial}{\partial a}}\right] \mathrm{Im}\, Q(a, h_i, k_0, y_0), \qquad (6.79)$$

where

$$Q(a, h_i, k_0, y_0) = -2\pi \int_{-\infty}^{\infty} \frac{dy}{y^4}\left[3\tilde{a} \ln \mathbf{s}_- - \frac{3}{4}\tilde{r}\left(\mathbf{s}_- - \frac{1}{\mathbf{s}_-}\right) + \frac{2}{\tilde{r}}\left(\mathbf{s}_- - \frac{1}{\mathbf{s}_-}\right)^{-1}\right]. \qquad (6.80)$$

6.7 Summary

The work presented in this chapter is still in progress. We have reported the very general result for the lateral Casimir force for dielectric slabs. We have taken the conductor limit, the dilute dielectric limit, the thick plate limit and the thin plate limit. Most strikingly in this study we have been able to understand the physical meaning of the thin plate limit. We have further derived an exact formula for the lateral Casimir force in the dilute dielectric limit. This provides a check for the approximate results. To be able to use it fully we need to extend the perturbative calculation to the next-to-leading order. The complexity of this task has resulted in slow progress. However, we still believe that the next-to-leading order should be able to accommodate the total result to better than 95 % similar to what was found in the scalar case [110].

Chapter 7

Conclusions and future directions

7.1 Conclusions

This thesis focuses on the response of the quantum vacuum to the geometric structure of the background potential confining it. The vacuum energy changes in the presence of the confining boundaries. Any variation in the confining parameters gives rise to a change in the energy causing a non-vanishing measurable effect, namely, the Casimir effect. We evaluate the Casimir energy for the electromagnetic field interacting with the dielectric slabs with and without corrugations using the multiple scattering formalism, which allows us to subtract off the divergences from the onset. We are able to reproduce the standard Lifshitz result for the case of parallel infinite dielectric semi-spaces, the Casimir result for two perfectly conducting parallel plates, the Casimir-Polder energy between a dielectric slab and an atom, and the Casimir-Polder energy between a perfect conductor and an atom in Chapter 4. We present a simple physical model that allows us to take the infinitesimally thin plate limit of the thickness of the slabs by modifying the expression of the plasma frequency of the material

to incorporate the finite size of the dielectric slab using the Drude-Sommerfeld free electron gas model. This is a remarkable result because it could be extended to study the vacuum energy in the presence of a single atom layer by modeling them using the semi-transparent δ-function potential, which simplifies the calculational burden enormously. The properties of the material are then encoded in the coupling constant. Our expressions for the case of the perfect conductor limit taken after the thin-plate limit for both the Casimir and the Casimir-Polder energy gives the expected results. We expect our results to provide understanding of infinitesimally thin plates in the presence of electromagnetic fields.

In Chapter 5 and 6 we calculate the leading order lateral Casimir torque and the lateral Casimir force for the two concentric corrugated cylinders and the two parallel dielectric corrugated surfaces respectively. We use the perturbative approximation for the corrugation amplitude being small in comparison to the corrugation wavelength. The analytical result obtained for the case of parallel dielectric slabs is very general and can be used to calculate the Lifshitz energy in the leading order by applying the appropriate model for describing the materials. Results are given for various limiting cases of the perfect conductor limit, the dilute dielectric (weak) limit, the thick plate limit and the thin plate limit. The complexity of doing the next-to-leading order calculation is immense; however, we believe that similarly to the scalar case it will bring down the theoretical error to about 1%. On the other hand we are limited by the approximation of keeping the corrugation amplitude smaller than the corrugation wavelength.

7.2 Future directions

One of the logical extensions of our work is to compare our results with other exact numerical results with respect to change in corrugation amplitude and separation distance. This also requires us to complete the next-to-leading order calculation for both parallel and cylindrical geometries. Our analytical results together with the above mentioned exact results would give a wide and more complete understanding in the study of the lateral Casimir force in real materials.

As mentioned briefly in the discussion of the Chapter 4, Bordag studied the Casimir force and Casimir-Polder force when the perfectly conducting plates are thin (plasma sheets). He has reported that the force between two thin perfectly conducting plates leads to exactly the same Casimir force as for thick slabs, but the Casimir-Polder force between a thin perfectly conducting plate and a molecule is smaller than the standard result by 13% [95]. This discrepancy seems to originate from a choice of boundary conditions on the electromagnetic fields. We, on other hand, obtain identical results for Casimir and Casimir-Polder force for both thick and thin perfect conductors. We believe it is important to explore this discrepancy more carefully. It is worth mentioning that Bordag predicts a similar kind of change in physics if the plates were anisotropic such that there is no conduction in the direction parallel to the thickness even if the plates were thick. Therefore an analogous calculation for anisotropic material slabs could help us in clarifying this issue further. An additional motivation for exploring anisotropic materials arise from the theoretical predictions of repulsive Casimir-Polder force in certain configurations [116]. A repulsive Casimir force is considered as a possible solution for the stiction problem in design of nano-mechanical devices.

Differences in the electromagnetic properties of a thin conductor versus a thick conductor has been considered earlier in literature. For example, in the paper [96] Fetter considers the dynamical properties of a charge in the presence of conducting plate. These differences in the context of Casimir effect has been studied by Barton in a series of papers [117, 118]. It is natural to reconsider the above studies using our methods and ask if a thin plate behaves differently from a thick plate. We tend to believe that there will be no difference in the properties of a thin perfect conductor and thick perfect conductor.

Although we model an idealized situation of an infinitely thin material sheet, the above discussions in the context of the conductivity of graphene, C_{60} molecule, or of carbon nanotube, are of great relevance. To model graphene the number density is derived using a two dimensional massless Dirac-like equation [119] instead of the Schrödinger equation. This will change the result in Section 4.2.1. We are currently exploring this and trying to predict the interlayer bonding strength of graphite. This will further reinforce our confidence in this model. Theoretical models describing graphene as discussed in [120] should also be kept in perspective. These are very interesting and pertinent problems to explore and have multi-disciplinary applications.

Bibliography

[1] H. B. G. Casimir. On the attraction between two perfectly conducting plates. *Kon. Ned. Akad. Wetensch. Proc.*, 51:793–795, 1948.

[2] K. A. Milton and M. Bordag, editors. *Quantum field theory under the influence of external conditions. Proceedings, 9th Conference, QFEXT09, Norman, USA, September 21-25, 2009.* 2010. Prepared for 9th conference on quantum field theory under the influence of external conditions (QFEXT 09): Devoted to the centenary of H. B. G. Casimir, Norman, Oklahoma, 21-25 Sep 2009.

[3] R. Eisenschitz and F. London. Über das Verhältnis der Waalsschen Kräfte zu den homöopolaren Bindungskräften. *Z. Physik*, 60:491–527, 1930.

[4] F. London. Zur Theorie und Systematik der Molekularkräfte. *Z. Physik*, 63:245–279, 1930.

[5] E. J. M. Verwey and J. T. G Overbeek. Long distance forces acting between colloidal particles. *J Chem Soc, Faraday Trans.*, 42A-B:117–123, 1946.

[6] H. B. G. Casimir and D. Polder. The influence of retardation on the London-van der Waals forces. *Phys. Rev.*, 73:360–372, 1948.

[7] H. B. G. Casimir. Sur les forces van der Waals-London. In *Colloque sur la theorie de la liaison chimique*, Paris, 12–17 April 1948. Published in *J. Chim. Phys.*, 46:407, 1949.

[8] Kimball A. Milton, Prachi Parashar, K. V. Shajesh, and Jef Wagner. How does Casimir energy fall? II. Gravitational acceleration of quantum vacuum energy. *J. Phys.*, A40:10935–10943, 2007, 0705.2611.

[9] Bordag, M. and Klimchitskaya, G. L. and Mohideen, U. and Mostepanenko, V. M. *Advances in the Casimir effect*. Oxford University Press, Oxford, UK, 2009.

[10] V. V. Nesterenko, G. Lambiase, and G. Scarpetta. Calculation of the Casimir energy at zero and finite temperature: Some recent results. *Riv. Nuovo Cim.*, 27N6:1–74, 2004, hep-th/0503100.

[11] E. Elizalde, S. D. Odintsov, A. Romeo, A. A. Bytsenko, and S. Zerbini. *Zeta Regularization Techniques with Applications*. World Scientific, Singapore, 1994.

[12] E. M. Lifshitz. The theory of molecular attractive forces between solids. *Zh. Eksp. Teor. Fiz.*, 29:94, 1956. [English transl.: *Soviet Phys. JETP* 2:73, 1956].

[13] I. D. Dzyaloshinskii, E. M. Lifshitz, and L. P. Pitaevskii. *Zh. Eksp. Teor. Fiz.*, 37:229, 1959. [English transl.: *Soviet Phys. JETP* 10:161, 1960].

[14] I. D. Dzyaloshinskii, E. M. Lifshitz, and L. P. Pitaevskii. General theory of van der Waals' forces. *Usp. Fiz. Nauk*, 73:381, 1961. [English transl.: *Soviet Phys. Usp.* 4:153, 1961].

[15] K. A. Milton. *The Casimir effect: Physical manifestations of zero-point energy*. World Scientific (2001) 301 p, River Edge, USA.

[16] Timothy H. Boyer. Quantum electromagnetic zero point energy of a conducting spherical shell and the Casimir model for a charged particle. *Phys. Rev.*, 174:1764–1774, 1968.

[17] H. B. G. Casimir. Introductory remarks on quantum electrodynamics. *Physica*, 19:846, 1953.

[18] B. Davies. Quantum electromagnetic zero-point energy of a conducting spherical shell. *J. Math. Phys.*, 13:1324, 1972.

[19] Roger Balian and Bertrand Duplantier. Electromagnetic waves near perfect conductors. II. Casimir effect. *Annals of Physics*, 112(1):165 – 208, 1978.

[20] Kimball A. Milton, Lester L. DeRaad, and Julian Schwinger. Casimir self-stress on a perfectly conducting spherical shell. *Annals of Physics*, 115(2):388 – 403, 1978.

[21] Kimball A. Milton. Semiclassical electron models: Casimir self-stress in dielectric and conducting balls. *Annals of Physics*, 127(1):49 – 61, 1980.

[22] Iver Brevik, Valery N. Marachevsky, and Kimball A. Milton. Identity of the van der Waals force and the Casimir effect and the irrelevance of these phenomena to sonoluminescence. *Phys. Rev. Lett.*, 82(20):3948–3951, May 1999.

[23] Ines Cavero-Pelaez, Kimball A. Milton, and Klaus Kirsten. Local and global Casimir energies for a semitransparent cylindrical shell. *J. Phys.*, A40:3607–3632, 2007, hep-th/0607154.

[24] Lester L. DeRaad and Kimball A. Milton. Casimir self-stress on a perfectly conducting cylindrical shell. *Annals of Physics*, 136(2):229 – 242, 1981.

[25] I. Brevik and G. H. Nyland. Casimir force on a dielectric cylinder. *Annals of Physics*, 230(2):321 – 342, 1994.

[26] Carl M. Bender and Kimball A. Milton. Scalar Casimir effect for a D-dimensional sphere. *Phys. Rev. D*, 50(10):6547–6555, Nov 1994.

[27] Peter Gosdzinsky and August Romeo. Energy of the vacuum with a perfectly conducting and infinite cylindrical surface. *Physics Letters B*, 441(1-4):265 – 274, 1998.

[28] Inés Cavero-Peláez and Kimball A. Milton. Casimir energy for a dielectric cylinder. *Annals of Physics*, 320(1):108 – 134, 2005.

[29] Israel Klich. Casimir energy of a conducting sphere and of a dilute dielectric ball. *Phys. Rev. D*, 61(2):025004, Dec 1999.

[30] Kimball A. Milton, A. V. Nesterenko, and V. V. Nesterenko. Mode-by-mode summation for the zero point electromagnetic energy of an infinite cylinder. *Phys. Rev. D*, 59(10):105009, Apr 1999.

[31] Kimball A. Milton. Calculating Casimir energies in renormalizable quantum field theory. *Phys. Rev. D*, 68(6):065020, Sep 2003.

[32] E. K. Abalo, K. A. Milton, and L. Kaplan. Casimir energies of cylinders: Universal function. *Phys. Rev. D*, 82(12):125007, Dec 2010.

[33] W. Lukosz. Electromagnetic zero-point energy and radiation pressure for a rectangular cavity. *Physica*, 56(1):109 – 120, 1971.

[34] Jan Ambjorn and Stephen Wolfram. Properties of the vacuum. I. Mechanical and thermodynamic. *Annals of Physics*, 147(1):1 – 32, 1983.

[35] Jan Ambjorn and Stephen Wolfram. Properties of the vacuum. 2. Electrodynamic. *Annals of Physics*, 147(1):33 – 56, 1983.

[36] I. Brevik and M. Lygren. Casimir effect for a perfectly conducting wedge. *Annals of Physics*, 251(2):157 – 179, 1996.

[37] I. Brevik, M. Lygren, and V. N. Marachevsky. Casimir-Polder effect for a perfectly conducting wedge. *Annals of Physics*, 267(1):134 – 142, 1998.

[38] I. Brevik and K. Pettersen. Casimir effect for a dielectric wedge. *Annals of Physics*, 291(2):267 – 275, 2001.

[39] K. Kirsten. *Spectral functions in mathematics and physics*. Chapman & Hall/CRC Press, Boca Raton, 2002.

[40] S A Fulling. Systematics of the relationship between vacuum energy calculations and heat-kernel coefficients. *Journal of Physics A: Mathematical and General*, 36(24):6857–6873, 2003.

[41] Roger Balian and Bertrand Duplantier. Electromagnetic waves near perfect conductors. I. Multiple scattering expansions. Distribution of modes. *Annals of Physics*, 104(2):300 – 335, 1977.

[42] Oded Kenneth and Israel Klich. Casimir forces in a T-operator approach. *Phys. Rev. B*, 78(1):014103, Jul 2008.

[43] Holger Gies, Kurt Langfeld, and Laurent Moyaerts. Casimir effect on the worldline. *Journal of High Energy Physics*, 2003(06):018, 2003.

[44] D. Dalvit, P. Milonni, D. Roberts, and F. da Rosa, editors. *Casimir Physics*, volume 834 of *Lecture Notes in Physics*. Springer, first edition, 2011.

[45] C. M. Hargreaves. *Proc. Kon. Ned. Akad. Wetensch. B*, 68:231, 1965.

[46] Kimball A. Milton. Resource Letter VWCPF-1: van der Waals and Casimir–Polder forces. *American Journal of Physics*, 79(7):697–711, 2011.

[47] Kimball A Milton. The Casimir effect: Recent controversies and progress. *Journal of Physics A: Mathematical and General*, 37(38):R209–R277, 2004.

[48] I. I. Abrikosova and B. V. Deriagin (Derjaguin). *Dokl. Akad. Nauk SSSR*, 90:1055, 1953.

[49] B. V. Deriagin (Derjaguin) and I. I. Abrikosova. Direct measurement of molecular attraction of solid bodies. 2. Method for measuring the gap results of experiments. *Zh. Eksp. Teor. Fiz.*, 30:993.

[50] B. V. Deriagin (Derjaguin) and I. I. Abrikosova. *Zh. Eksp. Teor. Fiz.*, 31:3, 1956. [English transl.: *Soviet Phys. JETP* 4:2, 1957].

[51] M. Y. Sparnaay. Measurements of attractive forces between flat plates. *Physica*, 24:751–764, 1958.

[52] A. Kitchener and A. P. Prosser. Direct measurement of the long-range van der Waals forces. *Proc. Roy. Soc. (London) A*, 242:403, 1957.

[53] W. Black, J. G. V. de Jongh, J. Th. G. Overbeck, and M. J. Sparnaay. Measurements of retarded van der Waals' forces. *Trans. Faraday Soc.*, 56:1597, 1960.

[54] A. van Silfhout. *Proc. Kon. Ned. Akad. Wetensch. B*, 69:501, 1966.

[55] R. H. S. Winterton. *Contemp. Phys.*, 11:559, 1970.

[56] J. N. Israelachivili and D. Tabor. The measurement of van der Waals dispersion forces in the range 1.5 to 130 nm. *Proc. Roy. Soc. (London) A*, 331:19, 1972.

[57] E. S. Sabisky and C. H. Anderson. Verification of the Lifshitz theory of the van der Waals potential using liquid-helium films. *Phys. Rev. A*, 7(2):790–806, Feb 1973.

[58] S. K. Lamoreaux. Demonstration of the Casimir force in the 0.6 to 6 micrometers range. *Phys. Rev. Lett.*, 78:5–8, 1997.

[59] Steve K. Lamoreaux. Systematic correction for "Demonstration of the Casimir force in the 0.6 to 6 μm range". 2010, 1007.4276.

[60] U. Mohideen and A. Roy. Precision measurement of the Casimir force from 0.1 to 0.9 microns. *Phys. Rev. Lett.*, 81:4549, 1998. [arXiv:physics/9805038].

[61] A. Roy, C.-Y. Lin, and U. Mohideen. Improved precision measurement of the Casimir force. *Phys. Rev. D*, 60:R111101, 1999. [arXiv:quant-ph/9906062].

[62] B. W. Harris, F. Chen, and U. Mohideen. Precision measurement of the Casimir force using gold surface. *Phys. Rev. A*, 62:052109, 2000. [arXiv:quant-ph/0005088].

[63] H. B. Chan, V. A. Aksyuk, R. N. Kleiman, D. J. Bishop, and F. Capasso. Nonlinear micromechanical Casimir oscillator. *Phys. Rev. Lett.*, 87:211801, 2001. [arXiv:quant-ph/0109046].

[64] G. Bressi, G. Carugno, R. Onofrio, and G. Ruoso. Measurement of the Casimir force between parallel metallic surfaces. *Phys. Rev. Lett.*, 88:041804, 2002, quant-ph/0203002.

[65] R. S. Decca, E. Fischbach, G. L. Klimchitskaya, D. E. Krause, D. López, and V. M. Mostepanenko. Improved tests of extra-dimensional physics and thermal quantum field theory from new casimir force measurements. *Phys. Rev. D*, 68(11):116003, Dec 2003.

[66] R. S. Decca, D. López, H. B. Chan, E. Fischbach, D. E. Krause, and C. R. Jamell. Constraining new forces in the casimir regime using the isoelectronic technique. *Phys. Rev. Lett.*, 94(24):240401, Jun 2005.

[67] R.S. Decca, D. López, E. Fischbach, G.L. Klimchitskaya, D.E. Krause, and V.M. Mostepanenko. Precise comparison of theory and new experiment for the casimir force leads to stronger constraints on thermal quantum effects and long-range interactions. *Annals of Physics*, 318(1):37 – 80, 2005. Special Issue.

[68] V. M. Mostepanenko et al. Present status of controversies regarding the thermal Casimir force. *J. Phys.*, A39:6589–6600, 2006, quant-ph/0512134.

[69] R. S. Decca, D. Lopez, E. Fischbach, and D. E. Krause. Measurement of the Casimir force between dissimilar metals. *Phys. Rev. Lett.*, 91:050402, 2003.

[70] Steve K. Lamoreaux. Progress in experimental measurements of the surface-surface Casimir force: Electrostatic calibrations and limitations to accuracy. 2010, 1008.3640.

[71] A. O. Sushkov, W. J. Kim, D. A. R. Dalvit, and S. K. Lamoreaux. Observation of the thermal Casimir force. *Nat Phys*, 7(3):230–233, Mar 2011.

[72] V. B. Bezerra, G. L. Klimchitskaya, U. Mohideen, V. M. Mostepanenko, and C. Romero. Impact of surface imperfections on the Casimir force for lenses of centimeter-size curvature radii. *Phys. Rev. B*, 83(7):075417, Feb 2011.

[73] B. V. Deryagin (Derjaguin). Untersuchungen über die Reibung und Adhäsion. IV. Theorie des Anhaftens kleiner Teilchen. *Kolloid Z.*, 69:155–164, 1934.

[74] Astrid Lambrecht and Valery N. Marachevsky. Casimir interaction of dielectric gratings. *Phys. Rev. Lett.*, 101(16):160403, Oct 2008.

[75] Sahand Jamal Rahi, Thorsten Emig, Noah Graham, Robert L. Jaffe, and Mehran Kardar. Scattering theory approach to electrodynamic Casimir forces. *Phys. Rev. D*, 80(8):085021, Oct 2009.

[76] H. C. Chiu, G. L. Klimchitskaya, V. N. Marachevsky, V. M. Mostepanenko, and U. Mohideen. Lateral Casimir force between sinusoidally corrugated surfaces: Asymmetric profiles, deviations from the proximity force approximation and comparison with exact theory. *Phys. Rev. B*, 81:115417, 2010.

[77] A. W. Rodriguez, F. Capasso, and S. G. Johnson. The Casimir effect in microstructured geometries. *Nature Photonics*, 5:211, 2011.

[78] L. Brillouin. *Wave propagation and group velocity*. Academic Press, Newyork and London, 1960.

[79] Julian. Schwinger, Jr. DeRaad, Lester L., Kimball A. Milton, and Wu-yang Tsai. *Classical electrodynamics*. Advanced book program. Perseus Books, 1998.

[80] J. Schwinger. The algebra of microscopic measurement. *Proc. Nat. Acad. Sci.*, 45:1542, 1959.

[81] J. Schwinger. The geometry of quantum states. *Proc. Nat. Acad. Sci.*, 46:257, 1960.

[82] J. Schwinger. Unitary operator bases. *Proc. Nat. Acad. Sci.*, 46:570, 1960.

[83] J. Schwinger. Unitary transformations and the action principle. *Proc. Nat. Acad. Sci.*, 46:883, 1960.

[84] J. Schwinger. The special canonical group. *Proc. Nat. Acad. Sci.*, 46:1401, 1960.

[85] J. Schwinger. Quantum variables and the action principle. *Proc. Nat. Acad. Sci.*, 47:1075, 1961.

[86] J. Schwinger. Exterior algebra and the action principle, I. *Proc. Nat. Acad. Sci.*, 48:603, 1962.

[87] J. Schwinger. *Particles, sources, and fields. Volume 1.* Reading, Mass., USA, (1970) 425 p.

[88] Kimball A. Milton, Lester L. DeRaad, Jr., and Julian S. Schwinger. Casimir selfstress on a perfectly conducting spherical shell. *Ann. Phys.*, 115:388, 1978.

[89] Kimball A. Milton and Jef Wagner. Multiple scattering methods in Casimir calculations. *J. Phys.*, A41:155402, 2008, 0712.3811.

[90] P. M. Morse and H. Feshbach. *Methods of theoretical Physics*. McGraw-Hill book companya, NY, USA, 1953.

[91] Julian S. Schwinger, Jr. DeRaad, Lester L., and Kimball A. Milton. Casimir effect in dielectrics. *Annals Phys.*, 115:1–23, 1978.

[92] Kimball A. Milton, Jef Wagner, Prachi Parashar, and Iver Brevik. Casimir energy, dispersion, and the Lifshitz formula. *Phys. Rev. D*, 81(6):065007, Mar 2010.

[93] L. D. Landau. Paramagnetism of metals. *Z. Phys.*, 64:629, 1930.

[94] Neil W. Ashcroft and David N. Mermin. *Solid state physics*. Holt, Rinehart and Winston (1976), USA.

[95] Michael Bordag. Reconsidering the quantization of electrodynamics with boundary conditions and some measurable consequences. *Phys. Rev.*, D70:085010, 2004, hep-th/0403222.

[96] Alexander L. Fetter. Electrodynamics of a layered electron gas. I. Single layer. *Annals of Physics*, 81(2):367 – 393, 1973.

[97] Ramin Golestanian and Mehran Kardar. Mechanical response of vacuum. *Phys. Rev. Lett.*, 78(18):3421–3425, May 1997.

[98] Ramin Golestanian and Mehran Kardar. Path-integral approach to the dynamic Casimir effect with fluctuating boundaries. *Phys. Rev. A*, 58(3):1713–1722, Sep 1998.

[99] H. B. Chan, V. A. Aksyuk, R. N. Kleiman, D. J. Bishop, and Federico Capasso. Quantum mechanical actuation of microelectromechanical system by the Casimir force. *Science*, 291:1941–1944, 2001.

[100] Arash Ashourvan, MirFaez Miri, and Ramin Golestanian. Noncontact rack and pinion powered by the lateral Casimir force. *Phys. Rev. Lett.*, 98(14):140801, Apr 2007.

[101] MirFaez Miri, Vahid Nekouie, and Ramin Golestanian. Nonlinear dynamics of a rack-pinion-rack device powered by the Casimir force. *Phys. Rev. E*, 81(1):016104, Jan 2010.

[102] Anushree Roy and U. Mohideen. Demonstration of the nontrivial boundary dependence of the Casimir force. *Phys. Rev. Lett.*, 82(22):4380–4383, May 1999.

[103] F. Chen, U. Mohideen, G. L. Klimchitskaya, and V. M. Mostepanenko. Experimental and theoretical investigation of the lateral Casimir force between corrugated surfaces. *Phys. Rev. A*, 66(3):032113, Sep 2002.

[104] H. B. Chan, Y. Bao, J. Zou, R. A. Cirelli, F. Klemens, W. M. Mansfield, and C. S. Pai. Measurement of the Casimir force between a gold sphere and a silicon surface with nanoscale trench arrays. *Phys. Rev. Lett.*, 101(3):030401, Jul 2008.

[105] Inés Cavero-Peláez, Kimball A. Milton, Prachi Parashar, and K. V. Shajesh. Noncontact gears. II. Casimir torque between concentric corrugated cylinders for the scalar case. *Phys. Rev. D*, 78(6):065019, Sep 2008.

[106] Yu. Barash. Moment of van der Waals forces between anisotropic bodies. *Radiophysics and Quantum Electronics*, 21:1138–1143, 1978. 10.1007/BF02121382.

[107] S. J. van Enk. Casimir torque between dielectrics. *Phys. Rev. A*, 52(4):2569–2575, Oct 1995.

[108] F.C. Lombardo, F.D. Mazzitelli, and P.I. Villar. Exploring the quantum vacuum with cylinders. *J.Phys.A*, A41:164009, 2008.

[109] F. C. Lombardo, F. D. Mazzitelli, M. Vázquez, and P. I. Villar. Computing the Casimir energy using the point-matching method. *Phys. Rev. D*, 80(6):065018, Sep 2009.

[110] Inés Cavero-Peláez, Kimball A. Milton, Prachi Parashar, and K. V. Shajesh. Noncontact gears. I. Next-to-leading order contribution to the lateral Casimir force between corrugated parallel plates. *Phys. Rev. D*, 78(6):065018, Sep 2008.

[111] Milton Abramowitz and Irene A. Stegun. *Handbook of Mathematical Functions with Formulas, Graphs, and Mathematical Tables*. Dover, New York, ninth dover printing, tenth gpo printing edition, 1964.

[112] Prachi Parashar, Kimball A. Milton, Ines Cavero-Pelaez, and K. V. Shajesh. Electromagnetic non-contact gears: Prelude. In proceedings of quantum field theory under the influence of external conditions (QFEXT09), World Scientific Singapore, page 48 (2010), Kimball A. Milton (ed.) and Michael Bordag (ed.). 1001.4105.

[113] T. Emig, A. Hanke, R. Golestanian, and M. Kardar. Normal and lateral casimir forces between deformed plates. *Phys. Rev. A*, 67(2):022114, Feb 2003.

[114] Kimball A. Milton, Prachi Parashar, and Jef Wagner. Exact results for Casimir interactions between dielectric bodies: The weak-coupling or van der Waals limit. *Phys. Rev. Lett.*, 101(16):160402, Oct 2008.

[115] Kimball A. Milton, Prachi Parashar, and Jef Wagner. From multiple scattering to van der Waals interactions: exact results for eccentric cylinders. 2008, 0811.0128.

[116] Kimball A. Milton, E. K. Abalo, Prachi Parashar, Nima Pourtolami, Iver Brevik, and Simen Å. Ellingsen. Casimir-Polder repulsion near edges: Wedge apex and a screen with an aperture. *Phys. Rev. A*, 83(6):062507, Jun 2011.

[117] G Barton. Casimir effects for a flat plasma sheet: I. energies. *Journal of Physics A: Mathematical and General*, 38(13):2997, 2005.

[118] G Barton. Casimir effects for a flat plasma sheet: Ii. fields and stresses. *Journal of Physics A: Mathematical and General*, 38(13):3021, 2005.

[119] P. R. Wallace. The band theory of graphite. *Phys. Rev.*, 71(9):622–634, May 1947.

[120] A. H. Castro Neto, F. Guinea, N. M. R. Peres, K. S. Novoselov, and A. K. Geim. The electronic properties of graphene. *Rev. Mod. Phys.*, 81(1):109–162, Jan 2009.

Appendix A

Thin plate approximation

A thin plate will be described by the model

$$(\varepsilon_i - 1)\zeta^2 = \frac{\lambda_i}{d_i}, \tag{A.1}$$

where λ_i is independent of d_i and is a material dependent parameter. In the thin plate limit we have the definitions

$$\varepsilon_i = 1 + \frac{\lambda_i}{d_i\zeta^2} = \frac{\lambda_i}{d_i\zeta^2}\left[1 + \zeta^2\frac{d_i}{\lambda_i}\right], \qquad \kappa_i^2 = \kappa^2 + \frac{\lambda_i}{d_i}. \tag{A.2}$$

Using the approximations

$$\zeta^2 \ll \frac{\lambda_i}{d_i} \qquad \text{and} \qquad k^2 \ll \frac{\lambda_i}{d_i}, \tag{A.3}$$

and with the understanding that the $\mathcal{O}(d)$ in the following should be read after scaling d, we have following approximations:

$$\kappa_i = \sqrt{\frac{\lambda_i}{d_i}}\left[1 + \frac{\kappa^2}{2}\frac{d_i}{\lambda_i}\right] + \mathcal{O}(d^{\frac{3}{2}}), \tag{A.4}$$

$$\bar{\kappa}_i = \zeta^2\sqrt{\frac{d_i}{\lambda_i}}\left[1 + \left(\frac{\kappa^2}{2} - \zeta^2\right)\frac{d_i}{\lambda_i}\right] + \mathcal{O}(d^2), \tag{A.5}$$

$$\alpha_i = 1 - 2\kappa\sqrt{\frac{d_i}{\lambda_i}} + 2\kappa^2\frac{d_i}{\lambda_i} + \mathcal{O}(d^2), \tag{A.6}$$

$$\bar{\alpha}_i = -1 + 2\frac{\zeta^2}{\kappa}\sqrt{\frac{d_i}{\lambda_i}} - 2\frac{\zeta^4}{\kappa^2}\frac{d_i}{\lambda_i} + \frac{\zeta^6}{\kappa^3}\left(\frac{d_i}{\lambda_i}\right)^{\frac{3}{2}}\frac{k^4}{\zeta^4} + \mathcal{O}(d^2), \tag{A.7}$$

$$\alpha_i^2 = 1 - 4\kappa\sqrt{\frac{d_i}{\lambda_i}} + 8\kappa^2\frac{d_i}{\lambda_i} - 8\kappa^3\left(\frac{d_i}{\lambda_i}\right)^{\frac{3}{2}} + \mathcal{O}(d^2), \tag{A.8}$$

$$\bar{\alpha}_i^2 = 1 - 4\frac{\zeta^2}{\kappa}\sqrt{\frac{d_i}{\lambda_i}} + 8\frac{\zeta^4}{\kappa^2}\frac{d_i}{\lambda_i} - 8\frac{\zeta^6}{\kappa^3}\left(\frac{d_i}{\lambda_i}\right)^{\frac{3}{2}}\left[1 + \frac{k^4}{4\zeta^4}\right] + \mathcal{O}(d^2). \tag{A.9}$$

The above can be used to further derive the following

$$e^{-\kappa_i d_i} = 1 - \sqrt{\lambda_i d_i} + \frac{1}{2}\lambda_i d_i + \mathcal{O}(d^{\frac{3}{2}}), \tag{A.10}$$

$$e^{-2\kappa_i d_i} = 1 - 2\sqrt{\lambda_i d_i} + 2\lambda_i d_i + \mathcal{O}(d^{\frac{3}{2}}), \tag{A.11}$$

$$(1 - \alpha_i^2)e^{-\kappa_i d_i} = 4\kappa\sqrt{\frac{d_i}{\lambda_i}}\left[1 - 2\kappa\sqrt{\frac{d_i}{\lambda_i}}\left(1 + \frac{\lambda_i}{2\kappa}\right) + 2\kappa^2\frac{d_i}{\lambda_i}\left(1 + \frac{\lambda_i}{2\kappa}\right)^2\right] + \mathcal{O}(d^2), \tag{A.12}$$

$$\begin{aligned}(1 - \bar{\alpha}_i^2)e^{-\kappa_i d_i} = 4\frac{\zeta^2}{\kappa}\sqrt{\frac{d_i}{\lambda_i}}\Bigg[1 - 2\frac{\zeta^2}{\kappa}\sqrt{\frac{d_i}{\lambda_i}}\left(1 + \frac{\lambda_i}{2\zeta^2/\kappa}\right) \\ + 2\frac{\zeta^4}{\kappa^2}\frac{d_i}{\lambda_i}\left\{\left(1 + \frac{\lambda_i}{2\zeta^2/\kappa}\right)^2 + \frac{k^4}{4\zeta^4}\right\}\Bigg] + \mathcal{O}(d^2),\end{aligned} \tag{A.13}$$

$$(1-\alpha_i)(1+\alpha_i e^{-2\kappa_i d_i})=4\kappa\sqrt{\frac{d_i}{\lambda_i}}\Bigg[1-2\kappa\sqrt{\frac{d_i}{\lambda_i}}\left(1+\frac{\lambda_i}{2\kappa}\right) +2\kappa^2\frac{d_i}{\lambda_i}\left(1+\frac{\lambda_i}{2\kappa}\right)\left(1+\frac{\lambda_i}{\kappa}\right)\Bigg]+\mathcal{O}(d^2), \quad (A.14)$$

$$(1+\bar{\alpha}_i)(1-\bar{\alpha}_i e^{-2\kappa_i d_i})=4\frac{\zeta^2}{\kappa}\sqrt{\frac{d_i}{\lambda_i}}\Bigg[1-2\frac{\zeta^2}{\kappa}\sqrt{\frac{d_i}{\lambda_i}}\left(1+\frac{\lambda_i}{2\zeta^2/\kappa}\right)\left(1+\frac{\lambda_i}{2\zeta^2/\kappa}\right) +\frac{\zeta^4}{\kappa^2}\frac{d_i}{\lambda_i}\Bigg\{\left(1+\frac{\lambda_i}{2\zeta^2/\kappa}\right)^2 +\left(1+\frac{\lambda_i}{2\zeta^2/\kappa}\right)+\frac{1}{2}\frac{k^4}{4\zeta^4}\Bigg\}\Bigg]+\mathcal{O}(d^2), \quad (A.15)$$

$$(1-\bar{\alpha}_i)(1+\bar{\alpha}_i e^{-2\kappa_i d_i})=4\frac{\zeta^2}{\kappa}\sqrt{\frac{d_i}{\lambda_i}}\left(1+\frac{\lambda_i}{2\zeta^2/\kappa}\right)\Bigg[1-2\frac{\zeta^2}{\kappa}\sqrt{\frac{d_i}{\lambda_i}}\left(1+\frac{\lambda_i}{2\zeta^2/\kappa}\right) +2\frac{\zeta^4}{\kappa^2}\frac{d_i}{\lambda_i}\left(1+\frac{\lambda_i}{2\zeta^2/\kappa}\right)\Bigg]+\mathcal{O}(d^2). \quad (A.16)$$

Using the above we can further derive the approximations

$$\Delta=16\kappa^2\sqrt{\frac{d_1}{\lambda_1}}\sqrt{\frac{d_2}{\lambda_2}}\left[\left(1+\frac{\lambda_1}{2\kappa}\right)\left(1+\frac{\lambda_2}{2\kappa}\right)-\frac{\lambda_1}{2\kappa}\frac{\lambda_2}{2\kappa}e^{-2\kappa a}\right]+\mathcal{O}(d^{\frac{3}{2}}), \quad (A.17)$$

$$\bar{\Delta}=16\kappa^2\sqrt{\frac{d_1}{\lambda_1}}\sqrt{\frac{d_2}{\lambda_2}}\left[\left(1+\frac{\lambda_1}{2\zeta^2/\kappa}\right)\left(1+\frac{\lambda_2}{2\zeta^2/\kappa}\right)-\frac{\lambda_1}{2\zeta^2/\kappa}\frac{\lambda_2}{2\zeta^2/\kappa}e^{-2\kappa a}\right]+\mathcal{O}(d^{\frac{3}{2}}). \quad (A.18)$$

And further

$$M(-\alpha_i,-\alpha_i')=-16\frac{\kappa\kappa'}{\zeta^2}\sqrt{\frac{d_1}{\lambda_1}}\sqrt{\frac{d_2}{\lambda_2}}\lambda_i\left[\kappa\left(1+\frac{\lambda_i}{2\kappa}\right)+\kappa'\left(1+\frac{\lambda_i}{2\kappa'}\right)\right]+\mathcal{O}(d^{\frac{3}{2}}), \quad (A.19)$$

$$M(-\alpha_i,\bar{\alpha}_i')=-16\frac{\kappa}{\kappa'}\sqrt{\frac{d_1}{\lambda_1}}\sqrt{\frac{d_2}{\lambda_2}}\lambda_i\left[\kappa\left(1+\frac{\lambda_i}{2\kappa}\right)+\frac{\zeta^2}{\kappa'}\left(1+\frac{\lambda_i}{2\zeta^2/\kappa'}\right)\right]+\mathcal{O}(d^{\frac{3}{2}}), \quad (A.20)$$

$$M(\bar{\alpha}_i,-\alpha_i')=-16\frac{\kappa'}{\kappa}\sqrt{\frac{d_1}{\lambda_1}}\sqrt{\frac{d_2}{\lambda_2}}\lambda_i\left[\frac{\zeta^2}{\kappa}\left(1+\frac{\lambda_i}{2\zeta^2/\kappa}\right)+\kappa'\left(1+\frac{\lambda_i}{2\kappa'}\right)\right]+\mathcal{O}(d^{\frac{3}{2}}), \quad (A.21)$$

$$M(\bar{\alpha}_i,\bar{\alpha}_i')=-16\frac{\zeta^2}{\kappa\kappa'}\sqrt{\frac{d_1}{\lambda_1}}\sqrt{\frac{d_2}{\lambda_2}}\lambda_i\left[\frac{\zeta^2}{\kappa}\left(1+\frac{\lambda_i}{2\zeta^2/\kappa}\right)+\frac{\zeta^2}{\kappa'}\left(1+\frac{\lambda_i}{2\zeta^2/\kappa'}\right)\right]+\mathcal{O}(d^{\frac{3}{2}}), \quad (A.22)$$

$$M(-\bar{\alpha}_i,-\bar{\alpha}_i')=-16\varepsilon_i\sqrt{\frac{d_1}{\lambda_1}}\sqrt{\frac{d_2}{\lambda_2}}\lambda_i\left[\frac{\zeta^2}{\kappa}\left(1+\frac{\lambda_i}{2\zeta^2/\kappa}\right)+\frac{\zeta^2}{\kappa'}\left(1+\frac{\lambda_i}{2\zeta^2/\kappa'}\right)\right]+\mathcal{O}(d^{\frac{3}{2}}). \quad (A.23)$$

Using the above expressions we can derive

$$\frac{1}{\Delta}\frac{1}{\Delta'}M(-\alpha_1,-\alpha_1')M(-\alpha_2,-\alpha_2')=-\frac{2\kappa}{\zeta^2}\frac{2\kappa'}{\zeta^2}I_s^{(2)}(\kappa,\kappa')+\mathcal{O}(d^{\frac{1}{2}}), \tag{A.24}$$

$$\frac{1}{\Delta}\frac{1}{\bar{\Delta}'}M(-\alpha_1,\bar{\alpha}_1')M(-\alpha_2,\bar{\alpha}_2')=-\frac{2\kappa}{\zeta^2}\frac{2\kappa'}{\zeta^2}I_s^{(2)}\left(\kappa,\frac{\zeta^2}{\kappa'}\right)\frac{\zeta^2}{\kappa'^2}+\mathcal{O}(d^{\frac{1}{2}}), \tag{A.25}$$

$$\frac{1}{\bar{\Delta}}\frac{1}{\Delta'}M(\bar{\alpha}_1,-\alpha_1')M(\bar{\alpha_2},-\alpha_2')=-\frac{2\kappa}{\zeta^2}\frac{2\kappa'}{\zeta^2}I_s^{(2)}\left(\frac{\zeta^2}{\kappa},\kappa'\right)\frac{\zeta^2}{\kappa^2}+\mathcal{O}(d^{\frac{1}{2}}), \tag{A.26}$$

where $I_s^{(2)}(\kappa,\kappa')$ is

$$I_s^{(2)}(\kappa,\kappa')=-\frac{\lambda_1}{2\kappa}\frac{\lambda_2}{2\kappa'}\frac{e^{-a(\kappa+\kappa')}}{\Delta_s\Delta_s'}\left[\kappa\left(1+\frac{\lambda_1}{2\kappa}\right)+\kappa'\left(1+\frac{\lambda_1}{2\kappa'}\right)\right] \times\left[\kappa\left(1+\frac{\lambda_2}{2\kappa}\right)+\kappa'\left(1+\frac{\lambda_2}{2\kappa'}\right)\right], \tag{A.27}$$

and is the $I^{(2)}$-kernel for the scalar cae (see Eq. (49) in Gears-I [110]), Δ_s is given by

$$\Delta_s=\left(1+\frac{\lambda_1}{2\kappa}\right)\left(1+\frac{\lambda_2}{2\kappa}\right)-\frac{\lambda_1}{2\kappa}\frac{\lambda_2}{2\kappa}e^{-2\kappa a}, \tag{A.28}$$

which was given in Eq. (A2) in Gears-I [110]. We also need

$$\frac{1}{\bar{\Delta}}\frac{1}{\bar{\Delta}'}M(\bar{\alpha}_1,\bar{\alpha}_1')M(\bar{\alpha_2},\bar{\alpha}_2')=-\frac{2\kappa}{\zeta^2}\frac{2\kappa'}{\zeta^2}I_s^{(2)}\left(\frac{\zeta^2}{\kappa},\frac{\zeta^2}{\kappa'}\right)\frac{\zeta^2}{\kappa^2}\frac{\zeta^2}{\kappa'^2}+\mathcal{O}(d^{\frac{1}{2}}), \tag{A.29}$$

$$\frac{1}{\bar{\Delta}}\frac{1}{\bar{\Delta}'}M(\bar{\alpha}_1,\bar{\alpha}_1')\frac{1}{\varepsilon_2}M(-\bar{\alpha_2},-\bar{\alpha}_2')=-\frac{2\kappa}{\zeta^2}\frac{2\kappa'}{\zeta^2}I_s^{(2)}\left(\frac{\zeta^2}{\kappa},\frac{\zeta^2}{\kappa'}\right)\frac{\zeta}{\kappa}\frac{\zeta}{\kappa'}+\mathcal{O}(d^{\frac{1}{2}}), \tag{A.30}$$

$$\frac{1}{\bar{\Delta}}\frac{1}{\bar{\Delta}'}\frac{1}{\varepsilon_1}M(\bar{\alpha}_1,\bar{\alpha}_1')M(-\bar{\alpha_2},-\bar{\alpha}_2')=-\frac{2\kappa}{\zeta^2}\frac{2\kappa'}{\zeta^2}I_s^{(2)}\left(\frac{\zeta^2}{\kappa},\frac{\zeta^2}{\kappa'}\right)\frac{\zeta}{\kappa}\frac{\zeta}{\kappa'}+\mathcal{O}(d^{\frac{1}{2}}), \tag{A.31}$$

$$\frac{1}{\bar{\Delta}}\frac{1}{\bar{\Delta}'}\frac{1}{\varepsilon_1}M(\bar{\alpha}_1,\bar{\alpha}_1')\frac{1}{\varepsilon_2}M(-\bar{\alpha_2},-\bar{\alpha}_2')=-\frac{2\kappa}{\zeta^2}\frac{2\kappa'}{\zeta^2}I_s^{(2)}\left(\frac{\zeta^2}{\kappa},\frac{\zeta^2}{\kappa'}\right)+\mathcal{O}(d^{\frac{1}{2}}). \tag{A.32}$$

Appendix B

Evaluation of contour integral

The integral

$$I(\tilde{a},\tilde{r}) = \frac{1}{2\pi}\int_0^{2\pi} d\theta(\tilde{a}-\tilde{r}\cos\theta)\tan^{-1}(\tilde{a}-\tilde{r}\cos\theta) \tag{B.1}$$

can be evaluated by integrating on a contour along the unit circle of a complex plane:

$$I(\tilde{a},\tilde{r}) = \frac{1}{2\pi i}\int_c \frac{dz}{z}\Big[\tilde{a}-\frac{\tilde{r}}{2}\Big(z+\frac{1}{z}\Big)\Big]\tan^{-1}\Big[\tilde{a}-\frac{\tilde{r}}{2}\Big(z+\frac{1}{z}\Big)\Big], \tag{B.2}$$

where we used the substitutions

$$z = e^{i\theta}, \qquad d\theta = \frac{1}{i}\frac{dz}{z}, \qquad \text{and} \qquad \cos\theta = \frac{1}{2}\Big(z+\frac{1}{z}\Big). \tag{B.3}$$

Further using the principal value of

$$\tan^{-1}\tilde{x} = \frac{i}{2}\ln\Big(\frac{1-ix}{1+ix}\Big) - \pi n, \tag{B.4}$$

we can write

$$I(\tilde{a},\tilde{r}) = I_0(\tilde{a}) + J(\tilde{a},\tilde{r}), \tag{B.5}$$

where

$$I_0(\tilde{a}) = \frac{1}{2\pi i}\frac{\pi}{4}\tilde{r}\int_c \frac{dz}{z^2}\Big[z^2 - 2\frac{\tilde{a}}{\tilde{r}}z + 1\Big], \tag{B.6}$$

$$J(\tilde{a},\tilde{r}) = \frac{\tilde{r}}{8\pi}\int_c \frac{dz}{z^2}\Big[z^2 - 2\frac{\tilde{a}}{\tilde{r}}z + 1\Big]\ln\frac{(z-\mathbf{s}_+)(z-\mathbf{s}_-)}{(z-\mathbf{s}_+^*)(z-\mathbf{s}_-^*)}, \tag{B.7}$$

expressed in terms of the complex numbers defined in Eq. (6.74).

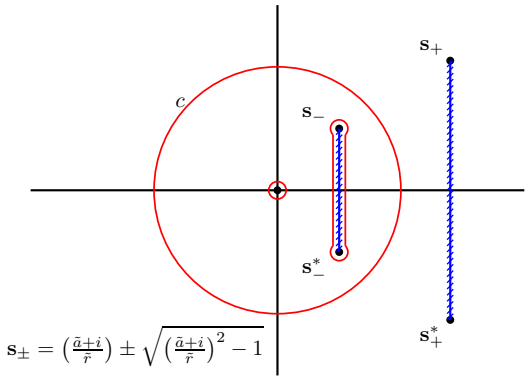

Figure B.1: Contour in the complex $\mathbf{s}$-plane. The integral in Eq. (B.7) has a pole at $\mathbf{s} = 0$ and branch points at $\mathbf{s}_\pm$ and $\mathbf{s}_\pm^*$. Strokes on a line represent branch cuts. The integral is evaluated over a contour on the unit circle and gets contributions from the pole at $\mathbf{s} = 0$, and from the discontinuity about the branch line connecting $\mathbf{s}_-$ and $\mathbf{s}_-^*$.

The integral in Eq. (B.6) is evaluated using residue theorem to be

$$I_0(\tilde{a}) = -\frac{\pi}{2}\tilde{a}. \tag{B.8}$$

The integral in Eq. (B.7) has a pole at the origin and the complex numbers $\mathbf{s}_\pm$ and $\mathbf{s}_\pm^*$ are branch points, which are described in Figure B.1 with the branch cuts. Observe that the discontinuities due the complex conjugates of the branch points are chosen to cancel out. The pole at the origin contributes exactly 1 to $J(\tilde{a}, \tilde{r})$. The discontinuity about the branch cut connecting $\mathbf{s}_-$ and $\mathbf{s}_-$ contributes the rest to yield

$$J(\tilde{a}, \tilde{r}) = -1 - \mathrm{Im}\left[\tilde{a}\ln \mathbf{s}_- - \frac{\tilde{r}}{4}\left(\mathbf{s}_- - \frac{1}{\mathbf{s}_-}\right)\right]. \tag{B.9}$$

Using solutions to $I_0(\tilde{a})$ in Eq. (B.8), and $J(\tilde{a}, \tilde{r})$ in Eq. (B.9), in Eq. (B.5) we have

$$I(\tilde{a}, \tilde{r}) = -\left(1 + \frac{\pi}{2}\tilde{a}\right) - \mathrm{Im}\left[\tilde{a}\ln \mathbf{s}_- - \frac{\tilde{r}}{4}\left(\mathbf{s}_- - \frac{1}{\mathbf{s}_-}\right)\right]. \tag{B.10}$$